technische universität dortmund

MAX-PLANCK-INSTITUT FÜR MOLEKULARE PHYSIOLOGIE

The Role of Cell Cycle, Growth, and Metabolism in Species-Specific Differentiation Timing

Dissertation

Zur Erlangung des akademischen Grades eines
Doktors der Naturwissenschaften
(Dr. rer. nat.)

an der Fakultät für Chemie und Chemische Biologie
der Technischen Universität Dortmund

Angefertigt am Max-Planck-Institut für molekulare Physiologie, Dortmund,
vorgelegt von

Julia Schröder

June 2024

Date of submission: 12.06.2024

1st Examiner: Prof. Dr. Philippe Bastiaens

2nd Examiner: Prof. Dr. Boris Pfander

Supervisor: Dr. Christian Schröter

The work presented in this thesis was performed under direct supervision of Dr. Christian Schröter in the Department of Systemic Cell Biology led by Prof. Dr. Philippe Bastiaens at the Max Planck Institute of Molecular Physiology, Dortmund, Germany.

Julia Schröder was affiliated with the International Max Planck Research School for Living Matter, Dortmund, Germany.

Declaration

Eidesstattliche Versicherung (Affidavit)

Schröder, Julia
Name, Vorname
(Surname, first name)

230072
Matrikel-Nr.
(Enrolment number)

Belehrung:

Wer vorsätzlich gegen eine die Täuschung über Prüfungsleistungen betreffende Regelung einer Hochschulprüfungsordnung verstößt, handelt ordnungswidrig. Die Ordnungswidrigkeit kann mit einer Geldbuße von bis zu 50.000,00 € geahndet werden. Zuständige Verwaltungsbehörde für die Verfolgung und Ahndung von Ordnungswidrigkeiten ist der Kanzler/die Kanzlerin der Technischen Universität Dortmund. Im Falle eines mehrfachen oder sonstigen schwerwiegenden Täuschungsversuches kann der Prüfling zudem exmatrikuliert werden, § 63 Abs. 5 Hochschulgesetz NRW.

Die Abgabe einer falschen Versicherung an Eides statt ist strafbar.

Wer vorsätzlich eine falsche Versicherung an Eides statt abgibt, kann mit einer Freiheitsstrafe bis zu drei Jahren oder mit Geldstrafe bestraft werden, § 156 StGB. Die fahrlässige Abgabe einer falschen Versicherung an Eides statt kann mit einer Freiheitsstrafe bis zu einem Jahr oder Geldstrafe bestraft werden, § 161 StGB.

Die oben stehende Belehrung habe ich zur Kenntnis genommen:

Official notification:

Any person who intentionally breaches any regulation of university examination regulations relating to deception in examination performance is acting improperly. This offence can be punished with a fine of up to EUR 50,000.00. The competent administrative authority for the pursuit and prosecution of offences of this type is the chancellor of the TU Dortmund University. In the case of multiple or other serious attempts at deception, the candidate can also be unenrolled, Section 63, paragraph 5 of the Universities Act of North Rhine-Westphalia.

The submission of a false affidavit is punishable.

Any person who intentionally submits a false affidavit can be punished with a prison sentence of up to three years or a fine, Section 156 of the Criminal Code. The negligent submission of a false affidavit can be punished with a prison sentence of up to one year or a fine, Section 161 of the Criminal Code.

I have taken note of the above official notification.

Dortmund, 12.06.2024
Ort, Datum
(Place, date)

Unterschrift
(Signature)

Titel der Dissertation:
(Title of the thesis):

The Role of Cell Cycle, Growth, and Metabolism in Species-Specific Differentiation Timing

Ich versichere hiermit an Eides statt, dass ich die vorliegende Dissertation mit dem Titel selbstständig und ohne unzulässige fremde Hilfe angefertigt habe. Ich habe keine anderen als die angegebenen Quellen und Hilfsmittel benutzt sowie wörtliche und sinngemäße Zitate kenntlich gemacht.
Die Arbeit hat in gegenwärtiger oder in einer anderen Fassung weder der TU Dortmund noch einer anderen Hochschule im Zusammenhang mit einer staatlichen oder akademischen Prüfung vorgelegen.

I hereby swear that I have completed the present dissertation independently and without inadmissible external support. I have not used any sources or tools other than those indicated and have identified literal and analogous quotations.

The thesis in its current version or another version has not been presented to the TU Dortmund University or another university in connection with a state or academic examination.*

*Please be aware that solely the German version of the affidavit ("Eidesstattliche Versicherung") for the PhD thesis is the official and legally binding version.

Dortmund, 12.06.2024
Ort, Datum
(Place, date)

Unterschrift
(Signature)

Abstract

Different mammalian species progress through similar stages during embryonic development and adult life but the pace of these transitions is species-specific. While classically, developmental timing was viewed merely as a consequence of varying body sizes between species, the use of pluripotent stem cells (PSCs) has shown that species-specific developmental timing is maintained during in vitro differentiation. Since then, uncovering cell-intrinsic mechanisms that regulate the timescales of development has become a rising topic of interest.

This project aimed to identify such cell-intrinsic mechanisms using in vitro neural progenitor differentiation of mouse, monkey and human PSCs. To facilitate inter-species comparisons, all cells were cultured and differentiated under harmonized conditions. Under these circumstances, mouse cells differentiated more than twice as fast as human cells, recapitulating species-specific differentiation timing. As differentiation and growth need to be tightly coordinated during development, I compared cell cycle durations across the species. Cell cycle durations followed a species-specific trend, with the human cell cycle being 1.47-fold and the monkey cell cycle 1.42-fold longer than the mouse cell cycle. To test if differentiation depends on proliferation, I performed cell cycle and growth manipulations by either a retinoblastoma knock-out line or inhibiting the mammalian target of rapamycin (mTOR). Strikingly, mTOR inhibition caused a drastic extension of cell cycle durations, yet single-cell transcriptomics revealed no systematic delay during early neural differentiation. This showed that differentiation can be uncoupled from growth and proliferation, suggesting alternative mechanisms. One candidate identified was the UDP-glucose pyrophosphorylase 2 (UGP2), required for glycogen synthesis. High UGP2 correlated with slow differentiation. Consequently, glycogen content was highest in human cells, intermediate in monkey and lowest in mouse. Thus, glycogen content is a species-specific cellular property that was unknown to this date. Neural differentiation of *UGP2* knock-out cells revealed premature expression of the forebrain marker FOXG1, indicating that UGP2 could contribute to setting differentiation timing. It remains to be tested, how loss of UGP2 globally affects differentiation and by which mechanisms UGP2 acts.

Taken together, these findings show that differentiation can be uncoupled from growth and cell cycling and implicate UGP2 and glycogen metabolism in the regulation of timing. This constitutes a novel mechanism by which cells could determine their differentiation speed.

Zusammenfassung

Verschiedene Säugetiere durchlaufen ähnliche Stadien während der Embryonalentwicklung und des adulten Lebens, allerdings passiert dies mit artspezifischer Geschwindigkeit. Während Entwicklungsgeschwindigkeit klassisch lediglich als Konsequenz variierender Körpergrößen zwischen Arten betrachtet wurde, zeigte der Einsatz pluripotenter Stammzellen (PSCs), dass Entwicklungsgeschwindigkeit während der in vitro-Differenzierung beibehalten wird. Seitdem ist die Entdeckung zellintrinsischer Mechanismen, die Entwicklungszeitabläufe regulieren, zu einem aufkommenden Interessensgebiet geworden.

Dieses Projekt beschäftigt sich mit der Identifizierung solcher zellintrinsischer Mechanismen. Dafür nutzte ich in vitro-Differenzierung neuraler Vorläuferzellen aus PSCs von Maus, Affe und Mensch. Um den Artvergleich zu erleichtern, wurden alle Zellen unter harmonisierten Bedingungen kultiviert und differenziert. Unter diesen Umständen differenzierten Mauszellen mehr als doppelt so schnell wie humane Zellen, was artspezifisches Timing widerspiegelte. Da Differenzierung und Wachstum während der Entwicklung eng koordiniert sein müssen, habe ich die Zellzyklusdauer zwischen den Spezies verglichen. Die Zellzyklusdauern folgten einem artspezifischen Trend; der humane Zellzyklus war 1,47-mal, der Affenzellzyklus 1,42-mal länger als der Mauszellzyklus. Um herauszufinden, ob Differenzierung von Proliferation abhängt, habe ich Zellzyklus und Wachstum durch eine Retinoblastom-Knockout-Linie oder durch Inhibition von mTOR (mammalian target of rapamycin) manipuliert. Auffällig war, dass mTOR-Inhibition eine drastische Verlängerung des Zellzyklus verursachte, jedoch zeigte Einzelzell-Transkriptomanalyse keine systematische Differenzierungsverzögerung. Das zeigte, dass Differenzierung von Wachstum und Proliferation entkoppelt werden kann und wies auf alternative Mechanismen hin. Ein identifizierter Kandidat war die UDP-Glukose-Pyrophosphorylase 2 (UGP2), notwendig für Glykogensynthese. Hohe UGP2-Expression korrelierte mit langsamer Differenzierung. Folglich war der Glykogengehalt humaner Zellen am höchsten, mittel beim Affen und am geringsten in Maus. Somit ist Glykogengehalt eine artspezifische Eigenschaft, die bisher unbekannt war. Neurale Differenzierung von *UGP2*-Knockout-Zellen zeigte vorzeitige Expression des Vorderhirnmarkers FOXG1, was darauf hinwies, dass UGP2 zur Regulierung von Differenzierungstiming beitragen könnte. Es muss weiterhin getestet werden, wie der Verlust von UGP2 Differenzierung global beeinflusst und durch welche Mechanismen UGP2 wirkt.

Zusammengefasst zeigen diese Ergebnisse, dass Differenzierung von Wachstum und Zellzyklus entkoppelt werden kann und dass UGP2 und Glykogensynthese zur Regulation von Timing beitragen könnten. Dies stellt einen neuartigen Mechanismus dar, durch den Zellen ihre Differenzierungsgeschwindigkeit bestimmen könnten.

Table of Contents

1 Introduction

1.1 Developmental timing is species-specific

During a lifespan, an organism typically progresses from a developmental stage over a mature period towards senescence. This sequence of events is universal across all mammalian species. However, the pace at which an organism transits through these phases is species-specific. This is also reflected at the level of maximum lifespans which are species-specific and can vary considerably. How the 'pace of life' arises and how it is regulated is a fundamental question of biology that has not been answered so far.

One of the most extreme examples for longevity is the Bowhead whale which can live for more than 200 years and takes over 22 years to reach maturity (Tacutu et al., 2018). The maximum lifespan of a human is approximately 120 years while the mouse has a much shorter maximum lifespan of four years (Figure 1A). Likewise, humans reach sexual maturity between thirteen and fourteen years and mice already at 42 days. The same trend applies to gestational time which is nine months for human and nineteen days for mouse (Tacutu et al., 2018).

Species-specific timing is also observed during embryonic development although embryos can be morphologically very similar between species (reviewed by Richardson, 1995). During embryonic development, a complex organism composed of various specialized cell types, tissues and organs arises from a single cell. The basic hallmarks of this developmental process are shared between all mammalian species but their timing differs drastically (Figure 1B). The mouse embryo at embryonic day 6.5 corresponds to the human embryo at two weeks (Otis & Brent, 1954) and only two days later, it closely resembles the human week 3 embryo (Copp, 2005; Sakai, 1989).

While little is known about how these differences emerge, it has been shown that developmental timing must be precisely regulated for normal development. For instance, in fruit flies, neuron differentiation is temporally coordinated; stem cells differentiate to specific neuronal subtypes along a precise temporal axis (reviewed by Toma et al., 2016). Species-specific timing may even be linked to the unique development of the human brain where protracted neurogenesis leads to a higher number of neurons and larger cortices (reviewed by Libé-Philippot & Vanderhaeghen, 2021).

Therefore, phenotypic differences between species arise not only as a consequence of different gene expression programs but also because of species-specific timing differences during development.

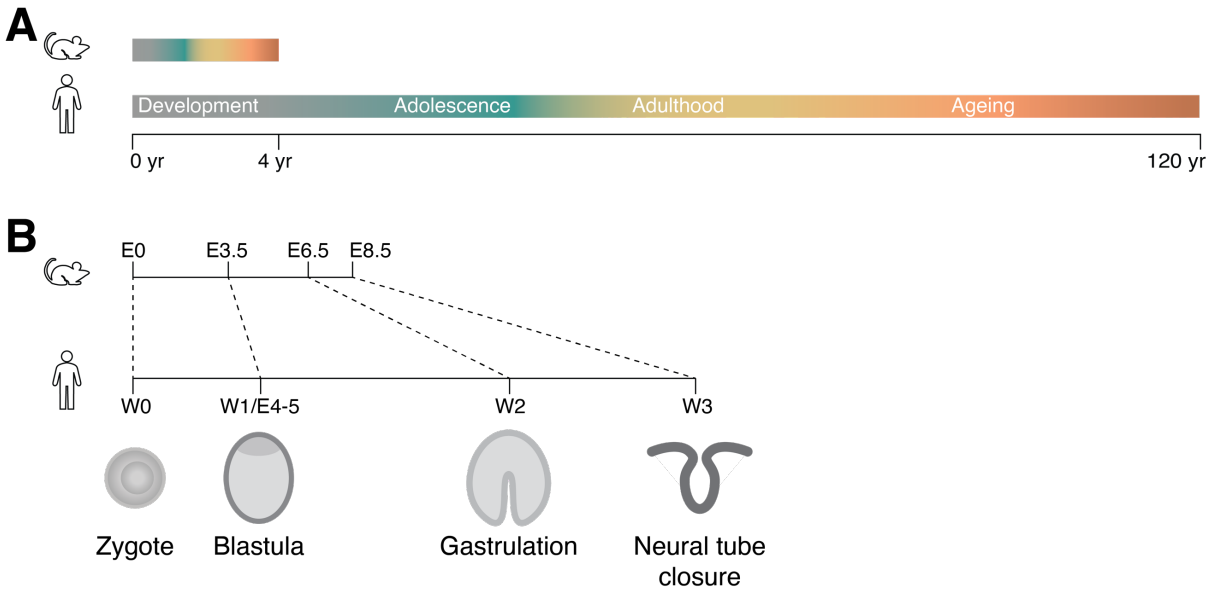

Figure 1: Schematic representation of species-specific developmental timescales.
A Lifespans of mouse and human are vastly different while both species undergo similar stages during their lives. Not drawn to scale. Based on Tacutu et al. (2018). **B** Mouse and human also develop along different timescales during embryogenesis. For mouse, the embryonic days of zygote, blastula, gastrulation and neural tube closure are indicated, for human either the embryonic day or week are indicated. Based on Cockburn & Rossant (2010); Copp (2005); Edwards et al. (1981); Otis & Brent (1954).

1.2 A classic view on developmental timing

Early studies on species-specific developmental timing view timing solely in the organismal context. Different animal species differ in various properties, one of which is timing, but another striking difference is body size. Mammalian body sizes span eight orders of magnitude, from the bumble-bee bat and the pygmy shrew at a body mass of 2 g to the blue whale at 180-200 tons (Smith & Lyons, 2011). In the early twentieth century, a link between a species' body size and lifespan was postulated (Rubner, 1908). Across most mammalian species, longevity is positively correlated with body size. Not only lifespan but several biological properties scale with body mass such as heart rate, gestation time and reproductive maturity (Lindstedt & Calder, 1981). This was explained by the observation that larger species tended to be metabolically less active than smaller species, suggesting that metabolic activity is limiting for developmental pace and adverse for longevity (Rubner, 1908). Later, this line of thinking became known as the *rate of living* theory, proposing that "the length of life […] inversely [depends] on the rate of living" (Pearl, 1928). Allometric scaling of body mass and metabolic rate was described more quantitatively in 1932 by Max Kleiber who found that metabolic rate scales with a ¾ exponent to the body mass (Kleiber's law, Kleiber, 1932). Following Kleiber's law, larger organisms have a lower mass-specific metabolic rate compared to smaller organisms. Three-quarter power-law scaling of metabolic rate and body mass has been explained by physical and geometric constraints of organisms. A mathematical model assuming that each cell of an organism has to be supplied with oxygen and nutrients by a fractal-like branched network such as the cardiovascular system with size-

invariant terminal units (e. g. capillaries) independent of species, can predict scaling of the cardiovascular system and metabolic rate (West et al., 1997). Thus, according to this, speed differences between species are just a consequence of body size and not actively regulated.

Biologically, metabolic rate and longevity have been linked by the *free radical theory of aging* (reviewed by Harman, 1992). High metabolic activity is thought to produce free radicals that damage mitochondria over time, possibly explaining the shorter lifespans in smaller organisms (reviewed by Harman, 1972). In support of this theory, inhibiting free radical reactions increased the mean lifespan in mice (Harman, 1968). However, the correlation between metabolic rate and longevity is subject to debate. As metabolic rates scale allometrically with body mass, the metabolic rates normalized for body mass did not correlate with longevity (de Magalhães et al., 2007). Collectively, past studies show a clear connection between body size and longevity but how the two are connected and which role metabolism plays remains elusive.

1.3 Species-specific developmental speed can be recapitulated in vitro

1.3.1 Timing during in vitro differentiation

Classically, the pace of life was mainly attributed to allometric scaling of body mass and metabolism. Timing was viewed solely in the organismal context and speed as an emergent property of body size. This line of thinking was disproved when mouse and human pluripotent stem cells were taken out their organismal context and maintained their species-specific time lines during in vitro differentiation (Barry et al., 2017), suggesting that timing is, at least in part, a cell-intrinsic property. In the 2017 study by Barry et al., mouse and human pluripotent stem cells (PSCs) were differentiated towards neuroectoderm under identical conditions and subjected to bulk RNA sequencing. They found that mouse PSCs activated neural markers earlier than human PSCs. Mouse day 3 of differentiation correlated best with human day 7 and similarly, mouse day 5 correlated best with human day 18 (Barry et al., 2017). Thus, in vitro differentiated PSCs recapitulate species-specific timescales of development (Figure 2). Co-culture of mouse and human PSCs during neural differentiation led to an upregulation of genes related to neuron maturation in human, suggesting that cell communication could contribute to setting differentiation speed. However, human cortical neurons xenotransplanted into the mouse cortex mature at a human-specific timeline rather than the host-specific time (Linaro et al., 2019). The same was observed when co-culturing human and macaque cortical progenitor cells which also differentiate along their species-specific timeline even if placed in an environment of faster or slower differentiating cells (Otani et al., 2016). These observations indicate that cells can regulate their differentiation speed autonomously.

Thus, the use of PSCs revealed the existence of cell-intrinsic mechanisms that contribute to timing. Moreover, this finding opens up new possibilities for studying timing, as PSCs can be used

to faithfully recapitulate species-specific differentiation timing in vitro in a controlled environment. PSCs can be obtained from different species and work on PSCs poses less legal and ethical challenges as opposed to embryo work, especially for human.

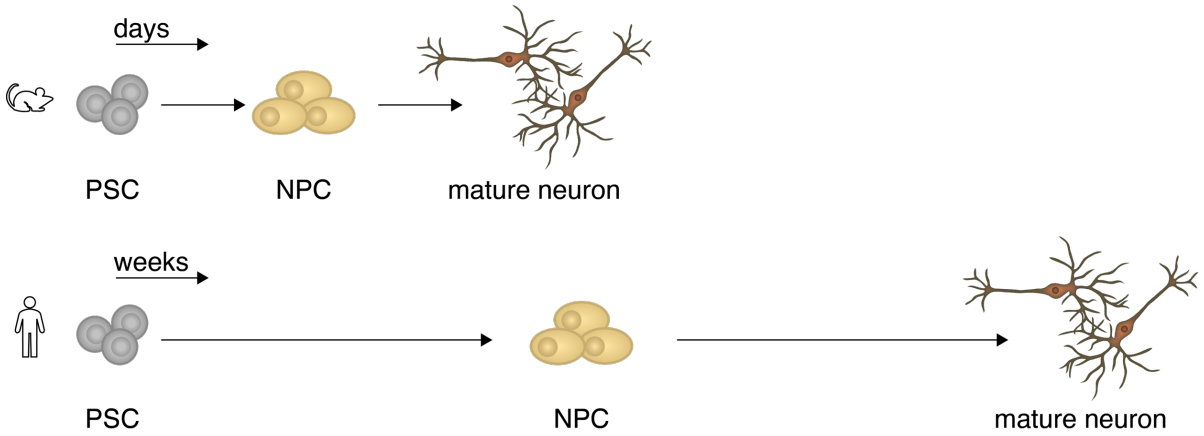

Figure 2: Species-specific differentiation is recapitulated during in vitro differentiation.
Human and mouse PSC differentiation to neural progenitor cells (NPC) and finally to mature neurons is shown. Differentiation in mouse cells occurs much faster than in human cells.

1.3.2 Pluripotent stem cells

Pluripotent stem cells represent a very early stage of development. Few days after fertilization, the embryo enters the blastocyst stage where an outer cell layer – the trophectoderm that later gives rise to the placenta – surrounds a cavity containing the inner cell mass (ICM). The ICM consists of pluripotent epiblast and hypoblast cells. Hypoblast (also called primitive endoderm) cells form the yolk sac and only the epiblast cells develop into the embryo-proper which will form the adult organism (reviewed by Rossant & Tam, 2022). Pluripotency is not a discrete state but rather a continuum. Before implantation into the uterus, the epiblast is in a naïve state. Post-implantation, the epiblast acquires a primed state which is thought to be required for later differentiation of the epiblast (reviewed by Nichols & Smith, 2009).

Pluripotent stem cells can also be cultivated in vitro. They are derived from the ICM and maintain their lineage potential in specific media conditions (Evans & Kaufman, 1981; Thomson, 1998). However, mouse and human embryonic stem cells (mESCs and hESCs) are distinct and rely on different signaling environments to maintain pluripotency. While hESCs need Activin/Nodal, mouse cells use LIF/STAT3 signaling (James et al., 2005; Niwa et al., 1998; Vallier et al., 2004). This reason for this discrepancy was resolved when mouse PSCs isolated from embryonic day 5.5 (E5.5) epiblast (~ 2 days later than mESCs) were, like hESCs, shown to be dependent on Activin/Nodal signaling to maintain their developmental potential (called EpiSCs, Brons et al., 2007; Tesar et al., 2007; Samanta & Kalantry, 2020). Thus, hESCs represent a later developmental stage than mESCs and resemble the primed mEpiSCs more closely.

Pluripotency can also be artificially induced (induced pluripotent stem cells, iPSCs). Overexpression of the core pluripotency factors OCT4, SOX2, c-MYC and KLF4 converts fibroblasts to pluripotent cells (Takahashi & Yamanaka, 2006). This finding drastically broadens the possibilities in research, allowing for personalized medicine or the derivation of PSCs from different animal species. When pluripotency-maintaining signals are removed, cells will differentiate (reviewed by Keller, 1995). Through directed differentiation, a broad variety of cell types including cardiomyocytes, neurons and intestinal tissues can be derived from PSCs in vitro (Kawasaki et al., 2000; Lee et al., 2000; Lian et al., 2012; Spence et al., 2010). Therefore, PSCs are a powerful tool for regenerative medicine and developmental biology.

1.4 Biological time

Biological time, as opposed to physical time, usually describes biochemical cycles that regulate the physiological state of an organism (reviewed by Lestienne, 1988). Consequently, biological time refers to cycles per unit time and is expressed in rates, like metabolic rate, protein turnover rate, or heart rate (reviewed by Günther & Morgado, 2004). These rates are typically not fixed and the same processes can transpire at different biological time scales. During embryonic development, growth rates and differentiation rates have to be coordinated in space and time. Growth and cell division require DNA and lipid synthesis as well as protein translation (reviewed by Tippetts et al., 2023). Furthermore, embryos undergo major epigenetic switches during development and rely on gene expression changes for cell fate acquisition (O'Neill, 2015). All of these processes can happen at different speeds and could be the bottleneck for an organism's developmental pace. Thus, biochemical, metabolic or cell division rates and epigenetic changes could determine species-specific developmental timescales. Therefore, these processes will be elucidated in the following.

1.5 Metabolism

1.5.1 The metabolism of pluripotent stem cells

Cells need a constant supply of energy in the form of ATP for survival and the production of biomass (e. g. during cell division). There are three major routes of ATP generation: glycolysis, the TCA/Krebs cycle and oxidative phosphorylation (OXPHOS) (reviewed by Rigoulet et al., 2020). During glycolysis, glucose is metabolized to pyruvate in the cytoplasm, yielding two ATP and two NADH per molecule glucose. Pyruvate is converted to Acetyl-CoA which feeds into the TCA/Krebs cycle in the mitochondrial matrix. The TCA/Krebs cycle produces two GTP, six NADH, two $FADH_2$ per molecule glucose (reviewed by Martínez-Reyes & Chandel, 2020). The reducing equivalents NADH and $FADH_2$ from the TCA/Krebs cycle then serve as electron donors for the

electron transport chain in the inner mitochondrial membrane. Here, electrons are transported through four protein complexes inside the mitochondrial membrane until they reach their final acceptor oxygen. Electron transfer through the membrane induces proton pumping into the intermembrane space, thereby generating an electrochemical gradient. This membrane potential fuels the ATP synthase which converts ADP to ATP (reviewed by Vercellino & Sazanov, 2021). One molecule of glucose yields 36 ATP during OXPHOS, making it the most efficient route of ATP production. Consequently, most somatic cells use OXPHOS for energy production (reviewed by Vander Heiden et al., 2009).

The metabolic landscape of pluripotent stem cells however is distinct from that of most somatic cell types (Figure 3). During the transition from naïve to primed pluripotency, stem cells undergo a metabolic switch from OXPHOS to glycolysis (Sperber et al., 2015; Zhou et al., 2012). This appears counterintuitive since stem cells are rapidly proliferating and consequently have a high energy demand. Proliferative cells are known to predominantly use glycolytic metabolism. For instance, tumor cells are characterized by aerobic glycolysis, also known as Warburg metabolism (Warburg, 1924). Originally, it was proposed that aerobic glycolysis is a consequence of a defective respiratory system (Warburg, 1956). Indeed, embryonic stem cells only have few mitochondria compared to somatic cells. These mitochondria are round and have immature cristae (Chung et al., 2007). However, rapidly proliferating cells have metabolic requirements that exceed the availability of ATP. Glycolysis, while less efficient in producing ATP, provides cells with reducing equivalents and carbon sources necessary for cell growth (reviewed by Vander Heiden et al., 2009). Glycolytic intermediates can be shunted away from glycolysis (1) via the pentose-phosphate pathway that produces pentose sugars required for nucleotide synthesis and NADPH and (2) via the serine synthesis pathway yielding amino acids, nucleotides and phospholipids (Labuschagne et al., 2014; reviewed by Mahmoud, 2023). In cancer cells, glycogen – the storage form of glucose, produced through a multi-step process involving UDP-glucose pyrophoshphorylase 2 (UGP2) – also feeds into glycolysis and the pentose-phosphate pathway, underlining the importance of glycolytic metabolism for highly proliferative cells (reviewed by Adeva-Andany et al., 2016; Favaro et al., 2012).

Metabolism and cell fate are tightly intertwined. As cells differentiate, they typically undergo a shift from Warburg-like metabolism to OXPHOS. It has been shown that upregulation of OXPHOS is crucial for cardiac differentiation (Chung et al., 2007). In agreement with that, reprogramming of somatic cells into induced pluripotent stem cells requires the upregulation of glycolytic metabolism; inhibition of glycolysis significantly reduces reprogramming efficiency (Folmes et al., 2011; Panopoulos et al., 2011). Interestingly, metabolic rewiring during differentiation is cell type-dependent. Upon neural progenitor differentiation, glycolytic rates increase and OXPHOS only takes over in terminally differentiated neurons (Birket et al., 2011). In either case,

metabolism and cell fate transition are closely intertwined such that metabolic intervention can alter cell fate.

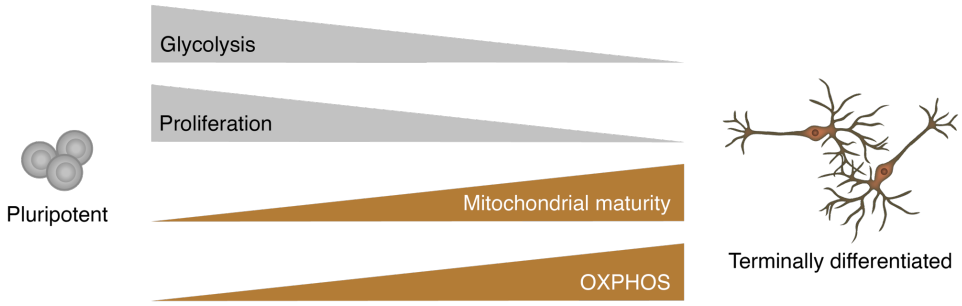

Figure 3: The metabolism of pluripotent and differentiated cells.
During differentiation, cells switch from a glycolytic, proliferative state to a resting state with mature mitochondria and OXPHOS metabolism.

1.5.2 mTOR signaling in development

The metabolic state of PSCs has evolved to meet the needs of a growing embryo with high proliferative capacity. A central metabolic hub that integrates various external signals to regulate cell growth is the mammalian target of rapamycin (mTOR) (Figure 4). mTOR is a kinase and mostly known as a positive regulator of translation (Brunn et al., 1997; Burnett et al., 1998; Gingras et al., 1999; Hara et al., 1997). It is the catalytic part of the mTOR complexes 1 and 2 (mTORC1/2). While mTORC2 stimulates cytoskeletal rearrangements and ion transport and counteracts apoptosis, mTORC1 positively regulates processes linked to translation and nucleotide synthesis and negatively regulates autophagy and lysosome biogenesis (reviewed by Liu & Sabatini, 2020). In general terms, mTOR promotes anabolic processes and inhibits catabolic processes. The effect of mTORC1 is mainly mediated through phosphorylation of the S6 protein kinase (S6K) and 4E-BP1. Unphosphorylated, 4E-BP1 sequesters eukaryotic translation initiation factor 4E (eIF4E) (Brunn et al., 1997; Chung et al., 1992). S6K is mainly involved in ribosome biogenesis through phosphorylation of several components of the ribosomal DNA transcription machinery, like UBF, TIF-1A and MAF1 (Hannan et al., 2003; Mayer et al., 2004; Michels et al., 2010). It is also linked to nucleotide synthesis by promoting purine and pyrimidine production (Ben-Sahra et al., 2013, 2016; Robitaille et al., 2013). Through S6K and 4E-BP1, mTOR furthermore promotes transition through the cell cycle. Upon mTORC1 inhibition by rapamycin, cells arrest in G1 phase (Fingar et al., 2004).

mTORC1 is regulated by the tuberous sclerosis complex 1/2 (TSC1-TSC2). TSC2 is a GTPase-activating protein (GAP) that activates RHEB which acts upstream of mTOR and inhibits it by phosphorylation (Inoki et al., 2003a). TSC2 itself is regulated by growth-promoting signals like AKT. Upon insulin stimulation, AKT phosphorylates TSC2, thereby destabilizing TSC1-TSC2 interaction (Inoki et al., 2002). mTOR is also coupled to cellular energy levels through AMP-

activated protein kinase (AMPK). AMPK is a sensor of a cell's AMP/ATP ratio and inhibits mTORC1 by phosphorylating TSC2 and RAPTOR, a component of mTORC1, to restrict anabolic processes under energy deprivation (Gowans & Hardie, 2014; Gwinn et al., 2008; Inoki et al., 2003b; Kim et al., 2002). Therefore, mTOR signaling links environmental signals to proliferation and tight regulation of mTOR is necessary for physiological growth.

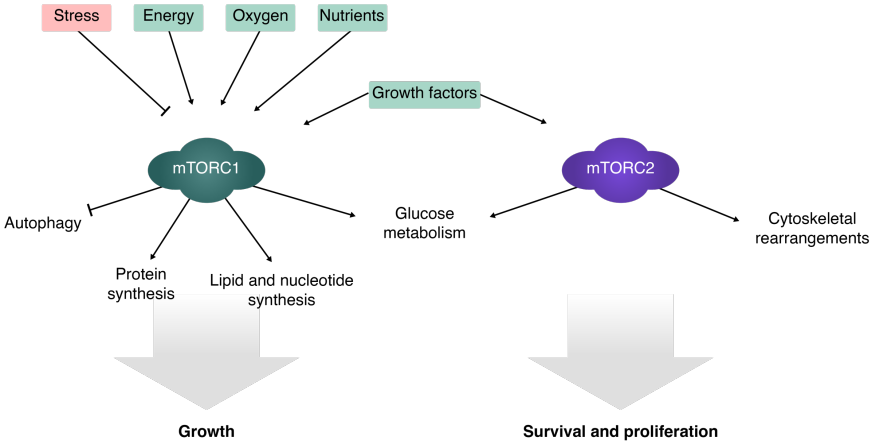

Figure 4: Effect and regulation of mTOR signaling.
Physiological stimulants and repressors of mTOR are shown in the top. The main processes regulated by mTORC1 and mTORC2 are indicated. They converge in the promotion of growth and survival/proliferation. Adapted from Liu & Sabatini (2020).

What happens to an organism, if mTOR is artificially depleted? When mouse blastocysts are subjected to pharmacological mTOR inhibition by the ATP-site inhibitor INK128 (Hsieh et al., 2012), they undergo a developmental arrest that is reminiscent of a natural diapause (Bulut-Karslioglu et al., 2016). During this state, cells do not proliferate and have reduced transcriptional activity while remaining pluripotent and able to re-enter normal development after inhibitor removal. The same was shown for mouse embryonic stem cells (Bulut-Karslioglu et al., 2016). Furthermore, evidence from multiple studies in different species, including mouse, suggests that a reduction in mTOR signaling slows down the ageing process and increases lifespan (Kaeberlein et al., 2005; Kapahi et al., 2004; Vellai et al., 2003; Wu et al., 2013). A similar phenomenon is observed upon caloric restriction (reviewed by Weindruch, 1996). Intriguingly, dietary restriction limited to methionine was sufficient to increase lifespan, indicating that negative regulation of translation promotes longevity (Grandison et al., 2009). In agreement with this, mTORC1 is constitutively active in senescent cells (Carroll et al., 2017).
Taken together, mTOR is a crucial regulator of translation, growth and cell cycling and inhibition of mTOR signaling pauses cells early in development and extends lifespans in adult organisms.

1.6 The cell cycle

1.6.1 Cell cycle regulation in somatic cells

During embryonic development, differentiation and growth happen in parallel and it is crucial that the two processes are coordinated with each other. In order for the embryo to grow, cells must undergo cell divisions to proliferate. The cell cycle is defined as the series of events taking place between two cell divisions. These events are broadly subdivided into phases of cell growth, DNA synthesis and division (Howard & Pelc, 1951), that were later termed gap phase 1 (G1), synthesis phase (S), gap phase 2 (G2) and mitosis (M). At the beginning of each cell cycle, cells are in G1 phase and mainly grow until they enter S phase where a second copy of DNA is synthesized. In G2 phase, cells continue to grow and synthesize proteins for cell division. Finally, M phase marks the nuclear division, followed by cytokinesis, producing two daughter cells with the same genetic information (Cooper, 2000).

Cell cycling is a highly complex and tightly regulated process. It is linked to cellular metabolism through mTOR and its effectors S6K1 and 4E-BP1 which are involved in regulating cell cycle phase transitions (Brown et al., 1994; Fingar et al., 2004). Deregulation of the cell cycle can cause uncontrolled cell proliferation and malignant growth (Hanahan & Weinberg, 2000). Progression through the cell cycle is largely mediated by cyclin-dependent kinases (CDKs). These serine/threonine kinases were first found in yeast (Hartwell, 1967, 1973; Hartwell et al., 1973) and form complexes with cyclins whose concentrations vary with the cell cycle (Evans et al., 1983; reviewed by Malumbres & Barbacid, 2005), making CDK activity cell cycle-dependent. There are over 20 different CDKs and 30 genes likely encoding cyclins described in mammals (reviewed by Chotiner et al., 2019; reviewed by Martínez-Alonso & Malumbres, 2020). CDKs have different roles during the cell cycle and associate with different cyclins. For instance, mitotic entry is regulated by CDK1-cyclin B as part of the M phase promoting factor (Dunphy et al., 1988; Gautier et al., 1988, 1990; Lohka et al., 1988). In contrast, S phase requires CDK2 to activate DNA synthesis (Pagano et al., 1993). CDK2 associates with cyclin A and cyclin E during G1 phase and its activity oscillates during the cell cycle (Lees et al., 1992; Rosenblatt et al., 1992; Tsai et al., 1991).

However, before cells enter S phase, they must pass the G1/S checkpoint. The G1/S checkpoint is a crucial component of the cell cycle. It is also referred to as the restriction (R) point because it decides whether a cell commits to the cell cycle or enters quiescence (Pardee, 1974). A central regulator during this restriction point is the retinoblastoma (RB) protein and its relatives p107 and p130, collectively referred to as the pocket protein family (reviewed by Henley & Dick, 2012; reviewed by Weinberg, 1995). RB restricts G1/S transition and is therefore a negative regulator of proliferation (Goodrich et al., 1991). The anti-proliferative effect of RB is mediated through sequestration of transcription factor E2F (Flemington et al., 1993; Helin et al., 1992, 1993). E2F is responsible for the expression of several S phase-related proteins like DHFR, N-MYC, c-MYC, c-

MYB, cyclin A, cyclin E (Hiebert et al., 1991; Mudryj et al., 1990; Ohtani et al., 1995; Schulze et al., 1995). RB activity is modulated through phosphorylation in a cell-cycle-dependent manner (Buchkovich et al., 1989; Chen et al., 1989; DeCaprio et al., 1989). CDK4/6-cyclin D complexes monophosphorylate RB in early G1 phase, allowing for E2F sequestration (Ezhevsky et al., 1997; Narasimha et al., 2014). In late G1, however, RB is hyperphosphorylated by CDK2-cyclin E complexes and thereby inactivated, resulting in the release of E2F and initiation of S phase (Ezhevsky et al., 2001).

1.6.2 Cell cycle in pluripotency and differentiation

During embryonic development, a single cell proliferates and differentiates to form a complex organism. Therefore, the cell cycle is an integral part of development. The embryonic cell cycle is drastically different to that of most somatic cells (Figure 5) and characterized by unusually short doubling times of as little as 6.5 hours in the mouse epiblast (Snow, 1977). Stem cells typically do not have fully-developed gap phases, especially G1, and spent most time in S phase (Becker et al., 2006; Mac Auley et al., 1993; Stead et al., 2002). Rapid cycling is necessary for the maintenance of pluripotency in human ESCs. Acceleration of doubling time increases reprogramming efficiency while cell cycle arrest abrogates reprogramming (Ruiz et al., 2011).

In mouse, progression through the cell cycle is less regulated in stem cells than in somatic cells. Mouse ESCs do not express CDK4-cyclin D up until gastrulation and subsequent differentiation (Savatier et al., 1995). At the same time, CDK2 and cyclin A/E are active throughout the entire cell cycle without any phase-dependent periodicity (Stead et al., 2002). Inhibition of CDK2 decreased cell cycle speed but did not alter the embryonic cell cycle structure, suggesting that the short G1 phase is caused by alternative mechanisms (Stead et al., 2002). Savatier et al. (1994) observed a lack of hypophosphorylated RB in mouse ESCs. E2F, that is usually sequestered by RB to prevent unrestricted passage into S phase, was mostly present in its free form (Stead et al., 2002). Thus, RB is hyperphosphorylated and therefore inactive and unable to bind E2F throughout the embryonic cell cycle, explaining the short dwell time in G1 phase. Another mechanism by which RB has been reported to counteract cell cycle progression is by direct inhibition of ribosomal DNA transcription factor UBF and therefore rRNA synthesis (Cavanaugh et al., 1995; Voit et al., 1997). Like mouse ESCs, primate ESCs have a shortened G1 phase, constitutively expressed cyclin E and hyperphosphorylated RB (Fluckiger et al., 2006). In contrast to murine ESCs, however, human ESCs have been reported to possess cell cycle-dependent expression of many CDKs and cyclins (Neganova et al., 2009). They also express CDK4-cyclin D2, a G1-related CDK-cyclin complex which could additionally promote G1/S progression (Becker et al., 2006). Because of a general lack of G1 control, both murine and primate ESCs do not arrest in G1 upon DNA damage and undergo apoptosis (Aladjem et al., 1998; Hong & Stambrook, 2004). Intriguingly, mouse ESCs

cultured under naïve conditions have been shown to possess a functional G1 checkpoint and hypophosphorylated RB (ter Huurne et al., 2017). Thus, cell cycle regulation is distinct in different pluripotency states.

Differentiation is accompanied by G1 lengthening (Calder et al., 2013). If one is causal for the other, is unknown. Concomitant differentiation and G1 lengthening suggests that both processes happen in parallel but there is also evidence showing that G1 arrest through CDK2 knockdown is promotes ESC differentiation to extraembryonic lineages (Neganova et al., 2009). Cells are generally more likely to differentiate during G1 phase, i. e. cellular responsiveness to differentiation cues is increased during G1 (Pauklin & Vallier, 2013; Sela et al., 2012). It has even been shown that cells activate distinct differentiation programs depending on differentiation induction timing during G1 phase; cells in early G1 only initiated endo- and mesoderm differentiation whereas cells in late G1 only initiated neuroectoderm differentiation. During G2, S and M phase, cells barely differentiated at all (Pauklin & Vallier, 2013). Terminal differentiation is marked by permanent exit from the cell cycle through downregulation of G1 cyclins, CDK inhibitor expression and epigenetic silencing of cell cycle genes (reviewed by Padgett & Santos, 2020).

Taken together, the cell cycle is a crucial part of growth and development. Not only is it indispensable for cell proliferation but it is also tightly linked to pluripotency and cell fate acquisition in the context of development.

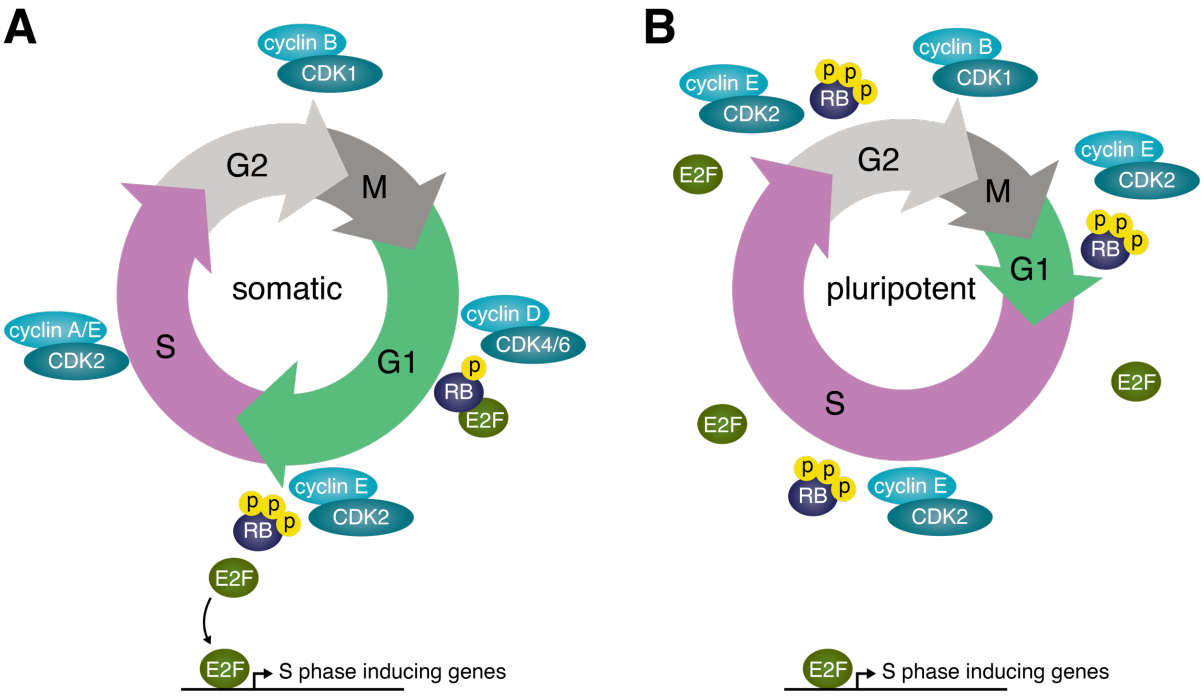

Figure 5: The cell cycle structure.
The cell cycle structure and the most important regulatory components are shown for **A** somatic cells and **B** mouse pluripotent stem cells. CDK/cyclin complexes are cell cycle phase-dependent in somatic cells while pluripotent cells

have CDK/cyclin activity throughout the cell cycle. The RB phosphorylation state is indicated as either monophosphorylated or hyperphosphorylated.

1.7 Epigenetics during development

Another crucial aspect of embryonic development is epigenetic regulation of gene expression. Epigenetics work through altering chromatin accessibility. Chromatin can either exist in a closed conformation as heterochromatin or in an open configuration as euchromatin (reviewed by Allis & Jenuwein, 2016). While heterochromatin cannot be accessed by transcription factors, euchromatin allows for transcription factor binding and therefore gene expression. Epigenetics can influence gene expression by DNA methylation or histone modifications. DNA methylation occurs at the 5'-carbon of cytosine, preferentially at CpG dinucleotides, referred to as CpG islands. It is generally associated with gene expression silencing (reviewed by O'Neill, 2015). As DNA is organized in nucleosomes, each constituting a histone octamer comprised of histones H2A, H2B, H3 and H4, histone modifications also influence chromatin structure and gene expression (reviewed by McGhee & Felsenfeld, 1980). Histone modifications are very diverse. A combination of histone phosphorylation, acetylation and methylation is used to determine the activity state of a genomic region. All of these modifications appear in active and inactive chromatin regions (reviewed by Jenuwein & Allis, 2001).

Epigenetic regulation of gene expression is also implicated in embryonic development. The early embryo is marked by global hypomethylation (reviewed by O'Neill, 2015). When stem cells exit naïve pluripotency and transition to a primed pluripotent state, DNA methylation increases, probably preparing cells for transcriptional restriction and lineage differentiation (reviewed by Gökbuget & Blelloch, 2019). Forced hypomethylation in embryonic stem cells through DNA methyltransferase knock-out has been shown to block lineage differentiation (Jackson et al., 2004). Furthermore, PSCs often exhibit genomic regions associated with active and repressive histone modifications at the same time. This bivalent histone state is believed to put genes in a poised state where they can be readily activated upon differentiation (reviewed by O'Neill, 2015). Thus, epigenetics represent another layer of gene regulation and are essential for correct embryonic development.

1.8 Theories for cell-intrinsic regulation of timing

With the use of PSCs, species-specific developmental timing became a rising topic of interest in the past years. Several studies investigate cell-intrinsic properties that could be involved in setting the pace of life, typically through comparison of mouse and human PSCs during in vitro differentiation. To this date, there is no definite answer to the question of developmental timing. It is also unknown whether timing mechanisms act globally or if they depend on the cell type and

differentiation direction. However, there are many theories and observations that link developmental timing to the speed of biochemical reactions, species-specific metabolic rates or epigenetics. Key findings from recent studies will be summarized in the following.

1.8.1 Species-specific speed of biochemical reactions

Developmental timing has been investigated using different differentiation paradigms. A key publication on species-specific timing uses motor neuron differentiation of mouse and human ESCs as a model system. Here, neural differentiation is induced, followed by specific differentiation to postmitotic motor neurons (Rayon et al., 2020). During differentiation towards a motor neuron fate, mouse cells differentiated 2.5-fold faster than human cells (Rayon et al., 2020). Interestingly, neither species-dependent differences in growth-factor responsiveness, nucleotide sequence differences in differentiation genes between mouse and human, nor different mRNA half-lives were responsible for the observed time shift (Rayon et al., 2020). However, protein half-lives perfectly correlated with differentiation speed and were therefore 2-2.5 times longer in human than in mouse, suggesting that higher protein turnover during differentiation makes mouse cells differentiate faster than human cells. In line with this, Matsuda et al. (2020) confirmed that protein half-lives are longer in human using the segmentation clock as a model. The segmentation clock refers to the process of somite formation from the presomitic mesoderm which occurs with a species-specific periodicity. Somite formation can be recapitulated in vitro and the periodic somite formation can be observed via HES7 oscillations (reviewed by Hubaud & Pourquié, 2014). Using this system, they also found that multiple biochemical reactions are slower in human than in mouse. These include transcription, translation and mRNA splicing (intron delay). Mathematical modeling indicated that a delay in these reactions can explain the slower differentiation in human (Matsuda et al., 2020). Indeed, when the number of introns in the HES7 gene was reduced, the segmentation clock was slightly accelerated (Harima et al., 2013). In support of these findings, a collection of stem cells derived from six different species, including mouse and human, showed differential expression of genes linked to biochemical reactions during presomitic mesoderm differentiation. Furthermore, the same study also implicated protein half-lives and intron delays in setting the segmentation clock period (Lázaro et al., 2023).

1.8.2 Metabolic rate scaling

The reason for species-specific biochemical reaction speeds could be different metabolic rates which in turn are dependent on the mitochondrial architecture. Human mitochondria mature much slower and are less active during neuronal differentiation than mouse mitochondria. Increasing mitochondrial activity in human sped up neuron maturation (Iwata et al., 2023). High

mitochondrial activity has also been linked to faster pancreatic and cardiac differentiation of human cells (Hu et al., 2018; Yang et al., 2019; Yoshihara et al., 2016).

During presomitic mesoderm differentiation, mouse cells have a 2-fold higher mass-specific metabolic rate than human cells in regards to oxygen consumption (OXPHOS) and extracellular acidification rate (glycolysis) (Diaz-Cuadros et al., 2023). Decreasing cellular metabolic rates by partially inhibiting the electron transport chain slowed down the segmentation clock, however, ATP was not responsible for this effect (Diaz-Cuadros et al., 2023). Instead, the NAD+/NADH ratio appeared to be different in mouse and human and decreased NAD+/NADH through pharmacological inhibition extended the segmentation clock period. This effect could be mediated by protein synthesis, as inhibition of the electron transport chain reduced translation. The mass-specific translation rate of mouse was almost 2-fold higher than in human and decreasing translation via cycloheximide treatment prolonged the segmentation period (Diaz-Cuadros et al., 2023). Like Rayon et al. (2020), Diaz-Cuadros et al. (2023) observed a 2-fold difference in protein half-lives between mouse and human that was likely mediated by higher mass-specific proteasome activity in mouse. However, proteasome inhibition only arrested the segmentation clock without prolonging the oscillation period.

In line with the findings of Diaz-Cuadros et al. (2023), comparison between multiple species showed that ATP levels do not follow a species-specific trend. However, the multi-species comparison also indicated that, while mouse has a lower metabolic rate than human, metabolic rates do not generally correlate with body mass or developmental speed (Lázaro et al., 2023). In contrast, comparison of mouse and naked mole rat cells – two rodents that are evolutionary close but differ vastly in lifespans (Buffenstein & Jarvis, 2002) – indicated that the long-lived naked mole rat has lower ATP levels than the mouse. Although this study was performed in fibroblasts, not PSCs, it indicates that ATP turnover might contribute to the regulation of timing (Swovick et al., 2021). As demonstrated by these results, metabolism influences developmental timing although it is still under debate which mechanisms are at play.

1.8.3 Epigenetic regulation of timing

Another line of evidence suggested that the slower-differentiating human cells have a higher epigenetic barrier for neuronal differentiation. Transient inhibition of repressive chromatin modifiers like polycomb repressive complex 2 (PRC2) component EZH2 at the progenitor level resulted in faster neuronal maturation (Ciceri et al., 2024). Furthermore, an exploratory compound screen identified four molecules that enhanced maturation of cortical neurons when combined. This molecule cocktail consisted of the epigenetic modifiers GSK-2879552 (inhibitor of lysine-specific demethylase 1), and EPZ-5676 (inhibitor of the methyltransferase disruptor of telomerase-like 1), as well as NMDA (glutamate receptor agonist) and Bay K 8644 (L-type Ca^{2+}

channel agonist) and was termed GENtoniK (Hergenreder et al., 2024). While the glutamate receptor and L-type Ca^{2+} channel agonist could directly affect neuronal firing, withdrawal of GENtoniK seven days prior to electrophysiological measurements still resulted in matured neurons. The treatment has also been shown to accelerate neural crest and pancreatic differentiation (Hergenreder et al., 2024).

1.8.4 Cell proliferation

Both in presomitic mesoderm cells and during motor neuron differentiation, the human cell cycle took double the time of the mouse cell cycle (Diaz-Cuadros et al., 2023; Rayon et al., 2020). This raises the possibility that cell cycling and differentiation are dependent processes. While arresting the cell cycle did not alter the segmentation clock period in human (Diaz-Cuadros et al., 2023), it has been shown that it can slow down differentiation in zebrafish in a cell type-specific manner (Kukreja et al., 2023). It was furthermore reported that the cell cycle phase of presomitic mesoderm cells influences the segmentation clock period (Carrieri et al., 2019). Moreover, the timing of oligodendrocyte differentiation was explained by the cell-division-counting hypothesis, proposing that progenitor cells count the number of cell divisions before differentiating (Temple & Raff, 1986). However, this hypothesis could not explain why slower-dividing progenitor cells cultured at lower temperatures differentiated sooner than under normal conditions (Gao et al., 1997). Taken together, there is conflicting evidence about the connection between cell division and differentiation. Whether the two processes are coupled is still unclear and has yet to be clearly determined.

1.9 Neural differentiation

As evident from the previous paragraph, species-specific timing has mostly been studied during motor neuron or presomitic mesoderm differentiation (Diaz-Cuadros et al., 2023; Lázaro et al., 2023; Rayon et al., 2020). Here, I will discuss neural progenitor differentiation as a suitable model system to investigate species-specific differentiation timing, as it offers advantages over other systems due to its easier adaptability to different cell lines and species.

Neural differentiation begins at E8.0 in the mouse embryo (reviewed by Kojima et al., 2014) and after approximately two weeks in human (reviewed by Stiles & Jernigan, 2010). Early neural differentiation is marked by the onset of PAX6 and SOX1 expression. PAX6 is a member of the paired-box transcription factor family and found in the developing brain, specifically in the forebrain, the eye and the olfactory bulb (Walther & Gruss, 1991). It is expressed in the neural plate of E18 embryos in human and first detected at E8.5 in the neural tube of mouse embryos (Walther & Gruss, 1991; Zhang et al., 2010). SOX1 is a transcription factor belonging to the B1 subgroup of the Sox family (Uchikawa et al., 1999) that is expressed in neural progenitor cells

where it represses neuronal differentiation to maintain an early neural fate (Bylund et al., 2003). In mouse, SOX1 expression starts from E7.5 on, in human it is expressed around E26 (Pevny et al., 1998; Zhang et al., 2010).

Neural differentiation occurs in the absence of growth factor signaling. This conclusion is based on three observations in *Xenopus laevis*. (1) Disaggregated ectoderm cells differentiated into neural cells while reaggregated cells differentiated to epidermis (Grunz & Tacke, 1989), suggesting that neural differentiation is a cell-autonomous process and does not require cell-cell communication. (2) Inhibition of an Activin receptor promoted neuralization and (3) BMP4 suppressed neuralization (Hemmati-Brivanlou & Melton, 1994; Wilson & Hemmati-Brivanlou, 1995). These findings led to the 'neural default' model, postulating that stem cells will acquire a neural fate when growth factor signaling, specifically Activin and BMP4, are inhibited (reviewed by Muñoz-Sanjuán & Brivanlou, 2002). In support of this idea, differentiation of mouse embryoid bodies (EBs) in chemically defined medium without growth factor addition resulted in an upregulation of neural markers (Wiles & Johansson, 1999). In a 2003 publication, it was shown that neural differentiation can be performed in vitro in mouse adherent cell culture in medium lacking growth factors (Ying et al., 2003). Contrasting the 'neural default' model, they showed a requirement of endogenous FGF4 for neural conversion. The first neural differentiation protocol for adherent human embryonic stem cells was developed by Chambers et al. (2009). Here, neural stem cells were derived from hESCs by differentiation in a medium containing Noggin, an inhibitor of SMAD1/5/8-mediated BMP4 signaling and SB-431542, an inhibitor of SMAD2/3-mediated Activin signaling. This strategy is referred to as dual SMAD inhibition and has proven as a useful base for differentiating various ectodermal lineages from multiple different hESC lines (Tchieu et al., 2017).

Over the past years, neural differentiation via dual SMAD inhibition has been well-established. As external addition of growth factors is not required, dual SMAD inhibition can be particularly useful when studying and comparing differentiation in cells of different species where timing of growth factor addition and sensitivity to growth factors could be species-specific. Moreover, the fact that neural differentiation does not heavily rely on cell-cell communication can facilitate the identification of cell-intrinsic mechanisms that regulate differentiation timing.

1.10 A PSC panel of three species

Most studies on species-specific differentiation timing are based on the comparison of mouse and human cells. These two species have the advantage of being well-studied and established for laboratorial research. However, rodents and humans have very different developmental timescales and the use of a third species with an intermediate timescale could bridge the gap between the two. Furthermore, trends observed in three species independently are more robust

than trends between only two. The importance of using multiple comparisons has been demonstrated by Lázaro et al. (2023) who observed that metabolic rate scaling between mouse and human was not a general trend that holds true in a multi-species comparison. Therefore, I aimed to use stem cells of not only mouse and human, but also the cynomolgus monkey (or Crab-eating macaque, *Macaca fascicularis*). With an average body weight of 6 kg, cynomolgus lies in between mouse (20 grams) and human (58-81 kg) (reviewed by Phifer-Rixey & Nachman, 2015; Tacutu et al., 2018; Walpole et al., 2012). Cynomolgus has a maximum lifespan of 39 years and a gestation time of approximately 165 days (Jewett & Dukelow, 1972; Tacutu et al., 2018). It reaches reproductive maturity at three to four years (Tacutu et al., 2018). Therefore, it represents a species with intermediate body size and timing compared to mouse and human, making it a suitable model organism for inter-species comparisons of developmental timing.

1.11 Objectives

In this project, I aimed to identify cell-intrinsic mechanism that contribute to the regulation of species-specific differentiation speed by manipulating candidate mechanisms and characterizing differentiation outcome in a panel of different stem cells. More specifically, I pursued the following objectives:

(1) First, cell culture of mouse, cynomolgus and human pluripotent stem cells needed to be established. For all species, I aimed to use harmonized culture conditions in pluripotency and during neural progenitor cell differentiation. This way, I minimized the influence of external biases on differentiation outcome. To assess if the in vitro differentiation protocol recapitulated species-specific differentiation timing, differentiation onset was monitored comparatively in all species via immunofluorescence and via single cell transcriptomics. Part of this work was performed by or in collaboration with Alexandra de la Porte (Drukker group, Helmholtz Munich) and Moritz Thomas (Marr group, Helmholtz Munich).

(2) Next, I sought to compare the cell cycle as a candidate mechanism for the regulation of differentiation timing in mouse, cynomolgus and human cells. I characterized the total cell cycle duration and the duration of individual cell cycle phases using a FUCCI sensor which allows for precise delineation of cell cycle phases at single-cell resolution.

(3) To test if changes in the cell cycle influence differentiation speed and outcome, I used a mouse cell line harboring a knock-out of all members of the pocket protein family which should abrogate G1/S transition control and therefore alter the cell cycle structure. I

characterized the cell cycle phenotype in pluripotency and differentiation and examined neural differentiation in the knock-out line via immunofluorescence and single-cell transcriptomics.

(4) In a next step, I manipulated cellular metabolism by inhibition of mTOR signaling. I assessed the effect of mTOR inhibition by characterizing the cell cycle in untreated and treated cells in pluripotency and differentiation. Differentiation outcome was monitored by immunofluorescence, single-cell transcriptomics and neural reporter time-lapse imaging.

(5) In an orthogonal approach, a single-cell RNA sequencing time course of neural differentiation in mouse, cynomolgus and human cells performed by my collaborators Alexandra de la Porte (Drukker group, Helmholtz Munich) and Moritz Thomas (Marr group, Helmholtz Munich) was used to identify candidate mechanisms for the regulation of differentiation timing. We identified UGP2, responsible for glycogen synthesis, as a potential candidate. Therefore, I measured glycogen content in the species panel and performed a neural differentiation time course of human UGP2 knock-out cell lines and analyzed differentiation outcome via immunofluorescence.

2 Results

2.1 Mouse, monkey and human stem cells are cultured under identical conditions

As most studies focusing on species-specific developmental timing exclusively compare mouse and human cells, I sought to expand the species panel by using stem cells of mouse (*Mus musculus*), human (*Homo sapiens*) and the cynomolgus monkey (*Macaca fascicularis*). To faithfully compare differentiation speed between the species, the starting conditions for all cell lines should be as similar as possible. Depending on the cell line used, the pluripotency state can be either naïve or primed. Mouse embryonic stem cells (mESCs) are usually in a naïve state whereas primate embryonic stem cells are primed and therefore developmentally further advanced than mESCs. I aimed to minimize this discrepancy by using mouse epiblast stem cells instead of mESCs, as they are in a primed state and more equivalent to primate stem cells. In the end, the species panel should consist of mouse epiblast stem cells (mEpiSCs), cynomolgus induced pluripotent stem cells (cyiPSCs) and human embryonic stem cells (hESCs).

Primed pluripotency is maintained through TGFβ/FGF2-based media (James et al., 2005; Vallier et al., 2004), however, cell culture media are usually used species-specifically and can vary substantially. This could introduce artifacts when comparing species-specific differentiation speeds as a result of varying growth factor and nutrient concentrations in the different media. Furthermore, different cell lines are grown on different surface matrices and handled differently during passaging. To circumvent this issue, I aimed to harmonize the cell culture conditions and use the same medium, surface matrix and passaging reagents for all species. First, I adapted mouse, cynomolgus and human cells to Matrigel coating and EDTA passaging. This allows cells to remain in multicellular clusters which facilitates cell survival and is especially important for primate cells. Establishing a common culture medium proved more challenging as the media composition strongly influenced cell survival. A published pluripotency medium for primate cells (Universal Primate Pluripotency Stem Cell, UPPS medium) is based on the commercial StemMACS iPS Brew XF, originally intended for the use on human PSCs, but supplemented with 1 µM WNT antagonist IWR-1 and 0.5 µM WNT agonist Chiron (Stauske et al., 2020). Cells were gradually adapted to UPPS and grown in 100% UPPS for at least two passages before rigorous testing by my collaborator Alexandra de la Porte (Drukker group, Helmholtz Munich). I adopted UPPS culture for mouse, cynomolgus and human cells and was able to keep cells alive and in a proliferative state (Figure 6A). They had typical PSC morphology with dense colonies (Figure 6B). An immunostaining of mouse, cynomolgus and human PSCs grown in UPPS for the core pluripotency marker OCT4 shows that cells remain pluripotent in UPPS (Figure 6C). Cynomolgus

and human cells expressed OCT4 very homogeneously while OCT4 staining in mouse was more heterogeneous. However, I did not observe a notable decrease in pluripotency with increasing passage number. All following experiments, unless specified otherwise, were performed using UPPS-adapted cells on Matrigel-coating routine-passaged using EDTA.

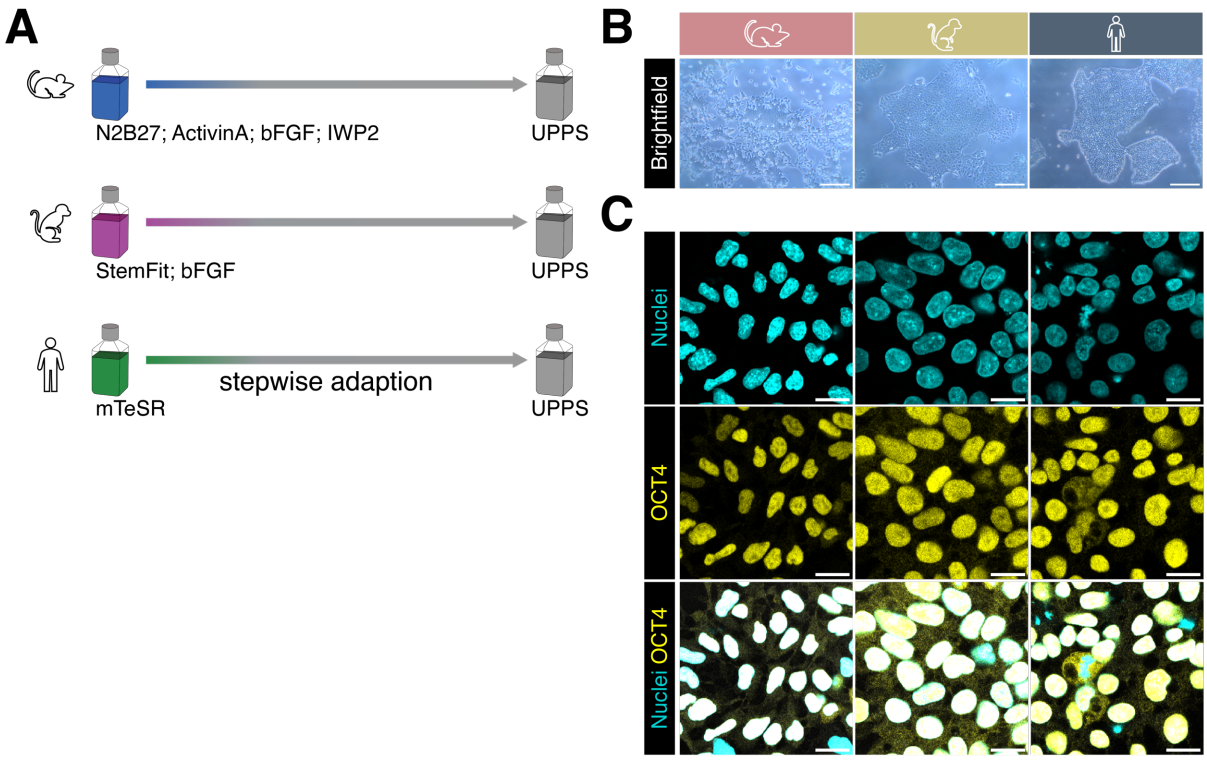

Figure 6: A multi-species panel of PSCs can be cultivated under identical conditions.
A Mouse EpiSCs, cynomolgus iPSCs and human ESCs in the indicated original media are adapted to a common pluripotency medium (UPPS). **B** Brightfield images of mouse, cynomolgus and human cells grown in UPPS. Scale bars = 200 µm. **C** Immunostaining of mouse, cynomolgus and human cells grown in UPPS for pluripotency marker OCT4, indicating that the majority of cells maintains pluripotency in UPPS. Nuclear signal (Hoechst33342) is shown as a control. An overlay of nuclei and OCT4 staining shows colocalization of both signals. Scale bars = 20 µm.

2.2 Species-specific differentiation timing is recapitulated during in vitro neural progenitor differentiation

Having established standardized culture conditions for mouse, cynomolgus and human PSCs, I next sought to compare differentiation speeds between the species. PSCs can be differentiated into a variety of different cell types by adjusting the culture conditions. This often involves the addition of growth factors to the culture medium and media changes at specific time points which could introduce external biases depending on the species origin of the growth factors used and the timing of media changes. To overcome this, I chose to perform neural progenitor cell (NPC) differentiation that does not require growth factor addition and timed media changes. NPC differentiation occurs in absence of pluripotency-maintaining signaling (reviewed by Muñoz-Sanjuán & Brivanlou, 2002). Thus, inhibition of TGFβ and BMP4 signaling drives cells towards a

neural fate. One commonly used NPC differentiation protocol is based on this principle and referred to as dual SMAD inhibition (Chambers et al., 2009). Here, cells are treated with inhibitors for SMAD2/3-mediated Activin/Nodal signaling and SMAD1/5/8-mediated BMP4 signaling which is sufficient to activate an early neural differentiation program. In collaboration with Alexandra de la Porte (Helmholtz Munich), I established identical media conditions for NPC differentiation in the species-panel, using two small molecular inhibitors, 10 μM SB431542 and 100 nM LDN193189 inhibiting Activin/Nodal and BMP4 signaling respectively, in an N2B27-based medium (NPCSL). Prior to NPC differentiation, cells were seeded in UPPS + ROCK inhibitor to facilitate cell survival. Mouse cells tended to grow faster than cynomolgus and human cells and were therefore seeded at half the density of the primate cells. After one day in UPPS + ROCK inhibitor, cells were confluent and the medium was changed to NPC differentiation medium containing SMAD inhibitors (Figure 7A). During differentiation, cells grew to high densities. Cell survival was supported by daily PBS-washes and media changes. To confirm successful NPC differentiation and compare differentiation timing between mouse, cynomolgus and human cells, I performed a differentiation time course by seeding multiple differentiations for each species and fixing cells daily. Early NPC differentiation is marked by the anterior neural markers PAX6 and SOX1 (gene and protein names will be referred to in the human convention, if in a multi-species context). PAX6 is expressed in the forebrain, the eye and the olfactory bulb (Walther & Gruss, 1991). In human embryos, expression is detected at E18 and in mouse at E8.5 (Walther & Gruss, 1991; Zhang et al., 2010). SOX1 is expressed in neural progenitor cells in mouse from E7.5 on and in human around E26 (Bylund et al., 2003; Pevny et al., 1998; Zhang et al., 2010). Immunostaining of the differentiation time course for PAX6 and SOX1 revealed that NPC differentiation was successful in all three species (Figure 7B). Although there was background signal in the PAX6 staining before NPC induction at day 0 in mouse, the onset of NPC differentiation could be detected at day 1 where single mouse cells had started to express PAX6 (Figure 7B, arrowheads). Throughout the time course, PAX6 signal rose until most cells were PAX6+ (Figure 7B). In cynomolgus and human, PAX6 was detected from day 3 on, albeit rather weakly and only in few cells in human. Human PAX6 was uniformly expressed at day 4 (Figure 7B). Staining for SOX1 showed that mouse cells already expressed SOX1 in pluripotency, indicating that mouse cells in UPPS are more biased towards differentiation. As differentiation progressed, SOX1 was expressed uniformly in most cells. In cynomolgus and human, SOX1 onset was observed at day 2, however, it did not rise to mouse levels in human (Figure 7B). Staining for pluripotency factor OCT4 revealed a rapid signal decrease upon differentiation in mouse where OCT4 signal was barely detected at day 2 anymore, whereas OCT4 signal was still strong at day 2 in cynomolgus. In human, day 3 OCT4 levels were comparable to cynomolgus day 2 levels. At day

4, OCT4 signal was still detected at low levels in human when most cells had already adopted a neural fate as indicated by PAX6 and SOX1 expression (Figure 7B).

Taken together, neural marker onset was earliest in mouse while cynomolgus and human expressed PAX6 and SOX1 at the same time point, although cynomolgus had higher PAX6 levels at day 3 than human. The OCT4 decrease also indicated that mouse differentiated fastest, followed by cynomolgus and human, suggesting that the differentiation protocol recapitulates species-specific differentiation timing.

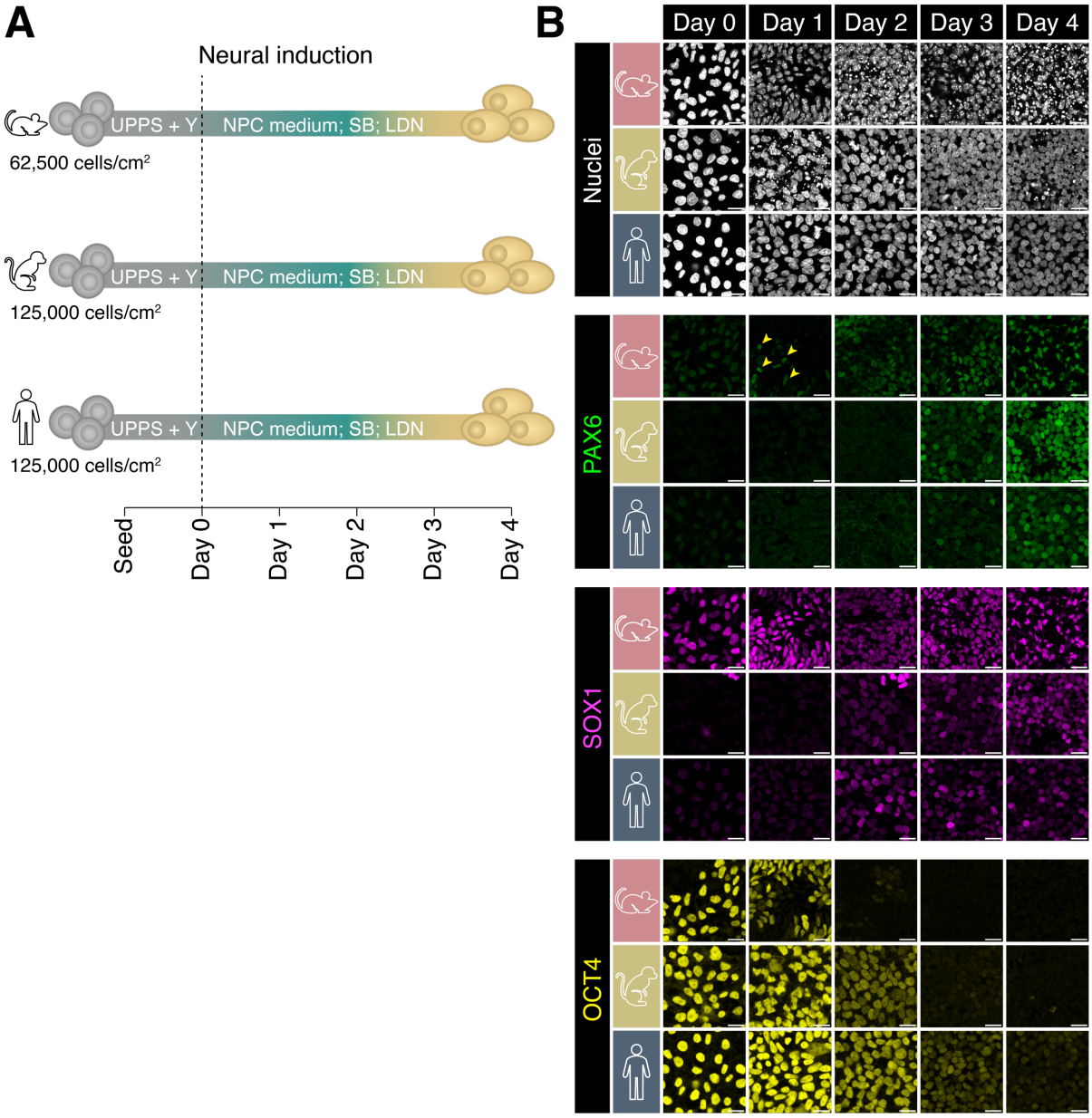

Figure 7: Neural progenitor differentiation of the harmonized species-panel.
A Schematic representation of the NPC differentiation protocol using dual SMAD inhibition. Cell numbers that were seeded for neural induction are indicated. **B** Immunostaining of an NPC differentiation time course of mouse, cynomolgus and human cells from day 0 (pluripotent control) up to day 4. Shown are the nuclear staining (Hoechst33258) and stainings for the early neural markers PAX6 and SOX1 and pluripotency marker OCT4. Arrow heads indicate PAX6+ cells in day 1 mouse cells. Minima and maxima were scaled channel-wise, the nuclei channel was adjusted for each image. Scale bars = 20 µm.

2.3 Mouse cells differentiate more than twice as fast as primate cells

To fully understand and quantify how different mouse, cynomolgus and human cells are during NPC differentiation, my collaborators Alexandra de la Porte and Moritz Thomas (Helmholtz Munich) conducted a single-cell RNA sequencing (scRNAseq) experiment where cells of all species were differentiated for ten days and sampled at eight different time points for single-cell transcriptomics (Figure 8A). The resulting data set spanned the time from pluripotency until ten days into NPC differentiation at high time resolution. To quantify how fast mouse cells differentiated relative to cynomolgus and human cells, cynomolgus and human sequencing data from each sampling time point were correlated with the mouse data from each sampling time point (Figure 8B). This 'mapped time' showed that the latest time point (day 10) in the primates corresponded best to day 4 in mouse, showing that mouse cells progress much faster through NPC differentiation and reach a differentiation state that is more advanced than both primate species. A linear fit through the mapped cynomolgus and human time revealed that mouse differentiates 2.2-fold faster than cynomolgus and 2.4-fold faster than human. This scaling factor shows that the NPC differentiation protocol recapitulates species-specific time scales in vitro and corresponds well to the differences observed in other differentiation systems (Matsuda et al., 2020; Rayon et al., 2020). Therefore, the scaling factor will serve as a reference for the following experiments.

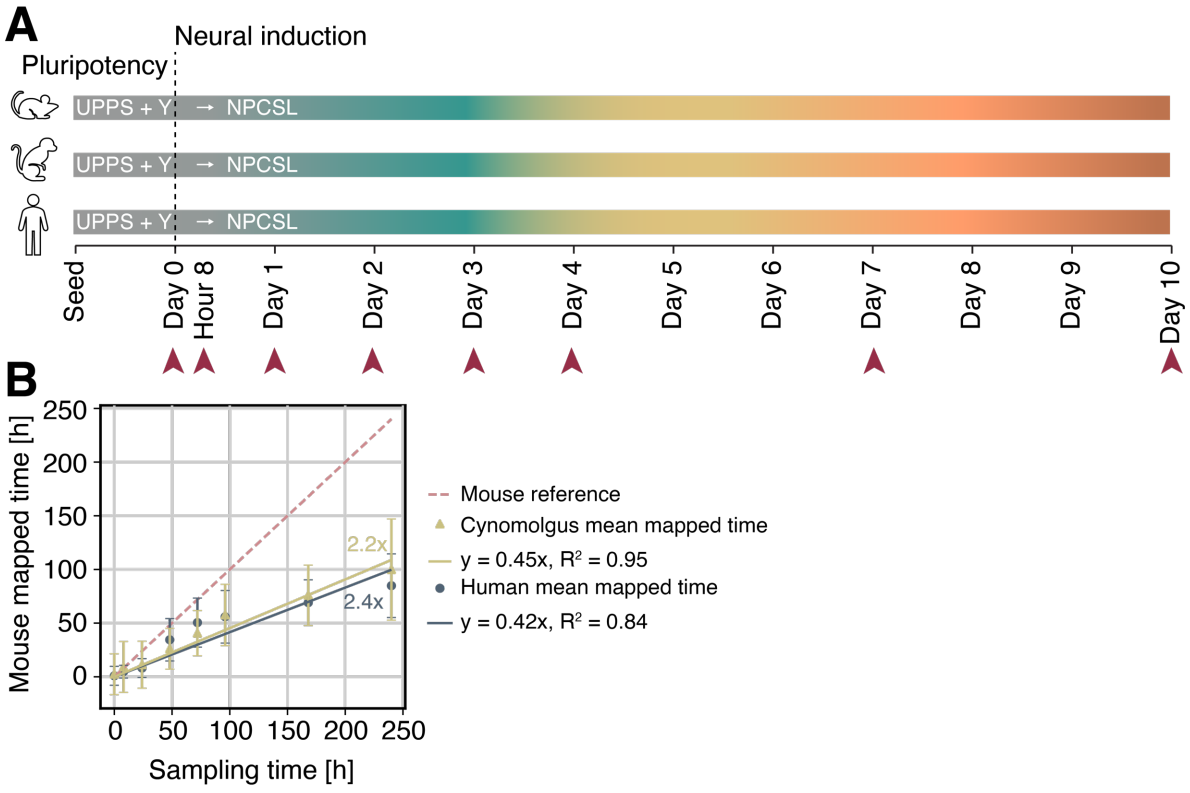

Figure 8: Single-cell transcriptomics reveal differentiation time shift between species.

A Schematic representation of the single-cell sequencing experiment performed by collaborators at Helmholtz Munich. Sampling times for sequencing are indicated by red arrow heads. **B** Gene expression at all sampling time points in cynomolgus and human was correlated with gene expression of mouse at corresponding sampling time points. The red, dashed line indicates the slope of mouse as a reference. X-axis shows original sampling time for cynomolgus and human, y-axis shows mouse mapped time, so the reference that cynomolgus and human were mapped to. Yellow triangles and blue points indicate the correlation between cynomolgus/mouse and human/mouse respectively. A linear fit (equation shown) was performed to quantify a scaling factor between the species. The indicated fold-changes of 2.2 and 2.4 indicate that mouse differentiation progression was 2.2 times faster than in cynomolgus and 2.4 times faster than in human. The experiment, data analysis and plotting were conducted by Alexandra de la Porte and Moritz Thomas (Helmholtz Munich).

2.4 Cell cycle durations are species-specific

During embryonic development, differentiation and growth have to be tightly coordinated to ensure proper tissue proportioning. Embryo growth is dependent on cell cycling and division. The correlation between cell cycle durations and differentiation speed observed in mouse and human cells by Rayon et al. (2020) opens the question whether cellular turnover and growth are required for differentiation. In this case, rapid proliferation would lead to fast differentiation. Another possible link between cell cycling and differentiation is the increased propensity of cells to differentiate in specific cell cycle phases, namely G1 (Pauklin & Vallier, 2013; Sela et al., 2012). Therefore, the time a cell spends in G1 phase could determine its differentiation speed. To explore both of these possibilities, I sought to characterize the cell cycle duration and structure in the species panel and assess whether the cell cycle follows a species-specific trend. If proliferation and differentiation are directly coupled, I expect the mouse cell cycle to be 2.2 times faster than the cynomolgus cell cycle and 2.4 times faster than the human cell cycle based on the scaling factor between the species during differentiation.

For cell cycle characterizations, I used the PIP-FUCCI system which constitutes a more precise version of the original FUCCI sensor. The PIP-FUCCI sensor uses the PCNA-interacting protein (PIP) degron ($Cdt1_{1-17}$) fused to mVenus and a nuclear localization signal, combined with Gem_{1-110} fused to mCherry (Grant et al., 2018; Sakaue-Sawano et al., 2008). As a licensing factor for DNA replication, Cdt1 accumulates during G1 phase and is degraded at the onset of S phase through interaction with PCNA, ensuring that DNA replication is initiated only once per cell cycle (Arias & Walter, 2005; Hofmann & Beach, 1994; Nishitani et al., 2000). Thus, $Cdt1_{1-17}$-mVenus confers mVenus fluorescence to G1 phase and its degradation is a direct marker of the G1/S transition. S phase is marked by Gem_{1-110}-mCherry. Geminin is present in S and G2 phase (Wohlschlegel et al., 2000). After DNA replication is completed, PCNA is released from the DNA and Cdt1 levels rise. As a consequence, both mVenus and mCherry fluorescence mark G2M phase (Grant et al., 2018). I generated polyclonal mouse, cynomolgus and human cell lines carrying the PIP-FUCCI sensor by Grant et al. (2018) under control of a CAG promoter and performed time-lapse imaging in 10 min intervals. Figure 9A shows exemplary stills of time-lapse movies in all three species. The PIP-mVenus signal marking G1 phase (displayed in green) is restricted to the first hour of the cell

cycle. It is followed by the gradual onset of Gem_{1-110}-mCherry signal (magenta) during S phase that takes up the largest proportion of the cell cycle. As cells enter G2M phase, PIP-Venus rises again, resulting in an overlay of mVenus and mCherry fluorescence (white). To quantify cell cycle and cell cycle phase durations, single cells were manually tracked and PIP-FUCCI signal was measured in a circular region of interest inside the nucleus. The resulting tracks (Figure 9B) show a sharp PIP-mVenus drop between G1 and S phase and a more gradual signal increase at the S/G2M boundary. Cell cycle phases were quantified based on PIP-mVenus signal. The G1/S transition was defined as the frame closest to half-maximal PIP-mVenus signal and the S/G2M boundary as the first frame of rising PIP-mVenus signal followed by five frames with an average signal increase of 1.5% (Chapter 5.9.4). The total cell cycle duration was defined as the time between cell birth and the last frame before the next division. Cell cycle durations were distributed very broadly in all species (Figure 9C). The mean cell cycle durations, however, were different and followed a species-dependent trend. With a total duration of 10.09 ± 0.92 h (mean ± SE), the mouse cell cycle was the fastest. Both primates had similar cell cycle durations with 14.27 ± 0.88 h (cynomolgus) and 14.82 ± 0.12 h (human), making the cynomolgus cell cycle 1.42-fold and the human cell cycle 1.47-fold longer than the mouse cell cycle (Figure 9C). This trend is reminiscent of species-dependent differentiation timing but the fold-changes in cell cycle durations between species cannot entirely explain the observed fold-change of > 2 during differentiation.

The cell cycle structure was similar in all three species (Figure 9D). The mean phase durations were characteristic of pluripotent stem cells. G1 phase was the shortest phase, taking only 0.97 ± 0.07 h in cynomolgus, 1.26 ± 0.15 h in mouse and 1.52 ± 0.05 h in human. S phase was the longest phase in all species, reflecting the fact that PSCs are highly proliferative. In mouse, S phase lasted 6.36 ± 0.74 h, in cynomolgus 7.73 ± 0.47 h and in human 8.00 ± 0.04 h. G2M duration was the most variable between the species, lasting from 2.46 ± 0.03 h (mouse) to 5.57 ± 0.49 h (cynomolgus). To test, if relative cell cycle phase durations are species-specific or rather scale with the total cell cycle duration, I normalized the phase durations to the total cell cycle length (Figure 9E). The proportions of individual phases were similar across species; however, mouse and human PSCs had a longer G1 phase compared to cynomolgus. Mouse had the longest relative G1 phase taking 13% of the total cell cycle and cynomolgus the shortest with 7%. At approximately 54%, S phase was very similar in the primate species whereas in mouse, S phase took up 63% of the cell cycle. In line with that, the relative G2M phase duration was between 36% and 39% in human and cynomolgus respectively and only at 24% in mouse.

In conclusion, the cell cycle analysis confirmed a species-dependent trend for total cell cycle durations where cells from fast-differentiating species tend to cycle faster than cells from slow-differentiating species. This trend cannot fully explain the timing difference between the species

during NPC differentiation quantitatively. However, it is possible that a change in cell cycle durations is not linearly translated to differentiation speed and that cell cycling is one of several factors contributing to the regulation of timing.

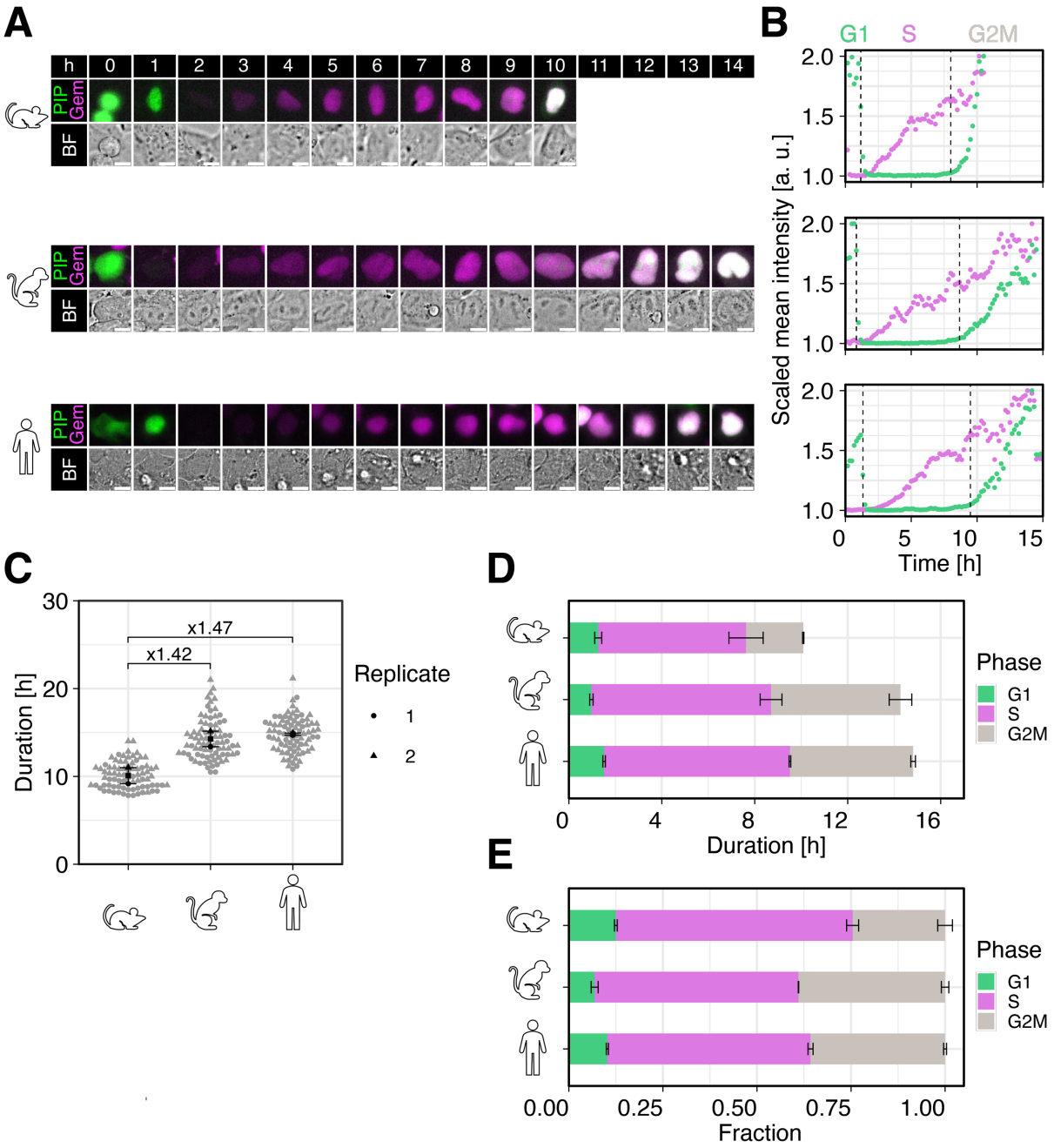

Figure 9: Cell cycle durations follow a species-specific trend.
A Time-lapse series of mouse, cynomolgus and human cells carrying the PIP-FUCCI sensor. The mVenus-tagged PIP degron (green) marks the G1 phase, mCherry-tagged Geminin$_{1\text{-}110}$ (magenta) marks S phase. Both markers combined indicate G2M phase (white). Scale bars = 10 µm. **B** Fluorescent tracks of cells shown in A. Colors correspond to PIP/Gem$_{1\text{-}110}$ color coding from A. G2M is indicated in gray. Fluorescence signal was measured in each frame and scaled between 1 and 2. G1, S and G2M phase could be distinguished by their fluorescence profiles. Dashed lines indicate the phase boundaries. **C** Distribution of total cell cycle durations in mouse, cynomolgus and human PSCs (N = 2 with n ≥ 40 cells each). Symbols correspond to replicate number; accordingly, black circles indicate the mean of replicate 1 and black triangles the mean of replicate 2. Black squares indicate the mean of both replicates ± SE. **D** Mean cell cycle phase durations as determined by fluorescent profiles as exemplified in B. The mean ± SE of N = 2 with n ≥ 40 cells each is

shown. **E** Same data as in D, but cell cycle phases were scaled to the total cell cycle duration. Mean ± SE of N = 2 with n ≥ 40 each is shown.

2.5 A retinoblastoma knock-out does not affect early NPC differentiation

2.5.1 Cell cycling in pluripotent cells is not perturbed by a retinoblastoma knock-out

Based on the observation that cell cycle durations are different depending on the species origin, I wanted to test if species-specific differentiation speed is a consequence of the cell cycle. Several studies link cell cycling to differentiation. G1 phase is often described as a window of opportunity in which cells are receptive to differentiation cues (reviewed by Boward et al., 2016). While I did not observe a systematic trend in relative G1 durations between the species, the cumulative time spent in G1 is also dependent on the number of cell divisions a cell experiences which is a direct consequence of cell cycle length. To test, if G1 duration influences NPC differentiation, I sought to manipulate the G1/S transition and analyze NPC differentiation. I obtained a mouse ESC line harboring knock-outs for all three members of the pocket protein family, *Rb*$^{-/-}$, *p107*$^{-/-}$, *p130*$^{-/-}$ (*Rb* triple knock-out, RbTKO hereafter) from Dannenberg et al. (2000). RB proteins are an essential part of the restriction point during the G1/S transition. When inactive, RB cannot repress E2F target gene expression, leading to immediate transition from G1 to S phase which truncates G1 phase (Chen et al., 1989; DeCaprio et al., 1989). Since the G1/S checkpoint is not active in ESCs (Savatier et al., 1994), the RbTKO does not affect ES cell growth (Dannenberg et al., 2000). It is however unknown, how EpiSCs which are developmentally further progressed than ESCs, are affected by the RbTKO. Here, I first differentiated RbTKO mESCs to mEpiSCs by culturing them in FAX medium for 10 passages and generated a PIP-FUCCI reporter line. RbTKO mEpiSCs and wild type mEpiSCs in FAX pluripotency medium were time-lapse imaged as described before. In pluripotency, RbTKO and wild type cells had indistinguishable cell cycle durations; the distributions of total cell cycle durations were not significantly different in both genetic backgrounds (Figure 10A). The mean cell cycle phase durations, including G1 duration were also very similar in both lines (Figure 10B). When normalized to the cell cycle length, there was no apparent difference between wild type and RbTKO, indicating that the cell cycle structure was the same (Figure 10C).

These results suggest that primed PSCs have a similar cell cycle regulation as naïve PSCs; both lack the restriction point at the G1/S boundary and the cell cycle is independent of RB activity.

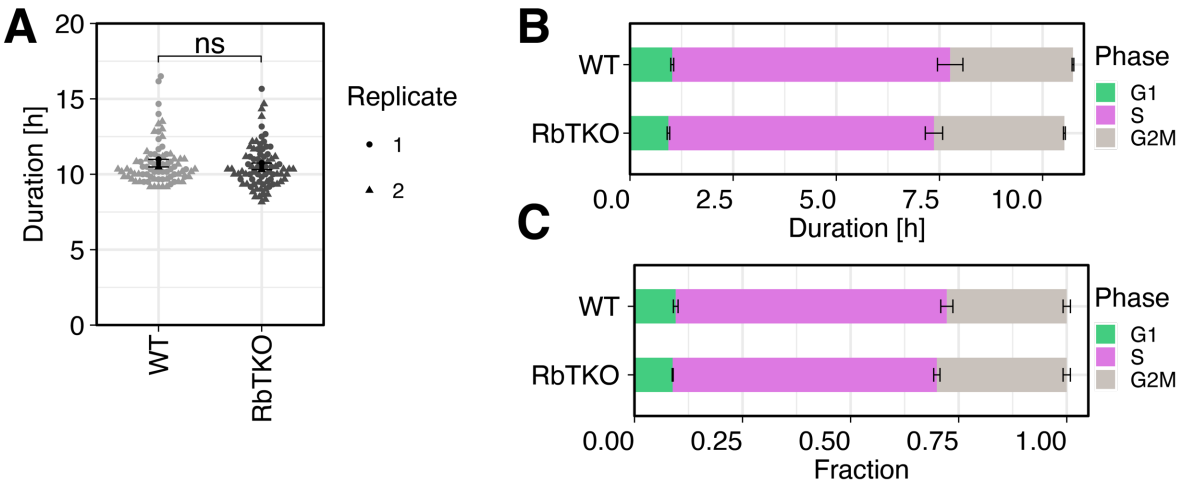

Figure 10: An RbTKO does not affect the pluripotent cell cycle.
A Beeswarm plot showing the distribution of cell cycle durations in mouse wild type EpiSCs and RbTKO EpiSCs. ns: p-value > 0.05 (not significant), Wilcoxon rank sum test comparing distributions. **B** Cell cycle phase durations as mean ± SE of N = 2 experiment with n = 40 each. **C** Same data as in B but normalized to the total cell cycle length.

2.5.2 The RbTKO affects the cell cycle of differentiating cells

As cells differentiate, RB becomes increasingly dephosphorylated, resulting in an extended G1 phase (Chen et al., 1989). Therefore, the RbTKO should affect differentiating cells more severely than pluripotent cells that typically do not have active RB (Savatier et al., 1994). To test if differentiating cells are affected by the RbTKO, I performed time-lapse imaging of wild type and RbTKO cells differentiated for two days prior to imaging. The total cell cycle duration was similar in both genetic backgrounds. RbTKO cells even had a slightly longer mean cell cycle duration than wild type (Figure 11A). The proportion of cell cycle phases did not reveal a drastic difference between the lines. G1 phase lasted for 3.1 ± 1.0 h (mean ± SD) in wild type and for 2.9 ± 1.0 h in RbTKO and therefore did not indicate the expected mutant phenotype with a truncated G1 phase (Figure 11B). Also, when normalized to the cell cycle length, both lines were very similar with 24% of the cell cycle spent in G1 for wild type and 21% for RbTKO (Figure 11C), suggesting that cells were still too undifferentiated to be affected by the knock-out. Tracking cells during later NPC differentiation was not possible due to increased cell death and debris. Therefore, I used flow cytometry to analyze the proportions of cell cycle phases during later differentiation. Wild type and RbTKO cells were differentiated for ten days and fixed on days 0-4 and 6, 8 and 10. PIP-FUCCI fluorescence was measured on a FACS Aria Fusion. At day 0, three distinct cell populations could be distinguished in the wild type and mutant line, corresponding to G1, S and G2M cells (Figure 11D). There was an overall downward shift of the RbTKO PIP-FUCCI signal which is likely caused by increased PIP-FUCCI sensor silencing compared to the wild type since the PIP-FUCCI sensor was selected for with puromycin and RbTKO cells contained a puromycin resistance gene from the start. Still, different trends could be observed for wild type and RbTKO cells. Upon NPC induction, the G1 fraction in the wild type increased while the S fraction decreased (Figure 11D-

E, G2M cannot be distinguished shortly post NPC induction anymore). This is in line with the literature as G1 becomes stretched when cells start differentiating (Calder et al., 2013; Coronado et al., 2013). In contrast, the fraction of RbTKO cells in G1 did not increase but stayed at a low level over the course of differentiation (Figure 11D, E). The S phase proportion stayed at a constant high level (Figure 11D, E), indicative of proliferating cells. In sum, these experiments suggested that the RbTKO affects the cell cycle later during NPC differentiation. The cell cycle structure of RbTKO cells remains pluripotency-like, even when cells are differentiated.

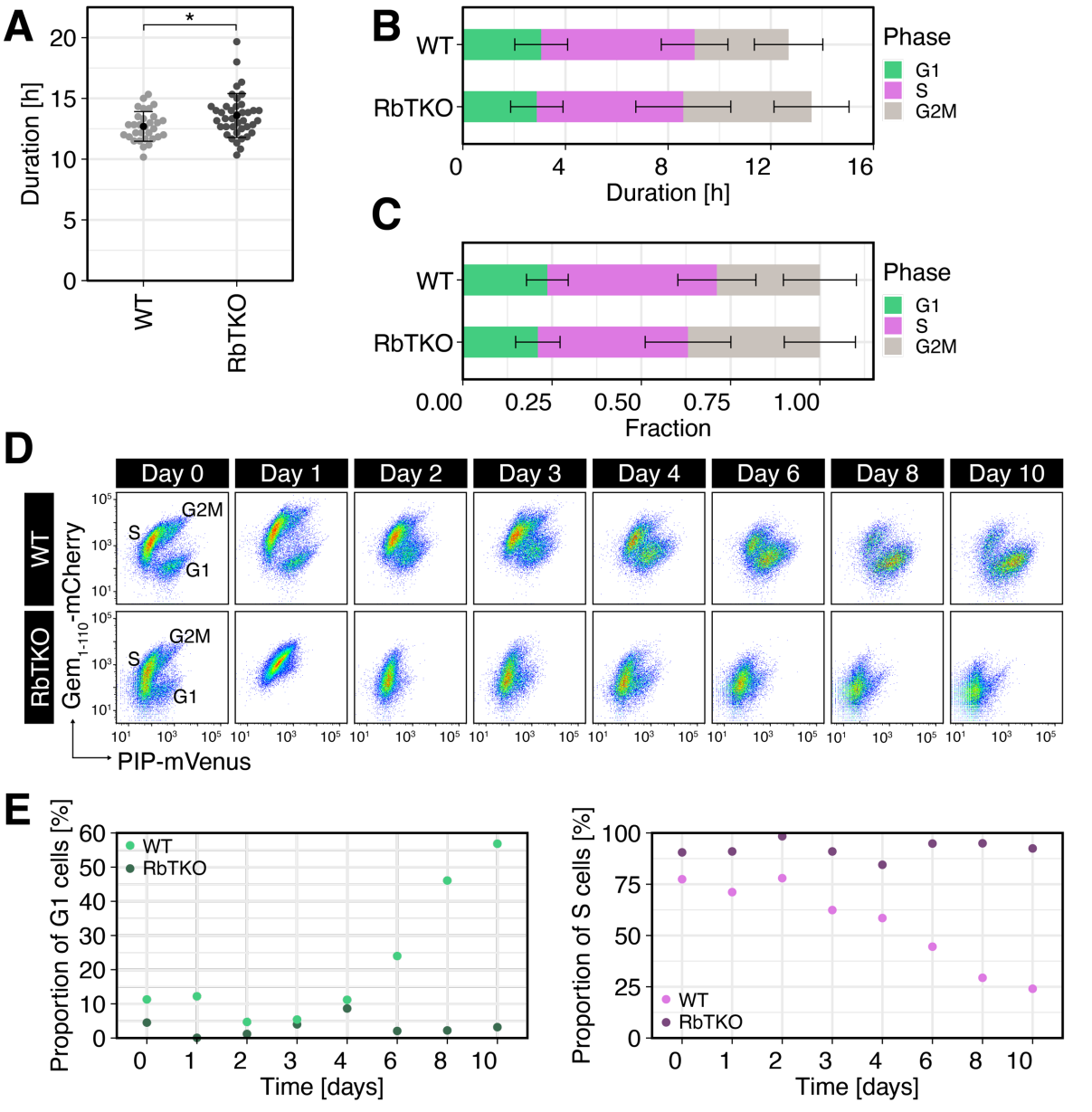

Figure 11: The RbTKO affects the cell cycle of differentiating cells.
A Beeswarm plot depicting the distribution of cell cycle durations of n ≥ 30 cells. Means ± SD are indicated. *: p-value < 0.05, Wilcoxon rank sum test comparing distributions. **B** Mean cell cycle phase durations ± SD. **C** Same as in B but scaled to the cell cycle length. **D** Flow cytometric analysis of differentiating wild type and RbTKO cells. **E** Quantification of data shown in D. Cells were assigned G1 phase when PIP-mVenus ≥ 600 and Gem_{1-110}-mCherry < 350. Cells were assigned S phase when PIP-mVenus < 600 and Gem_{1-110}-mCherry ≥ 350. To calculate the proportions of G1 and S cells, only cells that were not assigned double-negative (PIP-mVenus < 600 and Gem_{1-110}-mCherry < 350) were considered.

2.5.3 Neural differentiation appears unaffected in the RbTKO line

If the RbTKO affects differentiation speed, two scenarios are conceivable. (1) Differentiation speed is increased because G1 shortening leads to shortening of the overall cell cycle duration or (2) differentiation is slower or abrogated because cells need time in G1 to react to differentiation cues. To test this, I performed a differentiation time course of mouse wild type and RbTKO cells. Cells were fixed daily and stained for PAX6, SOX1 and OCT4. Neural marker onset was similar in both genetic backgrounds, although PAX6 at day 3 of differentiation was higher in the mutant than in the wild type (Figure 12A, B). Both lines exhibited a rapid decrease in OCT4 staining intensity immediately following NPC induction at day 1 (Figure 12A, B). Overall, wild type and RbTKO cells were not distinguishable during early NPC differentiation, showing that RbTKO cells are able to undergo normal early NPC differentiation. However, it was still unclear whether the differentiation outcome of RbTKO cells beyond PAX6 and SOX1 expression was affected.

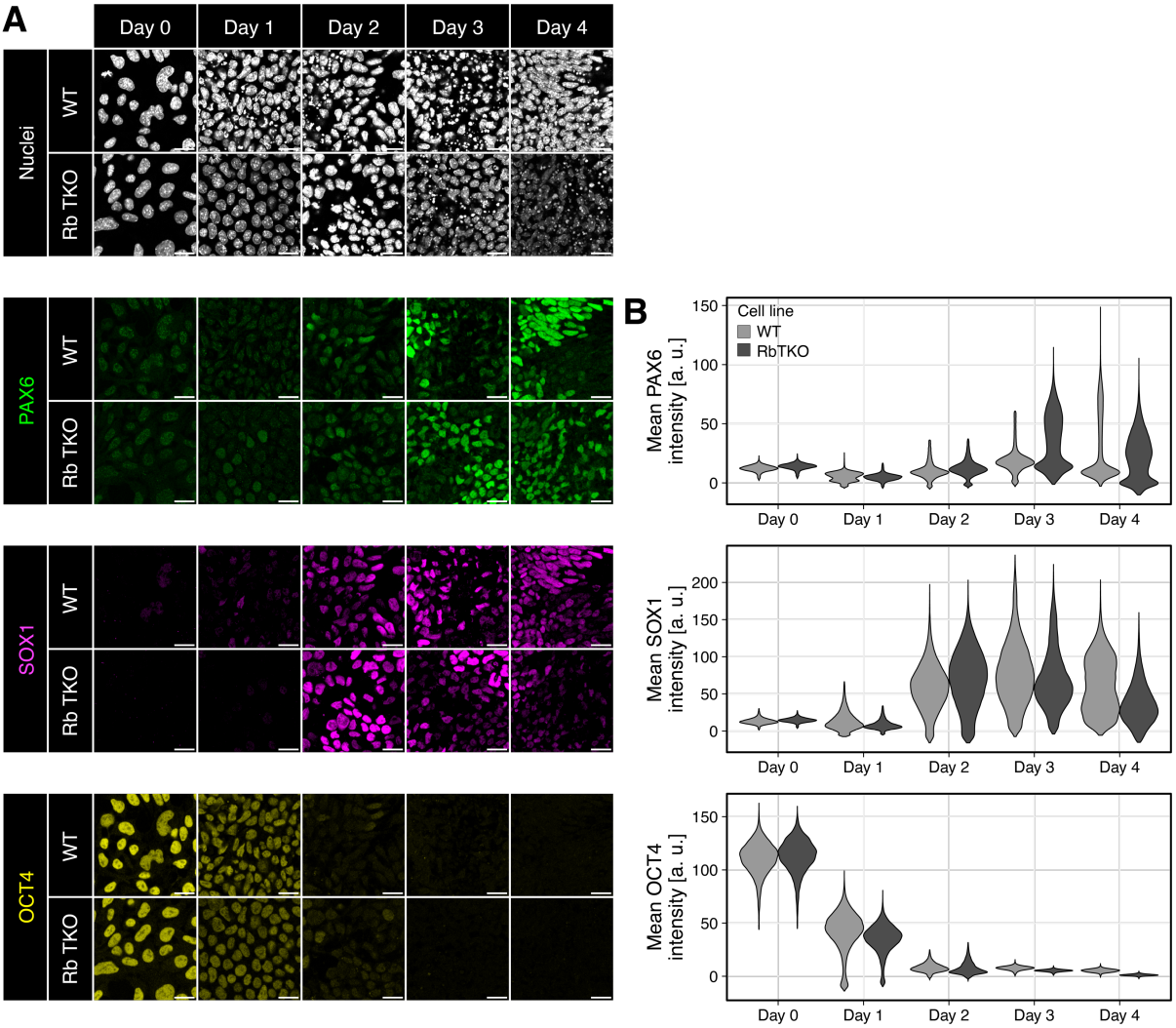

Figure 12: The RbTKO does not change differentiation marker onset.
A Immunostaining of a differentiation time course over four days. Representative images of N = 3 experiments are shown. Nuclei (Hoechst33258) indicate cell density, PAX6, SOX1 and OCT4 the differentiation status. Scale bars = 20 µm. **B** Single cell fluorescence measurements of immunostaining in A. Segmentation was done with StarDist 2D,

outlier removal and background subtraction were performed as described in chapter 5.5.3. Violins were stretched to the same maximum width.

2.5.4 Multiplexed single-cell RNA sequencing of RbTKO cells

To understand how wild type and RbTKO cells differ during differentiation, I used droplet-based single-cell RNA sequencing. This enabled me to analyze the expression of multiple neural markers as well as cell-to-cell heterogeneity during NPC differentiation.

In short, mouse wild type and RbTKO cells were seeded in FAX and harvested at days 0, 2 and 4 (Figure 13A). To reduce batch effects between the conditions, samples belonging to one time point were labeled with a unique Cell Multiplexing Oligo (CMO), binding to the plasma membrane, and pooled. Single cells were then compartmentalized into lipid droplets containing a gel bead providing barcoded primers. Inside the lipid droplets, cells were lysed and cDNA was synthesized using the barcoded primers. The cDNA contains sequencing adapters, a gel-bead-specific 10x barcode, a unique molecular identifier (UMI) and capture sequences. Two kinds of libraries were generated from each pool; (1) a Gene Expression Library with cDNA fragments carrying the UMI and a cell-specific barcode and (2) a Multiplexing Library with barcoded CMOs (Figure 13B). Samples were demultiplexed based on their CMO label. For the wild type day 0 sample, the CMO sequencing was very noisy and the sample could not be reliably demultiplexed. For this reason, the following analyses focus on wild type day 2 and 4 and RbTKO day 0, 2 and 4. Only cells with a mitochondrial gene proportion of less than 15% and a minimum feature count of 3000 were considered.

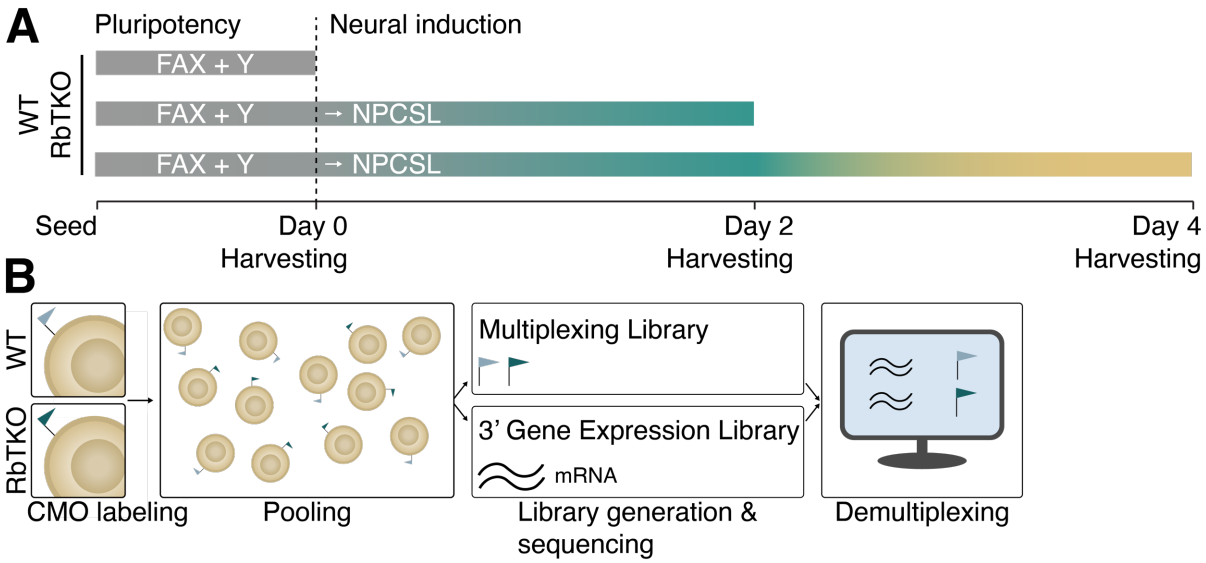

Figure 13: Schematic representation of experimental set-up for single cell-RNA sequencing.
A Mouse wild type and RbTKO cells were seeded in FAX + Y. The next day, cells were changed to NPCSL medium. At days 0, 2 and 4, cells were harvested for single-cell sequencing. **B** Work flow for multiplexed single-cell sequencing. Samples are labeled with a unique CMO and pooled. A Multiplexing Library and a 3' Gene Expression Library are generated and samples are bioinformatically demultiplexed.

2.5.5 RbTKO cells can be transcriptionally distinguished from wild type cells

To visualize the sequencing data, I performed non-linear dimensionality reduction (UMAP, McInnes et al., 2020) where each point represents the transcriptome of a single cell. In the UMAP projection, day 2 wild type and mutant cells are distinguishable but in close proximity whereas the day 4 wild type and mutant samples are localized further away from each other. The wild type day 4 sample is split into two distinct populations (Figure 14A).

To test if the cell cycle phase distribution was different between wild type and RbTKO, I performed cell cycle scoring using the *CellCycleScoring* function in Seurat (Hao et al., 2023). Here, cells are scored based on their expression of two sets of genes, (1) a set of genes typically expressed in S phase and (2) a set of genes typically expressed in G2M phase. Cells that score low in both sets compared to other cells, are assigned to G1 phase (Tirosh et al., 2016). Although expression-based cell cycle scoring is only an indirect measure of a cell's cell cycle phase, it is an indicator for differences between the analyzed cells. Using this method, there was a general overrepresentation of cells assigned to G2M (Figure 14B, C) which does not correspond to the time-lapse-based measurements. However, 23-24% of wild type cells were assigned to G1 phase at days 2 and 4, confirming the increased G1 length observed during NPC differentiation (Figure 11C). At days 2 and 4, no increase in G1 proportion was observed for RbTKO cells (Figure 14B, C), possibly indicating that RbTKO keeps differentiating cells in a pluripotency-like cell cycle structure.

Next, I wanted to assess how similar wild type and mutant cells are at the different time points of NPC differentiation apart from cell cycle differences. While UMAP plots are useful to visualize high-dimensionality data in 2D, they do not offer a quantitative clustering of cell groups. For this reason, I performed unsupervised Louvain clustering. By tuning the clustering resolution, cells are grouped into different numbers of clusters. First, I wanted to test, if clustering at low resolution produces clusters corresponding to the sampling time irrespective of the genotype. However, low-resolution clustering (Figure 14D, E) did not solely group cells after their sampling time. Day 2 wild type and mutant cells fell into the same cluster (cluster 0) while the day 4 wild type cells were split between clusters 2 and 0, indicating that part of the day 4 cells was still very similar to day 2 cells. RbTKO day 4 cells occupied their own cluster.

To test if day 2 wild type cells were different from day 2 RbTKO cells, I performed higher-resolution clustering (Figure 14F, G). Clustering at high resolution should produce more clusters and is more sensitive to differences between cells. Indeed, at a resolution of 0.57, the day 2 cells split into a wild type and a mutant cluster (clusters 3 and 6 respectively). This indicated that the wild type and mutant line were distinct from each other at day 2 albeit more similar than at day 4. Thus, with progressing NPC differentiation, the discrepancy between the lines increased.

In sum, single-cell transcriptomics indicated a lack of cells in G1 phase for the RbTKO during NPC differentiation. Furthermore, wild type and RbTKO cells become more different from each other as they undergo differentiation.

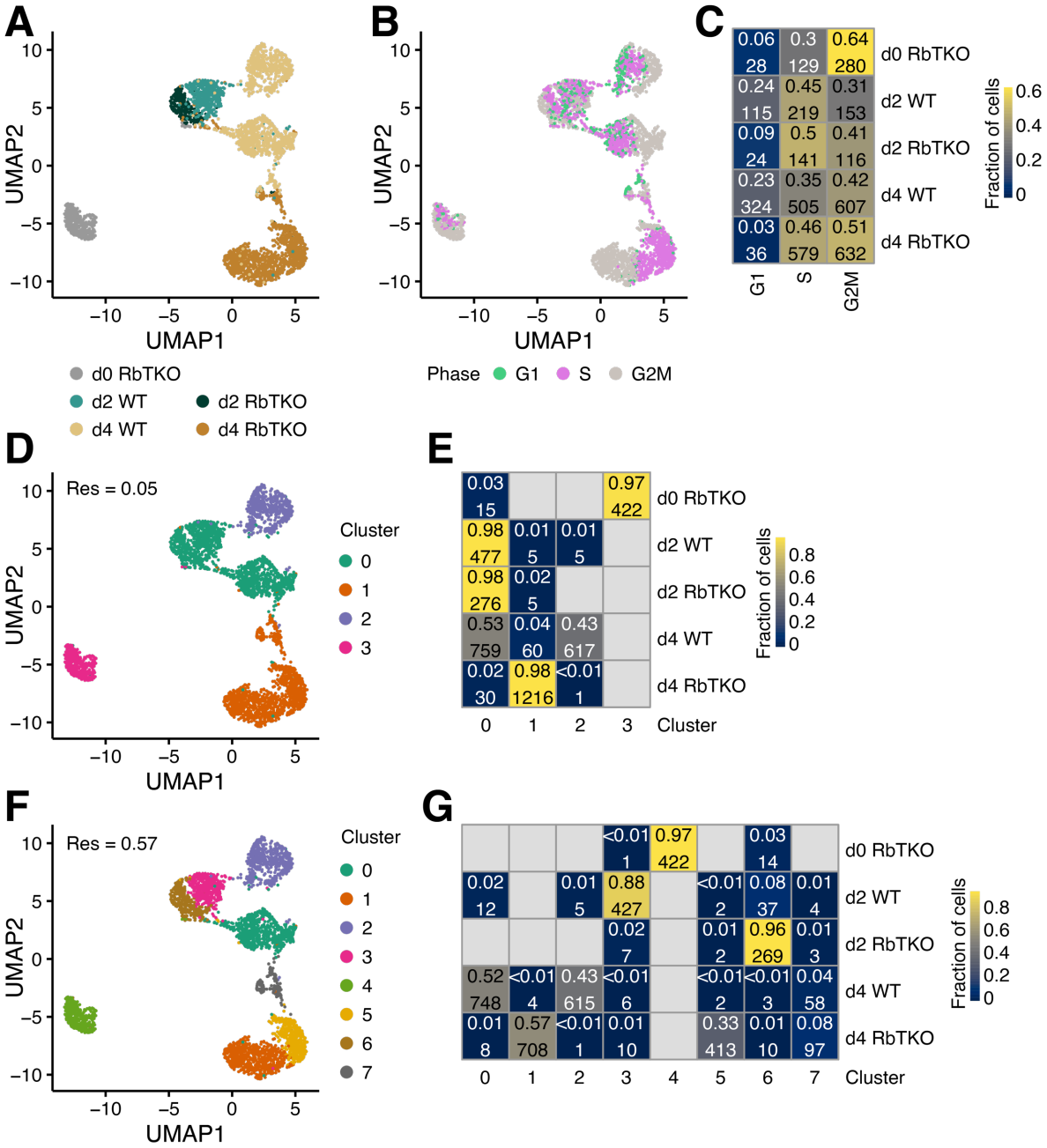

Figure 14: RbTKO and wild type cells form distinct clusters in a scRNAseq experiment.
A UMAP projection of mouse wild type and RbTKO sequencing data. Colors indicate the sample identity. **B** Cell cycle scoring shown as color-coding on a UMAP projection. **C** Quantification of cell cycle phase scoring from B. Upper number in each tile indicates the fraction of cells assigned to a specific cluster (also color-coded) and the lower number in each tile shows the absolute number of cells assigned to a cluster. Gray tiles indicate no assigned cells. **D** Low-resolution (0.05) Louvain clustering of sequencing data differentiates between 4 clusters. **E** Quantification of low-resolution clustering. **F** High-resolution (0.57) Louvain clustering detects eight clusters. **G** Quantification of high-resolution clustering. Rows in E and G correspond to sample identities, columns to detected clusters.

2.5.6 Several early neural markers are unaffected by RbTKO

To test, if wild type and RbTKO cells differentiated successfully in the sequencing experiment, I looked into the expression of several neural markers as well as pluripotency factors *Pou5f1* (encoding Oct4) and *Nanog* (Figure 15). The day 0 RbTKO sample showed high *Pou5f1* and *Nanog* expression that rapidly decreased at day 2. Like RbTKO cells, wild type cells had little *Pou5f1* and *Nanog* expression at days 2 and 4. Increasing neural marker expression (*Sox1*, *Pax6*, *Sox2*, *Map2*, *Nestin*, *Dcx*, *Sox5* and *Sox6*) indicated the onset of NPC differentiation. Strikingly, I did not observe a systematic difference in marker expression between wild type and RbTKO cells. Both lines expressed most markers at comparable levels in a similar proportion of cells. This suggests that RbTKO cells can undergo early NPC differentiation similar to wild type cells.

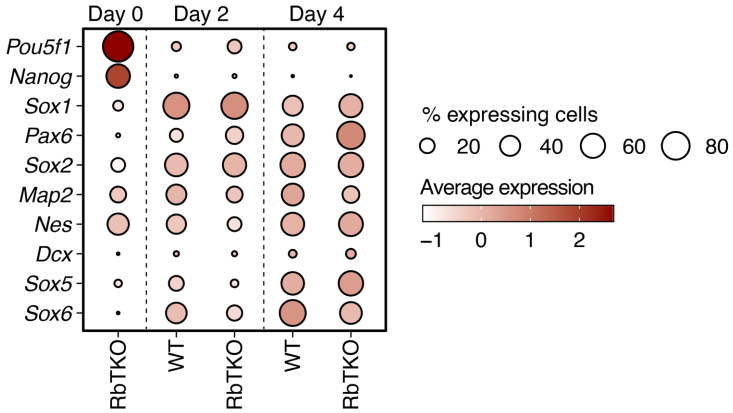

Figure 15: Early neural marker expression is similar in wild type and RbTKO cells.
Expression of a selection of neural markers and pluripotency genes *Pou5f1* (encoding Oct4) and *Nanog* are shown as a dotplot. Color indicates average expression; dot size indicates the proportion of cells with an expression level of > 0.

2.5.7 Early NPC differentiation occurs normally in RbTKO cells

Since clustering showed that RbTKO cells became progressively different from wild type cells during NPC differentiation and that these differences could be related to the cell cycle, I sought to understand which genes are differentially expressed between wild type and RbTKO and how they functionally relate to neural differentiation. Figure 16A shows all significantly differentially expressed genes (adjusted p-value < 0.01 and average log2FC > |1|) between RbTKO and wild type cells at day 4 of NPC differentiation. 675 genes were downregulated and 297 genes upregulated in RbTKO cells (Figure 16A). Among the most significantly downregulated genes, several genes encoding glycolytic enzymes were found (*Pgk1*, *Aldoa*, *Tpi1*, *Ldha*), suggesting lower glycolytic activity in RbTKO cells. In contrast, the most significantly upregulated genes contained genes related to neurogenesis like *Dbx1*, *Ntn1*, *Nell2*, *Ndnf*, *Sox2ot*. Interestingly, *Cdkn1c* was also found to be upregulated in RbTKO cells. *Cdkn1c* (also called *p57*) is a member of the CIP/KIP family of CDK inhibitors and a tumor suppressor gene (Matsuoka et al., 1995). As a CDKi, Cdkn1c antagonizes proliferation and its overexpression leads to G1 arrest (Lee et al., 1995;

Matsuoka et al., 1995). Cdkn1c was found to be upregulated in retinoblastomas (Madhavan et al., 2010), potentially explaining its upregulation in RbTKO cells.

To functionally group the differentially expressed genes, I performed gene ontology (GO) term analysis focusing on biological processes (Figure 16B, C). Here, genes are assigned to various biological processes that give a more comprehensive understanding of the functional relevance of differentially expressed genes. The top 10 most significantly enriched biological processes among the upregulated genes in RbTKO were mostly related to neurogenesis (Figure 16B,), suggesting that day 4 RbTKO cells upregulate neural markers more strongly than wild type cells at the same timepoint. Surprisingly, the top 10 most significantly enriched biological processes among the downregulated genes in RbTKO cells also contained many terms linked to neurodevelopmental processes (Figure 16C). This could happen due to the hierarchical nature of GO terms where a mother term can contain daughter terms for not only positive but also negative regulation of the mother process. It could however also mean that wild type and RbTKO cells both initiate neural differentiation but express different neural genes associated with the same GO term. Next, I wanted to test, how similar wild type and RbTKO cells were during NPC differentiation by comparing the differentially expressed genes at day 4 versus day 2 in both lines (Figure 16D-F). Only a fifth to a fourth of the upregulated genes at day 4 versus day 2 overlapped between wild type and RbTKO cells, possibly because of the different genetic backgrounds (Figure 16E). Yet, GO term analysis of the upregulated genes at day 4 versus day 2 showed that both lines expressed genes associated with neural development (Figure 16E), indicating that RbTKO cells undergo neural differentiation similar to wild type cells.

Taken together, I observed strong differences in gene expression between wild type and RbTKO cells but neural differentiation appears similar in both genetic backgrounds, suggesting that early NPC differentiation occurs normally in RbTKO cells.

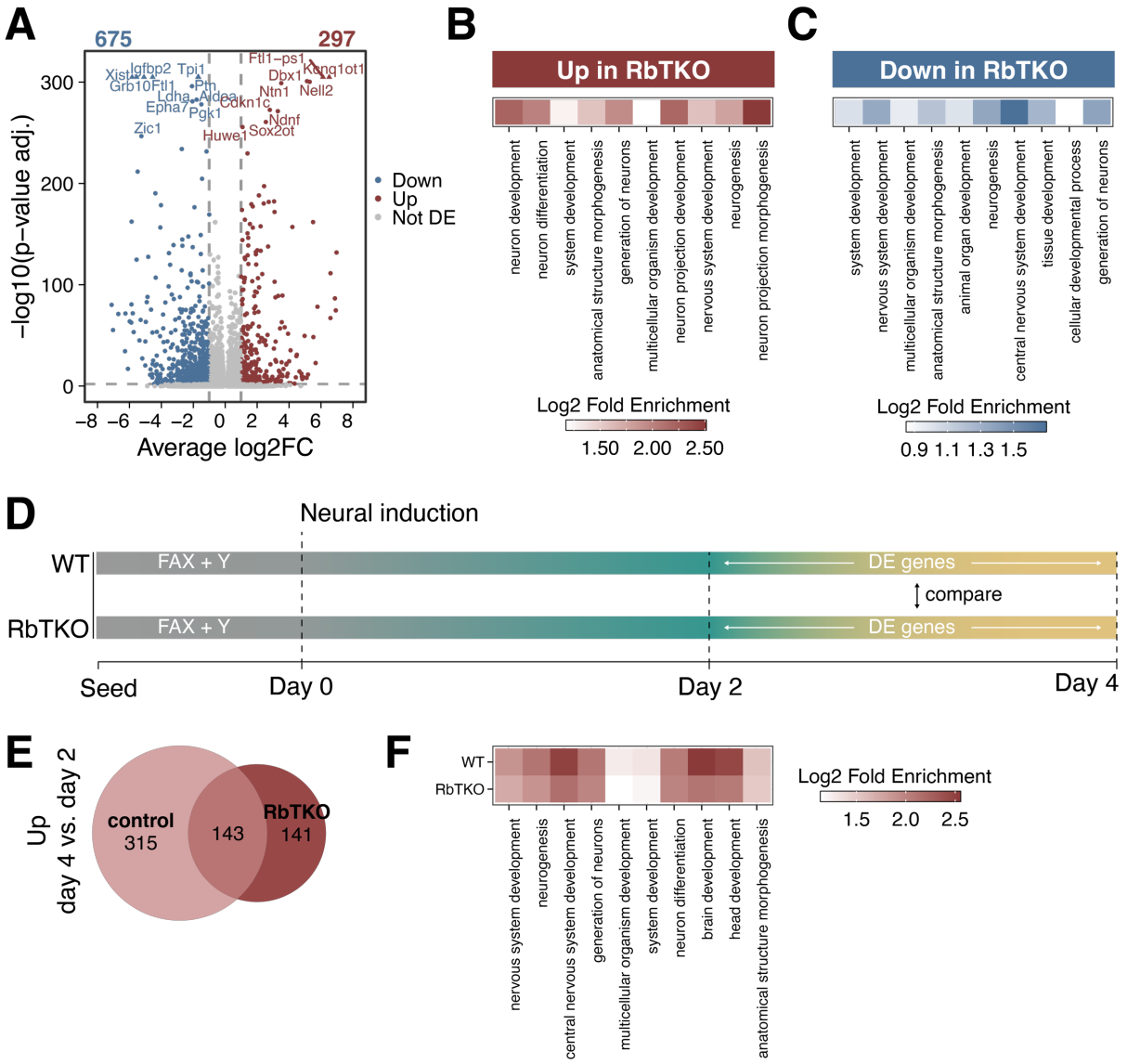

Figure 16: Differentially expressed genes between RbTKO and wild type cells.
A Volcano plot showing the differentially expressed genes between RbTKO and wild type cells at day 4 of NPC differentiation. Downregulated genes in RbTKO versus control are marked in blue, upregulated genes in red. Differentially expressed were all genes with an adjusted p-value < 0.01 and an average log2FC > |1|. Upregulated were all of these genes with an average log2FC > 0 and downregulated all with an average log2FC < 0. All other genes were considered not differentially expressed (gray). Vertical dashed lines indicate the log2FC cut-off for up- and downregulated genes, horizontal dashed lines indicate the adjusted p-value cut-off. Names of the top 20 most significantly differentially expressed genes are shown. Numbers of up- and downregulated genes are indicated in the top. **B** Heatmaps showing the top 10 most significantly enriched biological processes among the upregulated genes shown in A. **C** Heatmaps showing the top 10 most significantly enriched biological processes among the downregulated genes. **D** Scheme depicting the analysis strategy in E-F. **E** Euler diagram of the significantly higher expressed genes in day 4 cells versus day 2 cells comparatively in wild type and RbTKO cells (all significantly differentially expressed genes with an average log2FC > 0) **F** Heatmap displaying the top 10 most significantly enriched GO terms in the significantly higher expressed genes at day 4. GO terms were sorted after ascending false discovery rate (FDR) in the wild type. Tiles are colored after the log2 fold enrichment.

2.5.8 Early NPC differentiation is not delayed in RbTKO cells

To finally assess how fast RbTKO cells differentiate compared to the wild type, I used the time-resolved scRNAseq data obtained by Alexandra de la Porte and Moritz Thomas (Helmholtz Munich) as a reference. Using the Scanpy function *ingest* (Wolf et al., 2018), I integrated the

RbTKO scRNAseq data with the reference data. Here, the RbTKO data is mapped onto the reference data, allowing me to determine which time point in the reference data the RbTKO data resemble most closely. Figure 17B shows the RbTKO data projected onto the reference UMAP embedding and comparison with the reference time points (Figure 17A) reveals that RbTKO and wild type cells roughly occupied the same regions on the reference embedding. The quantification (Figure 17C) shows that the day 2 cells (wild type and RbTKO) corresponded to days 1 and 2 of the reference data, indicating that these cells were slightly slower than the reference cells. The day 4 wild type sample best corresponded to days 3 and 4 while RbTKO cells mapped onto days 4 and 7. Thereby, RbTKO tended to differentiate slightly faster than wild type cells.

In sum, this clearly shows that early neural differentiation was not delayed in RbTKO cells. In contrast, they appeared moderately faster than wild type cells. It is however not known, whether NPC differentiation is affected at later stages and if the observed cell cycle phenotype in RbTKO was strong enough at the chosen time points to conclude that loss of G1/S transition control does not affect NPC differentiation.

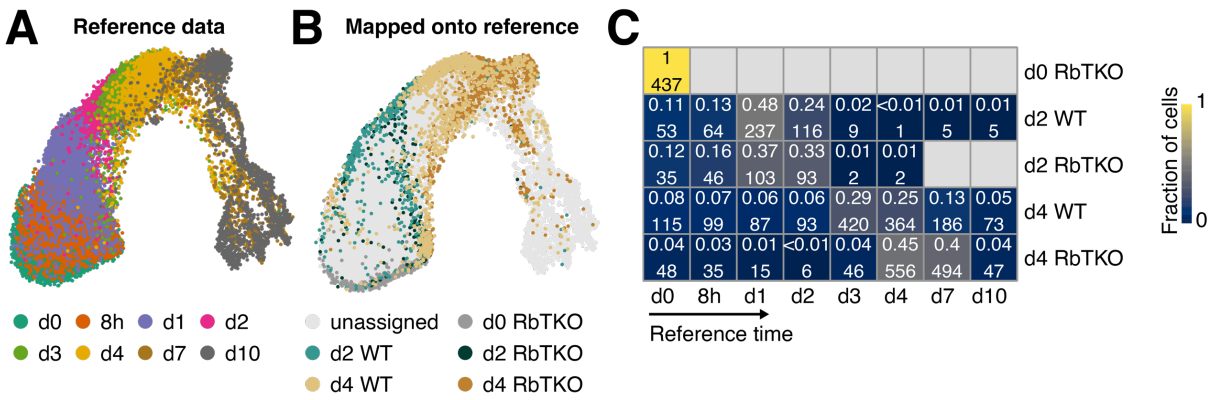

Figure 17: Integration with a time-resolved reference data set shows that early NPC differentiation is not delayed in RbTKO cells.
A UMAP projection of time-resolved reference data obtained by Alexandra de la Porte and Moritz Thomas (Helmholtz Munich). Color coding indicates the sampling time points. **B** scRNAseq data from RbTKO experiment integrated with the reference data and projected onto the reference UMAP embedding. Color-coding indicates sample identity. **C** Heatmap showing which fraction of cells from each sample was assigned to which reference time point (top number) and the total number of cells assigned to each time point (bottom number). Color-coding indicates the fraction of cells; gray corresponds to no assigned cells.

2.6 NPC differentiation and growth can be uncoupled

2.6.1 Inhibition of mTOR drastically slows down cell cycling in pluripotency

Stem cell proliferation and differentiation are highly dependent on metabolism. Rapid stem cell division is fueled by high glycolytic activity whereas cells shift to oxidative phosphorylation during differentiation (reviewed by Folmes et al., 2012). It has been reported that mouse cells have a higher mass-specific metabolic rate than human cells (Diaz-Cuadros et al., 2023) which could drive the fast differentiation in mouse. In line with this observation, I found that fast-

differentiating species had a faster cell cycle than the slow-differentiating species (Figure 9). Based on these previous experiments and observations from the literature, I hypothesized that growth and differentiation are functionally coupled. Therefore, I sought to manipulate cellular metabolism to alter growth and test whether differentiation speed is changed. One central regulator of proliferation and growth is mTOR. mTOR is a kinase and a positive regulator of translation (Brunn et al., 1997; Burnett et al., 1998; Gingras et al., 1999; Hara et al., 1997). Inhibition of mTOR signaling with 200 nM of the ATP-site inhibitor INK128 in mouse ESCs and blastocysts induced a diapause-like state in which the cell cycle was arrested and development paused (Bulut-Karslioglu et al., 2016). Here, I sought to impair growth and proliferation via mTOR inhibition and test if and to what degree differentiation is affected. A causal link between cell proliferation and differentiation has so far not been shown. I titrated the mTOR inhibitor INK128 and finally used a dose of 50 nM which was tolerated by all species and led to a notable growth reduction. First, I quantified the effect of mTOR inhibition (mTORi) on the cell cycle using the PIP-FUCCI system. Mouse, cynomolgus and human cells were cultured in UPPS or UPPS + 50 nM INK128 and time-lapse imaging was performed as described before. When comparing control with mTOR-inhibited cells (Figure 18A), I observed an increase in cell cycle durations in all species. This increase was very drastic in cynomolgus (46%) and human (53%) and milder in mouse cells (23%). The distribution of cell cycle durations was significantly different and much broader under mTORi treatment compared to control cells; some cells exhibited a control-like cell cycle duration while others had a total cell cycle duration of close to 35 hours in human and cynomolgus. The cell cycle structure (Figure 18B, C), i. e. the absolute and relative durations of individual phases was very similar in mouse control and mTORi -treated cells. In cynomolgus and human, G1 length scaled superlinearly with the total cell cycle duration, with cynomolgus exhibiting a 3.34-fold and human a 2.28-fold increase in G1 length. However, G1 phase was still the shortest phase in absolute time and relative to the total cell cycle. In contrast, G2M phase was shorter relative to the total duration in cynomolgus and human mTORi-treated cells. The relative duration of S phase however scaled with the total cell cycle duration and remained at a constant 53-58% in both primate species, irrespective of the treatment.

In conclusion, mTOR inhibition drastically slowed down proliferation in a species-dependent manner during pluripotency. Next, I wanted to test if this effect is preserved during NPC differentiation.

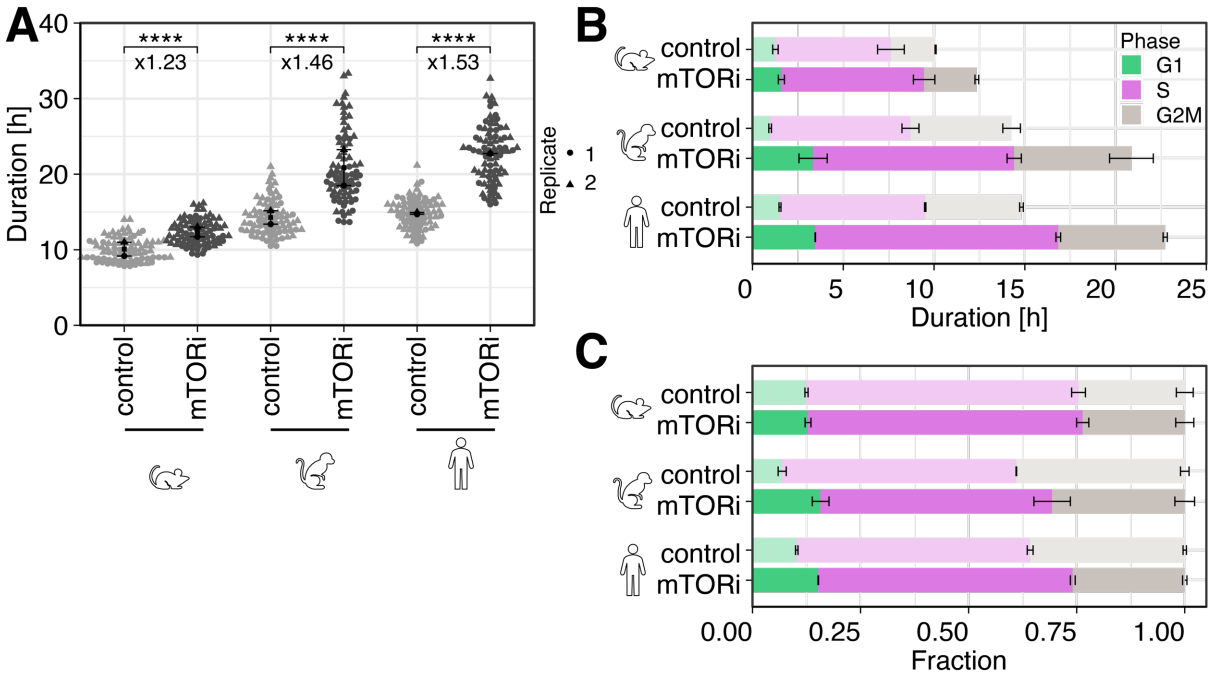

Figure 18: mTOR inhibition drastically extends cell cycle durations in pluripotency.
A Distributions of total cell cycle durations in mouse, cynomolgus and human PSCs +/- mTOR inhibition (same data for control as in Figure 9). N = 2 experiments with n ≥ 39 cells each are shown, the mean between replicates (square) and replicate means (circle and triangle) are indicated. Fold-changes between control and mTORi-treated cells are shown. ****: p-value < 0.001, Wilcoxon rank sum test comparing distributions. **B** Cell cycle phase durations comparing control (transparent) and mTORi-treated cells. **C** Same as in B but scaled to the total cell cycle duration. Error bars indicate SE.

2.6.2 mTORi effect on cell cycling is preserved during NPC differentiation

Changes in cell fate are reflected in cell cycle structure and duration. As cells differentiate, they spend more in the G1 phase (Chen et al., 1989). Due to these major cell cycle changes, I tested if and how mTOR inhibition influences the cell cycle during NPC differentiation. I induced NPC differentiation +/- mTOR inhibition in mouse, cynomolgus and human cells and started time-lapse imaging at day 2 of differentiation +/- mTOR inhibition (Figure 19A). Compared to pluripotent cells, differentiating cells had extended cell cycles (Figure 19B). This extension affected mouse the least and human the most. On average, differentiating mouse control cells cycled for 13.96 ± 1.42 h (mean ± SD), cynomolgus control cells for 18.34 ± 2.66 h and human control cells for 24.92 ± 5.47 h. When mTOR was inhibited during NPC differentiation, the distribution of cell cycle durations was significantly different from the control in all species. The human cell cycle was increased 1.45-fold to 36.08 ± 5.03 h and cynomolgus mTORi-treated cells cycled at 29.63 ± 10.53 h, corresponding to a 1.62-fold increase in cell cycle length. Strikingly, the distributions of cell cycle durations were again much broader in the mTORi-treated cells than in control cells, meaning that some cells were hardly affected by the treatment while others were highly affected (Figure 19B). In contrast to the primate species, differentiating mouse cells did not exhibit an elongated cell cycle upon mTORi treatment; mouse mTORi-treated cells cycled at 13.06 ± 1.12 h and were thereby 6% faster than control cells.

The cell cycle structure in mouse was very similar between control and mTORi, both in absolute time and relative to the total cell cycle duration (Figure 19C, D). In line with pluripotency measurements, cynomolgus and human cells had an elongated G1 phase in mTORi compared to the control (Figure 19C), also when normalized to the total cell cycle duration (Figure 19D). The relative G2M phase duration was decreased in mTOR-inhibited human cells.

Taken together, mTOR inhibition extended the cell cycle duration in pluripotency in all species tested whereas mTOR inhibition during NPC differentiation only affected cynomolgus and human cells. Quantitatively, the mTOR-induced cell cycle extension in cynomolgus and human during NPC differentiation (cynomolgus 1.62-fold, human 1.45-fold) was comparable to the extension observed in pluripotency (cynomolgus 1.46-fold, human 1.53-fold). In both states, the relative duration of G1 phase was increased. These results show that the mTORi-dependent cell cycle phenotype observed in pluripotent cells is largely maintained during NPC differentiation. In a next step, I will therefore use mTOR inhibition to manipulate proliferation of differentiating cells and test whether slowing down growth and cell cycling leads to slower differentiation.

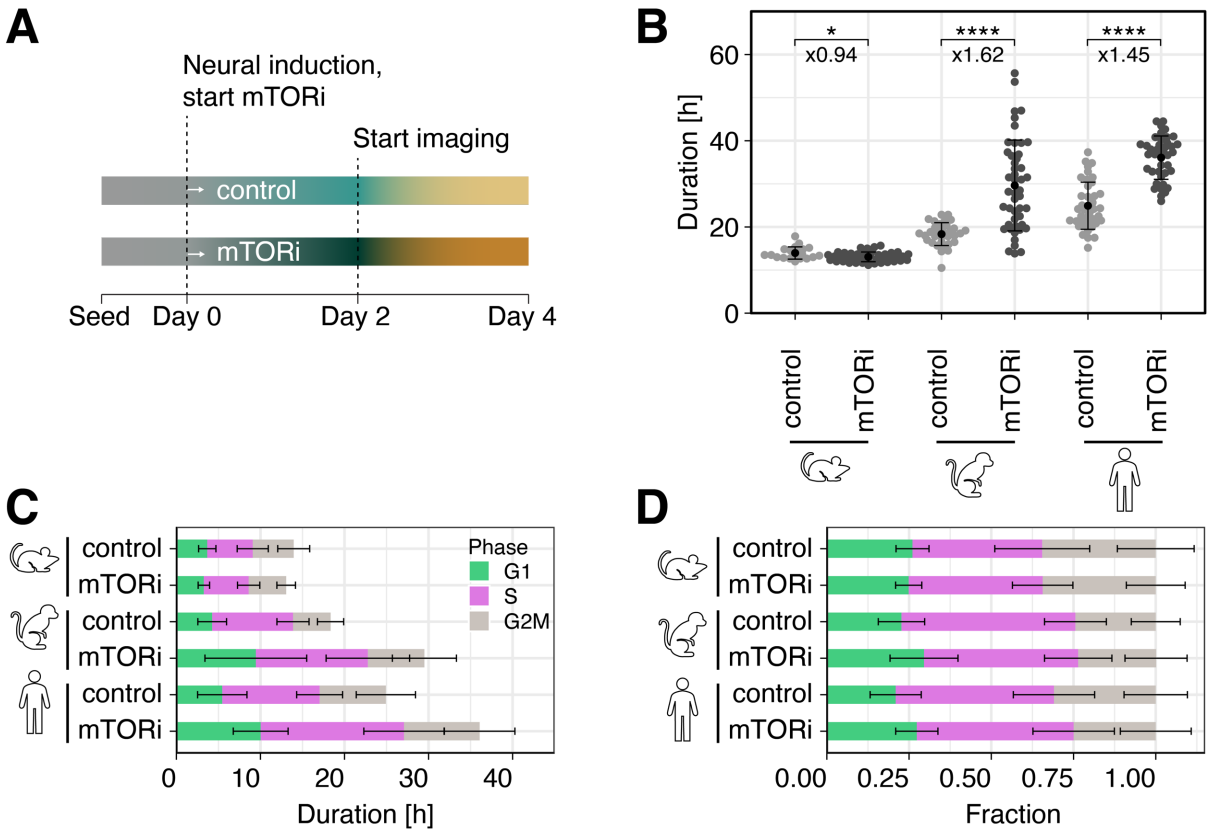

Figure 19: Cell cycle duration is slowed down by mTOR inhibition during NPC differentiation.
A Schematic representation of experimental procedure. PSCs are seeded and differentiation +/- mTORi is started at day 0. After two days of differentiation +/- mTORi, time-lapse imaging is started. **B** Total cell cycle durations in all cells measured. Means ± SD between cells (n = 20 for mouse control, n = 40 for all others) are indicated. *: p-value < 0.05; ****: p-value < 0.001, Wilcoxon rank sum test comparing distributions. **C** Average cell cycle phase durations in each condition. Error bars indicate SD between cells. **D** Same data as in C, but the fraction of individual cell cycle phases of the total cell cycle duration is shown. Error bars indicate SD between cells.

2.6.3 Neural differentiation appears unaffected by mTOR inhibition

If cell cycling was required for neural differentiation, the expression onset of neural marker genes would be delayed in mTOR inhibitor-treated cells where the cell cycle is drastically elongated. In case of direct coupling of differentiation to the cell cycle, differentiating mTORi-treated human and cynomolgus cells should thus acquire neural marker expression 50% later than control cells. Based on previous NPC differentiation time courses, this would mean that PAX6 expression in cynomolgus and human would be shifted from day 3 to day 4.5 and SOX1 from day 2 to day 3 of differentiation upon mTOR inhibition. In mouse, the difference is expected to be much smaller or absent.

To test this, I performed a neural differentiation time course in mouse, cynomolgus and human cells where I treated half of the cells with 50 nM INK128 and let the other half differentiate without mTOR inhibition (control). Cells were fixed daily and stained for neural markers PAX6, SOX1 and pluripotency marker OCT4. As expected from the cell cycle measurements, mTOR inhibition did not influence mouse differentiation. PAX6 and SOX1 onset and OCT4 decrease were similar in mouse control and treated cells (Figure 20A-C). Unexpectedly however, PAX6 onset was not delayed in either cynomolgus or human cells (Figure 20A). PAX6 signal rose at day 3 in the control and mTORi condition. SOX1 signal was slightly weaker in the mTORi condition at day 2 in both cynomolgus and human (Figure 20B). However, the onset was not delayed until the expected day 3, suggesting that early neural marker onset is not affected by mTOR inhibition to the expected degree. Only OCT4 signal revealed a difference between control and mTORi-treated cells (Figure 20C). This was most pronounced in human, where OCT4 was maintained until day 4 in mTORi-treated cells whereas OCT4 was not detected after day 3 in control cells. The delay in OCT4 downregulation however, does not necessarily constitute evidence for an mTORi-mediated differentiation delay. A decrease in protein levels can be caused by active degradation or cell division-dependent dilution. Since mTORi-treated cells cycled slower and therefore divided less than control cells, OCT4 signal could be maintained through lack of protein dilution.

In conclusion, mTOR inhibition did not affect neural differentiation drastically, suggesting that differentiation speed does not depend on cell proliferation speed. However, differentiation outcome cannot be precisely evaluated solely based on PAX6 and SOX1 expression. To better understand the differentiation status of mTORi-treated cells, I sought to characterize differentiation more globally using single cell transcriptomics.

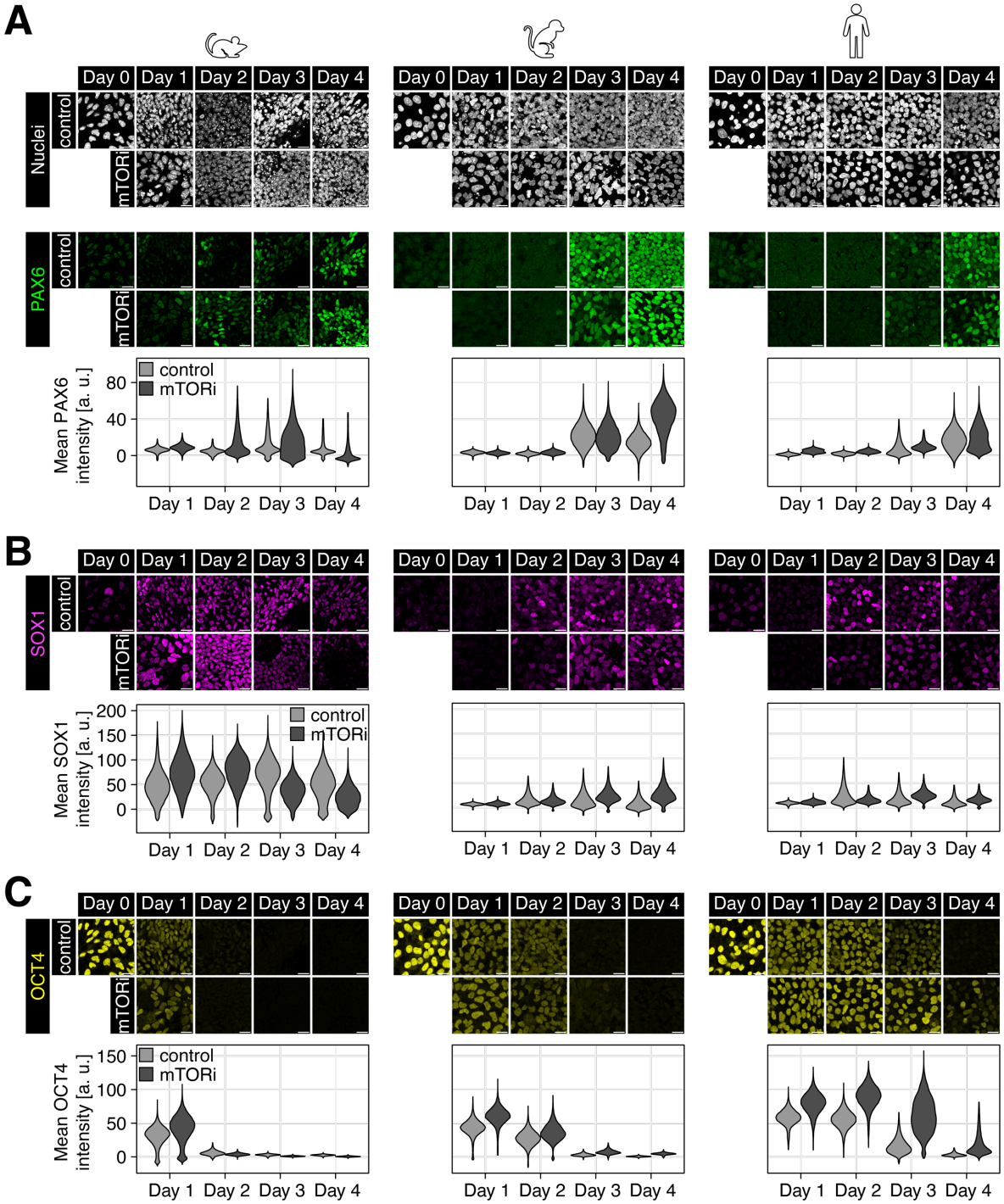

Figure 20: mTOR inhibition does not have an apparent effect on neural differentiation onset.
A Immunostaining of an NPC differentiation time course in mouse, cynomolgus and human. Cells were either differentiated without mTOR inhibitor (control) or treated with 50 nM mTOR inhibitor INK128 from day 0 onwards (mTORi). The nuclear channel (Hoechst33258) indicates nuclear positioning (top), PAX6 marks early neural differentiation. Immunofluorescence images (middle) and single cell PAX6 intensity measurements (bottom) are shown. **B** Same staining as in A, but SOX1 signal and quantification are shown. **C** Same as in A, B but OCT4 images and quantification are shown. Scale bars = 20 µm. Immunostaining image brightness was adjusted species-wise, nuclei brightness was adjusted image-wise. Segmentation performed using StarDist 2D, outlier removal and background subtraction done as described in chapter 5.5.3. Violins were set to the same maximum width.

2.6.4 Multiplexed single-cell RNA sequencing of mTOR-inhibited cells

To examine the differentiation status of mTOR-inhibited cells and analyze the expression of multiple neural markers at once, I used single-cell RNA sequencing. Mouse, cynomolgus and human cells were seeded following the NPC differentiation protocol and INK128 treatment was started in parallel to neural induction. Days 0 (pluripotent control), 2 and 4 were sampled for single-cell RNA sequencing (Figure 21A). The experiment was conducted in parallel to the RbTKO sequencing experiment. Cells were labeled with a CMO for sample demultiplexing as described before.

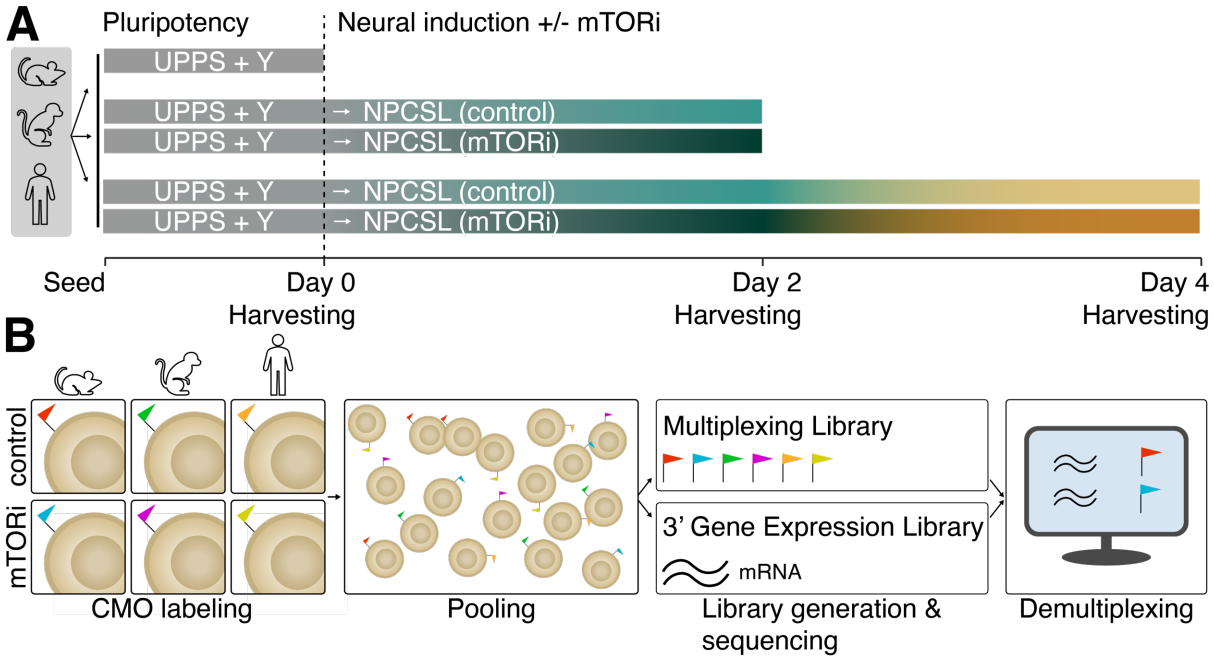

Figure 21: Schematic representation of experimental set-up for single cell-RNA sequencing.
A Mouse, cynomolgus and human cells are seeded in UPPS + Y. After one day, cells are changed to NPC medium +/- mTOR inhibitor. At days 0, 2 and 4, cells were harvested for single-cell sequencing. **B** Work flow for multiplexed single-cell sequencing. Samples are labeled with a unique CMO and pooled. A Multiplexing Library and a 3' Gene Expression Library are generated and samples are bioinformatically demultiplexed.

2.6.5 mTOR inhibited cells form distinct clusters in cynomolgus and human

For data visualization, I performed non-linear dimensionality reduction shown as UMAP projections (McInnes et al., 2020). In cynomolgus and human, all conditions, i. e. time points and control/mTORi treatment, were separated in UMAP space (Figure 22A, F). The day 0 cells occupied two distinct regions in the UMAP plot, one consisting of the majority of cells, and another containing fewer cells. In both species, but especially in cynomolgus, control and mTORi-treated cells were closer together at day 2 than at day 4.

To quantitatively assess how different or similar the different time points and the control versus the mTORi conditions were, they were clustered by unsupervised Louvain clustering. I used different clustering resolutions to test if cells can cluster (1) purely based on the sampling time

point irrespective of the mTORi treatment and (2) based on their sample identity in which case I can distinguish control from treated cells based on their transcriptome. At a resolution of 0.01, cynomolgus cells clustered according to their sampling time (Figure 22B). Day 0, 2 and 4 each occupied their own cluster. A fourth cluster (cluster 3) mainly consisting of day 0 cells was found, corresponding to the day 0 cells that were localized away from the other day 0 cells in UMAP space. At higher clustering resolution (0.25), seven clusters were detected. Most cells were grouped according to sample identity, confirming that control and mTORi-treated cells can be distinguished based on their transcriptome (Figure 22C). Quantification of the clustering analysis showed that day 4 control and mTORi-treated cells were well separated while the day 2 control and mTORi-treated cells occupied a main cluster but partially split into different clusters (Figure 22E).

In human, low-resolution clustering (0.03) clustered cells into three distinct groups according to their sampling time (Figure 22G, I). At a higher resolution of 0.20, human cells were grouped into eight clusters according to their sample identity (Figure 22H, J). Day 0 fell in clusters 2 and 6 with the majority of cells (79%) falling into cluster 2, and a smaller subgroup into cluster 6 (21%). In contrast to cynomolgus, the human day 2 samples occupied only one main cluster each (clusters 3 and 5). The day 4 control sample split between clusters 0 and 4 while the mTORi-treated day 4 cells almost exclusively occupied cluster 1 (Figure 22J).

In summary, control and mTORi-treated cells can be distinguished based on their transcriptome showing that mTORi had an effect on the cells. Since mTORi-treated cells were mostly only assigned to one cluster with the exception of day 2 in cynomolgus, it appears unlikely that mTORi treatment drives unspecific or random differentiation along multiple trajectories.

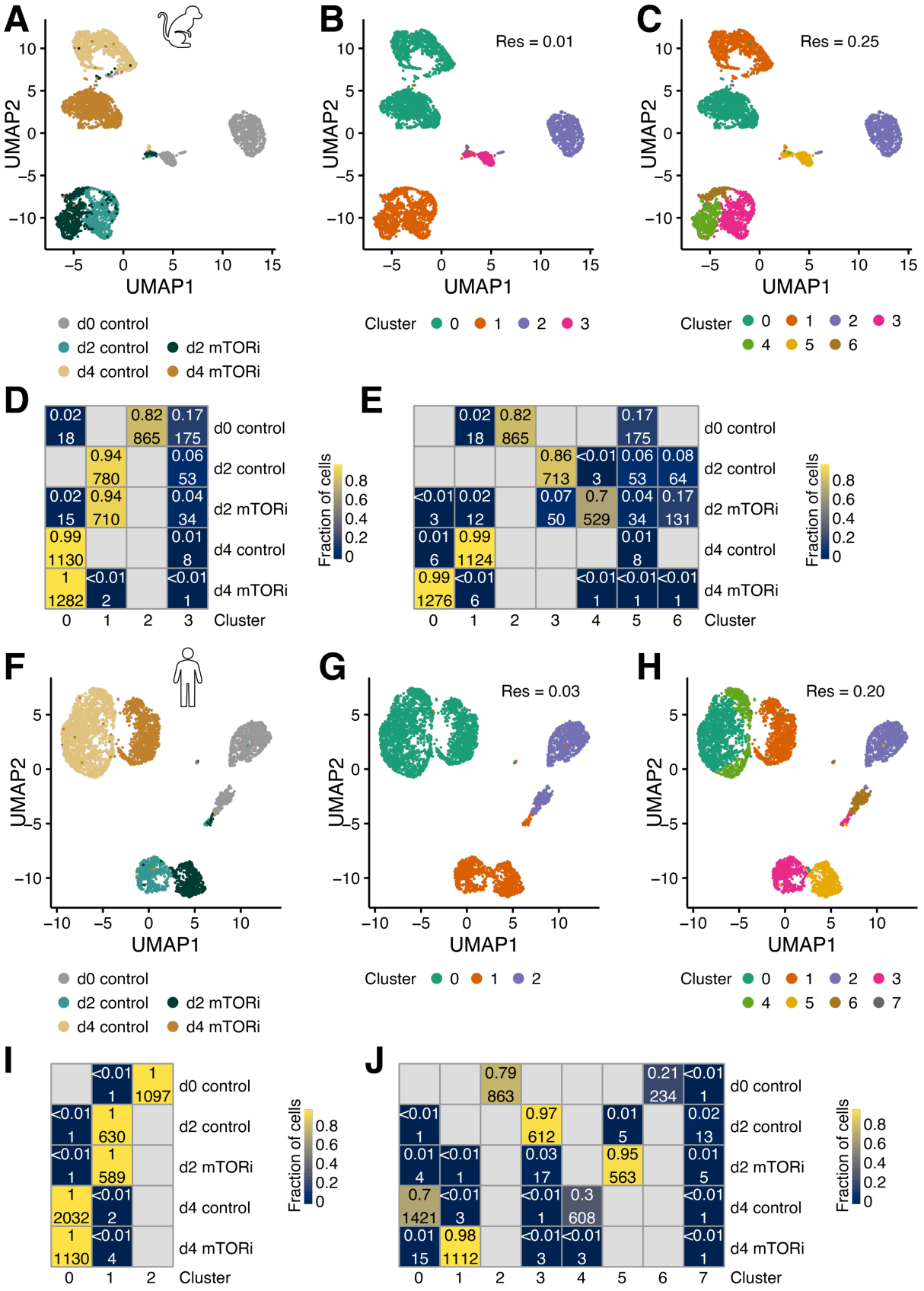

Figure 22: mTORi-treated cells form distinct clusters in cynomolgus and human.
A UMAP projection of cynomolgus scRNAseq data. Colors correspond to indicated sample identities. **B** Low-resolution (0.01) Louvain clustering separates cells after sampling time. Colors correspond to indicated cluster identities. **C** High-resolution (0.25) clustering groups cells according to their sample identity. **D** Quantification of clustering shown in B. Numbers in top of each tile show the fraction of cells in each row per indicated cluster. Numbers in tile bottom indicate

number of cells per row and cluster. Colors correspond to the fraction of cells per row and cluster. **E** Same quantification method as in D, but with data from C. **F** UMAP projection of human scRNAseq data. Colors correspond to indicated sample identities. **G** Low-resolution (0.03) clustering of human sequencing data splits cells according to their sampling time. **H** High-resolution (0.20) clustering groups cells after their sample identity. **I** Clustering quantification as in D, E, but with human low-resolution clustering data from G. **J** Clustering quantification with high-resolution clustering data from H.

2.6.6 Mouse mTORi-treated cells are more similar to control cells than in the primates

Of all species tested, the mouse cell cycle was affected least by mTOR inhibition (Figure 18, Figure 19). Therefore, I expected the transcriptomic effect of mTOR inhibition to be smaller in mouse than in the primates. In line with the expectation, mouse control and mTORi-treated cells were localized in close proximity in UMAP space (Figure 23A). Unsupervised clustering at a resolution of 0.05 grouped cells into three clusters which corresponded to sampling time, irrespective of mTORi (Figure 23B, D). Increasing the clustering resolution did not result in a clean separation of control and mTORi-treated cells as in cynomolgus and human. At a resolution of 0.39, cells of the same sample identity fell into separate clusters but mTORi-treated cells could still not be distinguished from control cells (Figure 23C, E). For example, both, control and mTORi-treated cells, split between clusters 2 and 4 at day 2 and between clusters 1 and 3 at day 4 in similar proportions. These results indicate that mouse cells are heterogeneous during NPC differentiation and mTORi-treated cells are similar to control cells. Differences between treated and untreated cells are smaller than naturally occurring heterogeneities, caused by e. g. the cell cycle phase. Species-specific mTOR inhibition effect sizes observed for cell cycle durations are thus reflected on the transcriptomic level.

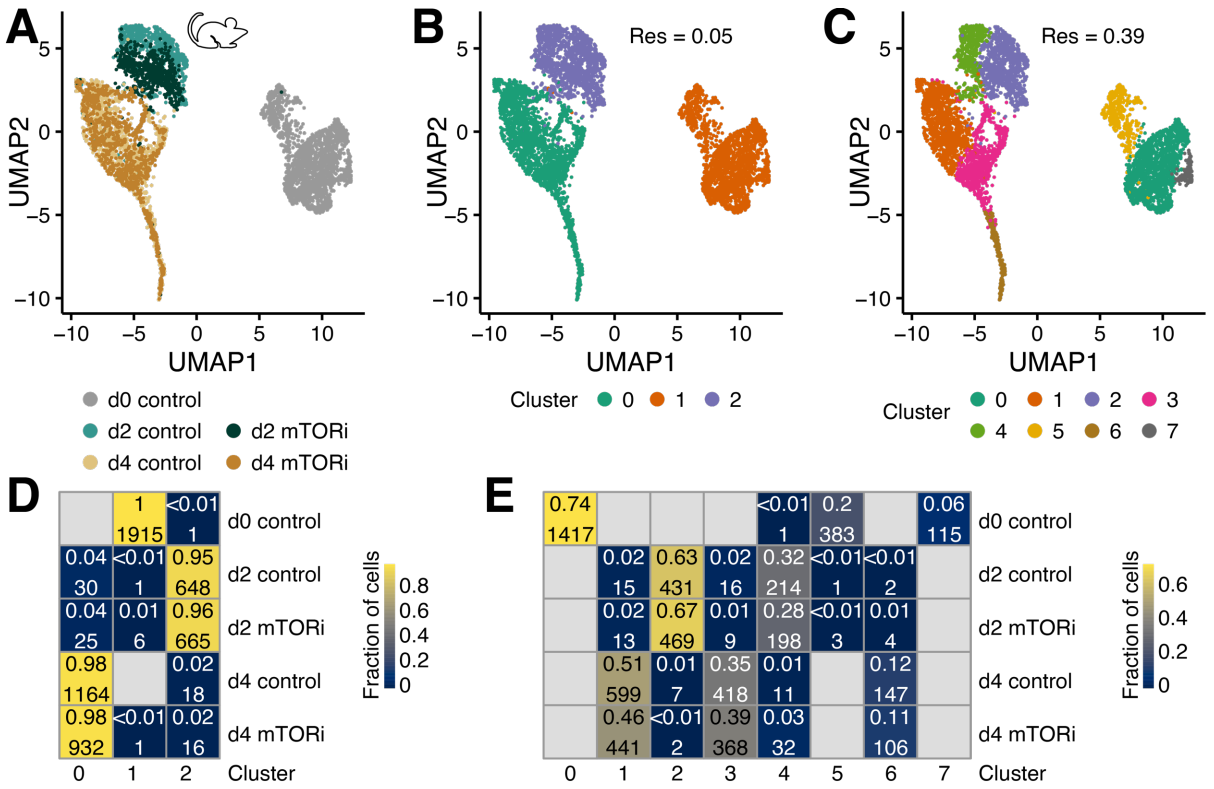

Figure 23: mTORi-treated mouse cells do not form distinct clusters.
A UMAP projection of mouse single cell sequencing data. Colors indicate the sample identity. **B** Low-resolution (0.05) clustering groups cell after their sampling time. **C** High-resolution (0.39) clustering distinguishes eight clusters that did not differentiate between control and treated cells. **D** Quantification of low-resolution clustering. **E** Quantification of high-resolution clustering. Rows in D and E correspond to sample identities, columns to detected clusters. Each tile in D + E shows the fraction of cells in each cluster (top number, also color-coded) and the absolute number of genes per cluster (bottom number).

2.6.7 Early neural marker expression is unaffected by mTOR inhibition

Next, I wanted to test for successful NPC differentiation in the single cell RNA sequencing experiment. Furthermore, I sought to compare differentiation in untreated control and mTORi-treated cells, since they formed distinct clusters in cynomolgus and human, raising the question, if they also differ in their differentiation status. I checked the sequencing data for several early neural markers as well as the two pluripotency markers *POU5F1* (encoding OCT4) and *NANOG*. Both control and mTORi-treated cells showed an upregulation of neural markers and downregulation of pluripotency markers over the differentiation time course, indicating successful NPC differentiation in both conditions (Figure 24). *NANOG* was downregulated very abruptly in all species and conditions, *POU5F1* expression persisted in cynomolgus and human until day 2 of differentiation. The *POU5F1* expression level and percentage of expressing cells was very similar between control and mTORi-treated cells, suggesting that different OCT4 levels observed on the protein level are caused by reduced protein dilution in the less proliferative mTORi-treated cells. In line with previous immunostainings, mouse showed early *PAX6* expression at day 2 in a subset of cells at a low level (Figure 24A) while the primate species only showed *PAX6* expression at day 4 (Figure 24B, C). There was a minor difference in *PAX6* levels

between control and mTORi-treated cells at day 4 in cynomolgus and human, but in different directions; cynomolgus control cells had higher *PAX6* expression in a slightly larger subset of cells than mTORi-treated cells but human mTORi-treated cells had a slightly higher average expression than control cells (Figure 24B, C). Similarly, no clear difference between control and mTORi-treated cells was observed for a selection of other neural marker genes, namely *SOX1*, *SOX2*, *MAP2*, *NESTIN*, *DCX*, *SOX5* and *SOX6*, indicating that mTOR inhibition does not systematically change the expression of the analyzed marker genes.

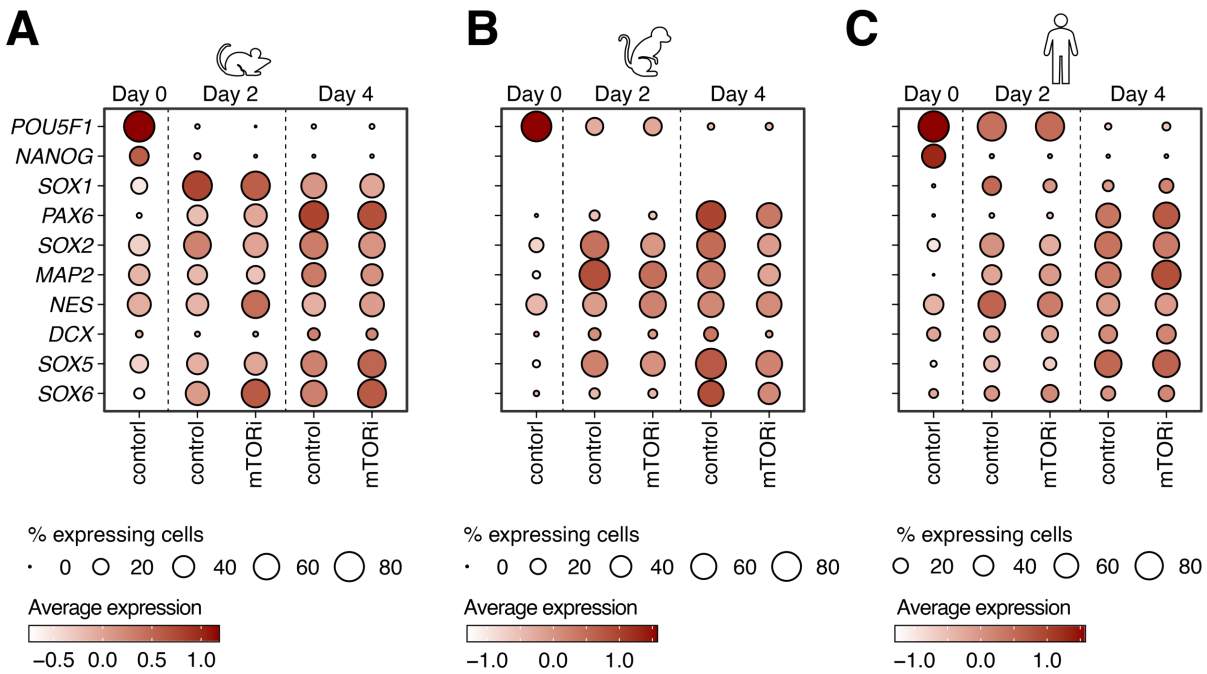

Figure 24: Early neural marker expression is similar between control and mTORi-treated cells.
A Selection of pluripotency and early neural markers during mouse differentiation. Color indicates average expression and dot size shows what percentage of cells expressed the respective marker. **B** Same as in A but for cynomolgus. *NANOG* and *SOX1* are not annotated in the genome. **C** Same as in A, B but for human.

2.6.8 NPC-related genes are differentially expressed upon mTOR inhibition

To assess the effect of mTOR inhibition in an unbiased manner, I focused on the differentially expressed genes between control and mTORi-treated cells at day 4 of NPC differentiation. Expectedly, only few genes were differentially expressed between treated and untreated cells in mouse (36 genes differentially expressed with an adjusted p-value < 0.01 and average log2FC > |1|). With 774 up- or downregulated genes, cynomolgus had the most differentially expressed genes between mTORi-treated and control cells, followed by human with 641 differentially expressed genes (Figure 25A). In all species, mTOR inhibition led to down- and upregulation of gene expression to similar degrees with no clear trend in either direction. Part of the downregulated genes under mTOR inhibition (*PGK1*, *PKM*, *LMAN1*) was related to metabolism, as is expected upon mTOR inhibition (Figure 25A). Interestingly, the upregulated genes in

cynomolgus and human included genes like *SLIT2*, *PAX3*, *NRG3* and *NXPH2* which are connected to neural development (Figure 25A). To functionally assess the differentially expressed genes, I performed GO term analysis of all significantly down- and upregulated genes, focusing on biological processes. Due to the low number of differentially expressed genes, GO term analysis of mouse cells has to be interpreted with caution. In the upregulated genes upon mTORi of mouse and human, GO terms related to neurogenesis were significantly enriched (Figure 25B). This indicates that mTOR inhibition did not slow down neural differentiation but rather the opposite. However, both primate species but especially human, also upregulated genes linked to other differentiation paths than neural, e. g. circulatory system development, renal and urogenital system development and kidney development (Figure 25B) which could indicate deregulated, unspecific differentiation upon mTOR inhibition.

GO term analysis of downregulated genes in mTORi-treated cells showed no clear trend in mouse (Figure 25C). In cynomolgus, however, downregulated genes were mostly categorized as neurodevelopmental. In human, the top 10 most downregulated GO terms were related to metabolism and specifically purine metabolism. Neurodevelopmental terms were also present in human but unlike in cynomolgus, these terms were not represented in the top 10 most significantly enriched terms (Figure 25C). As neurodevelopmental terms were enriched among the downregulated genes under mTOR inhibition in cynomolgus, it is conceivable that mTOR inhibition impairs neural differentiation. On the other hand, in human, neural terms were enriched among the upregulated genes under mTOR inhibition, together with terms linked to other differentiation paths. This could suggest that mTORi-treated cells activate other differentiation programs at the expense of neural differentiation.

If mTOR inhibition delayed NPC differentiation, there would only be NPC-related GO terms among the downregulated genes in mTORi-treated cells. Since these terms were found among the down- and upregulated genes, it is likely that NPC differentiation was affected but not necessarily delayed by mTOR inhibition.

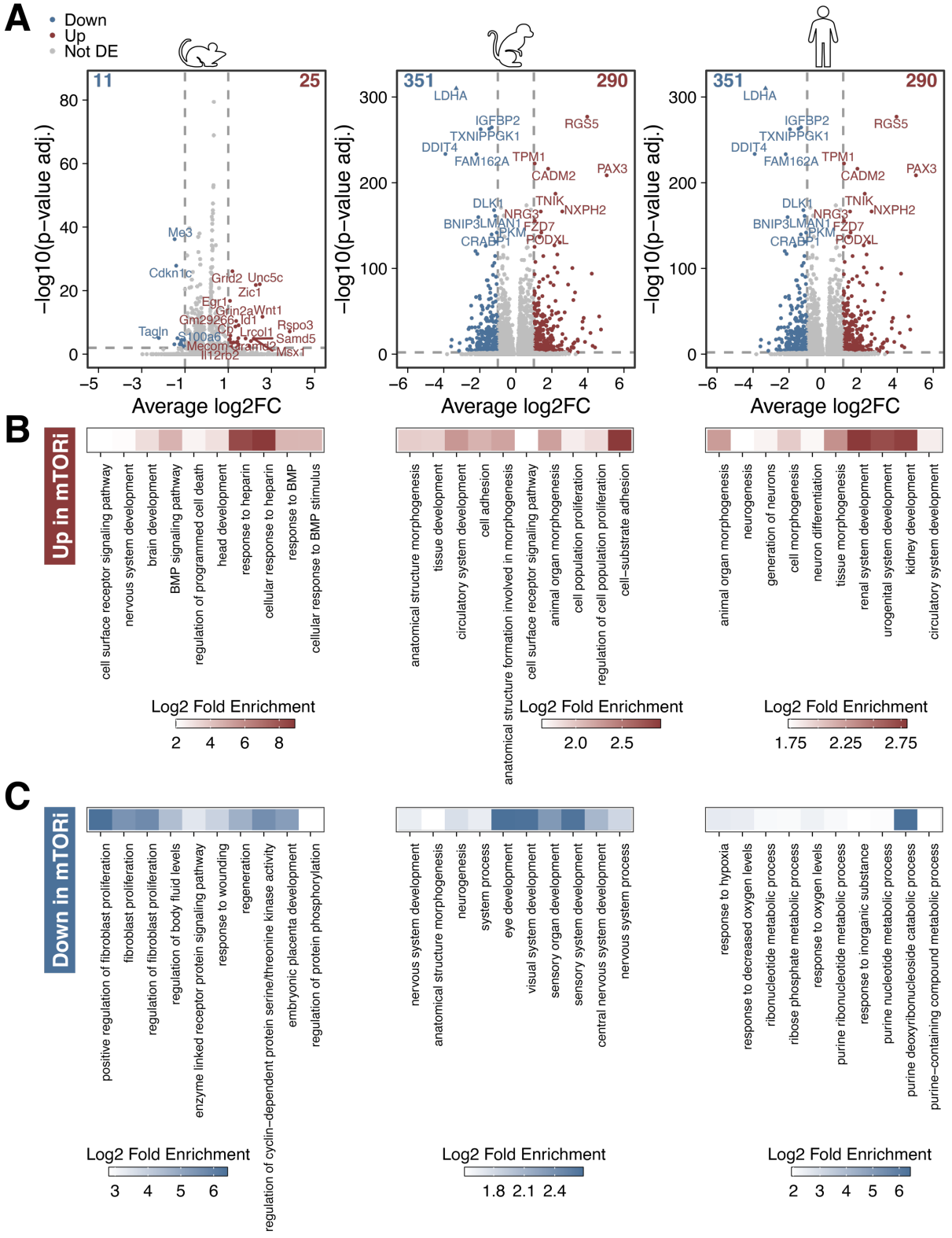

Figure 25: NPC-related GO terms were among the differentially expressed genes upon mTOR inhibition.
A Volcano plots showing the differentially expressed genes between mTORi-treated and control cells at day 4 of NPC differentiation in the three species. Downregulated genes in mTORi versus control are displayed in blue, upregulated genes in red. Genes were considered differentially expressed with an adjusted p-value < 0.01 and an average log2FC > |1|. Of these genes, all with an average log2FC > 0 were upregulated and all with average log2FC < 0 downregulated. All other genes were considered not differentially expressed (gray). Vertical dashed lines indicate the log2FC cut-off for up- and downregulated genes, horizontal dashed lines indicate the adjusted p-value cut-off. The top 20 most significantly differentially expressed genes are indicated. Numbers at the top show the number of up- and downregulated genes for each species. **B** Heatmaps displaying the top 10 most significantly enriched biological

processes among the upregulated genes shown in A. **C** Heatmaps displaying the top 10 most significantly enriched biological processes among the downregulated genes.

2.6.9 NPC differentiation occurs normally under mTOR inhibition

Since the direct comparison of control and mTORi-treated cells did not give conclusive results, I examined differentiation in control and mTORi-treated cells by comparing the significantly differentially expressed genes of day 4 versus day 2 of differentiation in control and mTORi-treated cells (Figure 26A). This way, I compared all genes that were different between a later and an earlier time point of differentiation in control and mTORi-treated cells. In both conditions, several significantly differentially expressed genes were found. In all species, more genes were significantly downregulated between day 4 and 2 than upregulated (Figure 26B, D). No clear trend emerged when comparing the number of differentially expressed genes between control and mTORi-treated cells. Strikingly, mouse had the least differentially expressed genes, followed by cynomolgus and human (Figure 26B). To characterize differentiation in control and mTORi-treated cells, I obtained the GO terms for all significantly differentially expressed genes at day 4 versus day 2 of differentiation. The heatmaps in Figure 26C show the top 10 most significantly enriched GO terms among the upregulated genes in the day 4 versus day 2 comparison (sorting based on control condition) in control and mTOR inhibition. In all species, GO terms related to neural differentiation were enriched in the control and the mTORi condition. Only GO terms related to cell division and cell cycling were not present in the mTORi-treated cells (Figure 26C, right). This suggests that NPC differentiation in the mTORi-treated cells was not perturbed. The top 10 biological processes in the downregulated genes at day 4 were mostly unrelated to differentiation or pluripotency (Figure 26E). Like the GO terms for the upregulated genes, they were largely shared between mTORi-treated and control cells, indicating that mTOR inhibition does not drastically alter the NPC differentiation process.

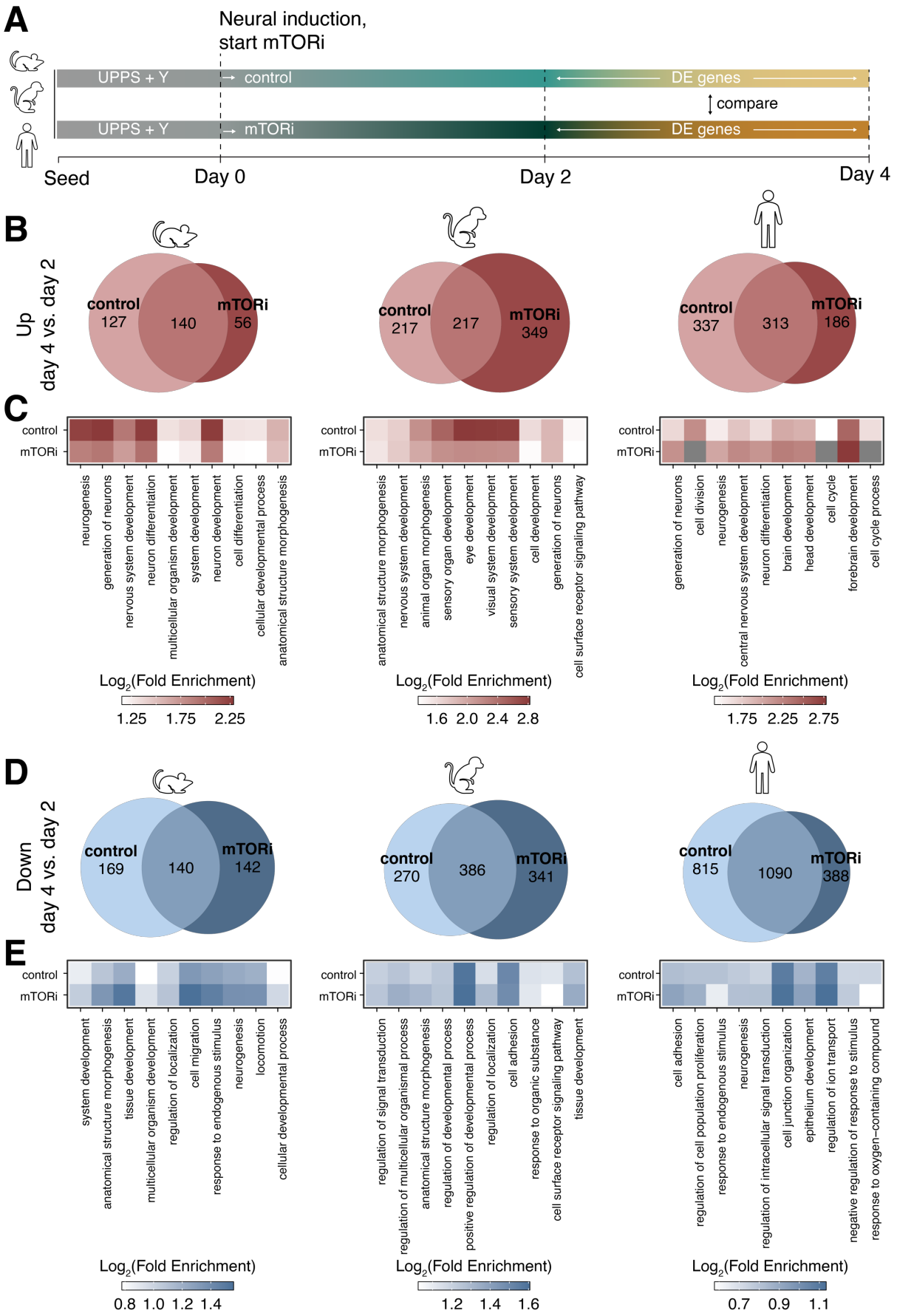

Figure 26: mTORi-treated cells differentiate normally.

A Schematic depicting analytical strategy. **B** Euler diagrams showing significantly higher expressed genes in day 4 cells versus day 2 cells comparatively in control and mTORi-treated cells (adjusted p-value < 0.01, average log2FC > 1) **C** The top 10 most significantly enriched GO terms in the significantly higher expressed genes at day 4. Sorting of the most significant GO terms is based on the control sample. Coloring indicates the log2 fold enrichment. **D** Euler diagrams showing significantly lower expressed genes in day 4 cells versus day 2 cells comparatively in control and mTORi-treated cells (adjusted p-value < 0.01, average log2FC < -1) **E** The top 10 most significantly enriched GO terms in the significantly lower expressed genes at day 4 versus day 2. Sorting of the most significant GO terms is based on the control sample. Coloring indicates the log2 fold enrichment.

2.6.10 mTOR inhibition does not cause a systematic differentiation delay

To determine the differentiation status of mTORi-treated cells versus control cells, I made use of the time-resolved scRNAseq data set obtained by my collaborators (Helmholtz Munich) as described before. Via integration of the mTORi sequencing data with the reference data set that spans eight time points of NPC differentiation, I can assess to which time point in the reference data the mTORi-treated cells best corresponded. Using the Scanpy function *ingest* (Wolf et al., 2018), the mTORi data (query) from each species were integrated with the time-resolved reference data set of the corresponding species. Figure 27A, D, G show the reference data with color-coding indicating the sampling time point. Through *ingest* integration, the mTORi data was forced into the UMAP embedding of the reference data (Figure 27B, E, H). Visual comparison of the mTORi data in the UMAP (Figure 27B, E, H) with the reference sampling time (Figure 27A, D, G) reveals that the query sampling time points follow a similar temporal trajectory as the reference. mTORi-treated and control cells mostly occupied the same regions of the reference UMAP, suggesting that they were in a similar differentiation state. Next, I quantified the proportion of query cells that were assigned to each reference time point. The majority of mouse control and mTORi-treated cells was assigned to the same time point (Figure 27C) which was expected since the mouse cell cycle did not strongly respond to mTOR inhibition.

In cynomolgus, the day 2 control sample corresponded best to the day 2 reference (83%); the day 2 mTORi sample however, was mostly assigned to day 1 (63%), indicating that control cells are more advanced than mTORi-treated cells (Figure 27F). Of all day 4 control cells, 52% were assigned to day 4, but for mTORi, it was only 26%. The majority of day 4 mTORi-treated cells (57%) corresponded best to day 7 in the reference, suggesting that they were further progressed than control cells.

In human, both control and mTORi-treated cells differentiated slower than the reference (Figure 27I). Most day 2 cells were assigned to day 1 in both conditions, however, 22% of control cells were assigned to day 2. Similarly, the day 4 samples mostly fell into the day 3 group. Surprisingly, half of the day 4 cells were assigned to days 7 and 10 in the control and only to day 10 in mTORi, suggesting that differentiation at day 4 was very heterogeneous in human. Furthermore, it shows that the 'fast' cells under mTORi were even further advanced than 'fast' cells in the control (control: 22% assigned to d10, mTORi: 49% assigned to day 10).

Overall, this analysis allows for the determination of a cell's biological state. While mTORi-treated cells at day 2 tended to be less advanced than control cells, this effect was not seen at the later day 4. In fact, day 4 mTORi-treated cells even corresponded to later time points than the control. Taken together, these results suggest that mTOR inhibition does not systematically delay NPC differentiation.

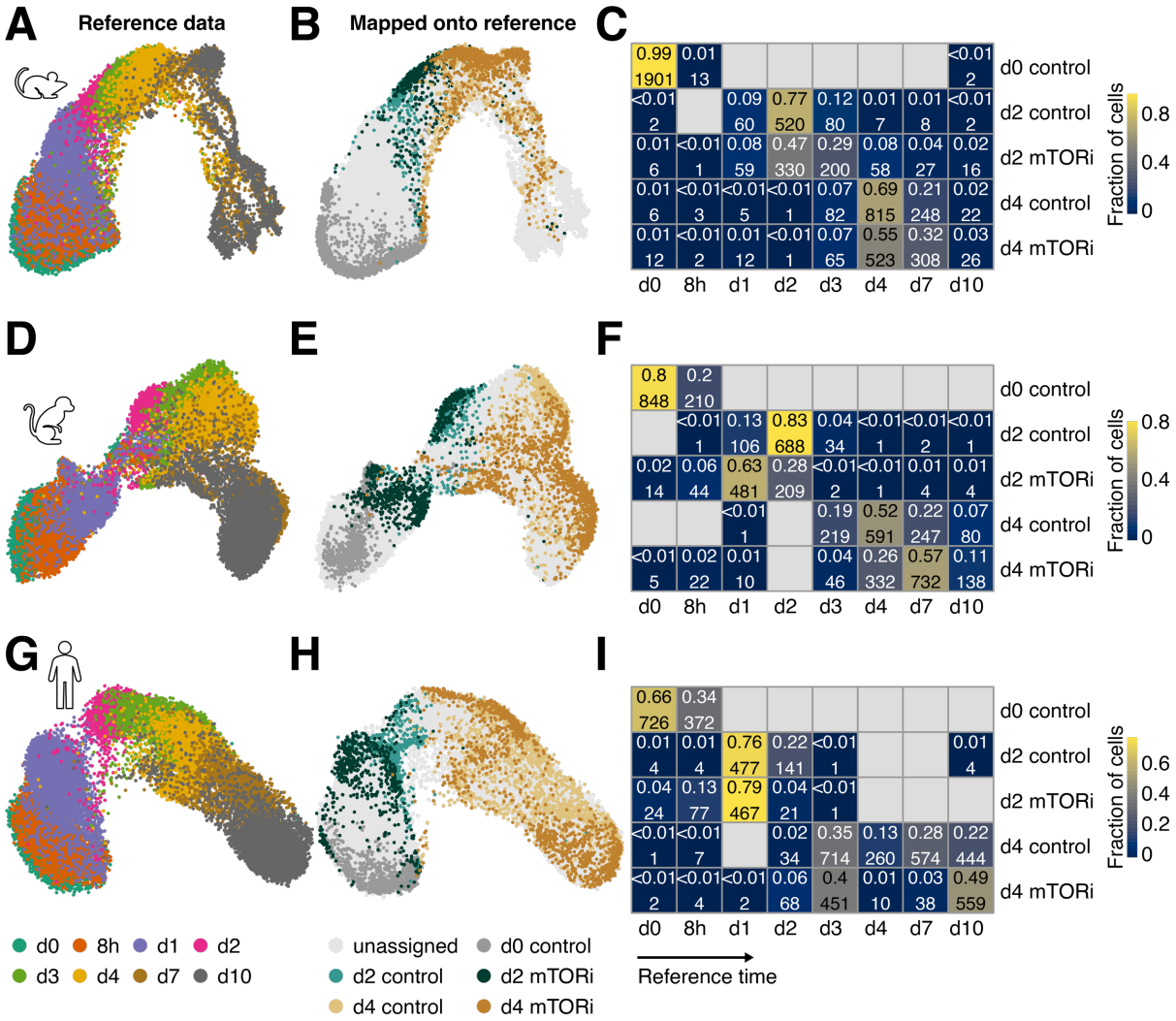

Figure 27: Integration with a time-resolved reference data set shows that mTORi-treated cells are not systematically delayed during NPC differentiation.
A UMAP representation of mouse reference data set spanning from day 0 to day 10 of NPC differentiation. **B** Mouse mTORi scRNAseq data mapped onto reference data set. **C** Quantification of B. The heatmap shows how many cells from each sample of the mTORi experiment were mapped onto which time point of the reference data set. Each tile indicates the proportion (top) and the absolute number (bottom) of cells of the corresponding sample mapped onto a specific time point. **D-F** Same analysis as in A-C, but for cynomolgus. **G-H** Same analysis, but for human. Legend in bottom indicates color coding for all species.

2.6.11 PAX6 onset is independent of mTOR inhibition

Single-cell RNA sequencing showed that neural differentiation was not delayed in mTORi-treated cells. Still, it was possible that mTOR inhibition delayed differentiation on a smaller time scale that could not be resolved with scRNAseq. Therefore, I wanted to test the influence of mTOR

inhibition on NPC differentiation with higher temporal resolution. I obtained a human ESC line with an endogenously tagged *PAX6* gene (H9 PAX6::H2B-GFP from Tchieu et al., 2017) and sought to perform time-lapse imaging under mTORi treatment and track the emergence of the *PAX6* reporter. The cells were adapted to UPPS and tagged with an H2B-Cerluean reporter to facilitate cell tracking using the piggyBAC system. I seeded reporter cells and kept them in UPPS + ROCK inhibitor overnight, then changed them to neural differentiation medium with and without mTOR inhibitor INK128. Imaging was performed on a widefield microscope for up to five days. Reporter cells under mTOR inhibition were however less viable than control cells. I changed different parameters of the experiment to be able to compare *PAX6* onset with and without mTOR inhibition and finally increased the starting cell number from 125,000 cells/cm^2 to 250,000 cells/cm^2 and reduced the concentration of mTOR inhibitor INK128 from 50 nM to 30 nM and 40 nM. Since I knew PAX6 emergence to be between day 2 and 3 of differentiation from previous immunostainings, I started image acquisition only after one day of differentiation. Cells were then imaged for five consecutive days in 30 min intervals (Figure 28A, B). Following image acquisition, cells were segmented based on H2B-Cerulean signal in each frame and fluorescence was measured in the PAX6::H2B-GFP channel. Since media changes introduced slight focal shifts and intensity changes due to removal of fluorescent debris, I measured PAX6::H2B-GFP intensities after subtraction of a Gaussian blur image of the same frame. This did not completely even out the effect of media changes and noise caused by fluorescent debris but confirmed that PAX6::H2B-GFP signal steadily rose from just before 72 hours of differentiation on under control conditions (Figure 28C). This was in line with previous observations from immunostainings. PAX6::H2B-GFP increase was comparable in control and mTORi conditions, with the first notable rise in PAX6::H2B-GFP signal around the 72 hours mark. After that, the signal kept rising until the end of the time series. The curves for control and 30 nM/40 nM INK128 treatment were very similar although signal increase under mTORi slowed down at ~ 100 hours while signal in the control cells kept rising (Figure 28C). However, despite of the noise in the mTORi conditions, it can be concluded that *PAX6* onset was not drastically different between control and mTORi-treated cells. Taken together, I show that mTOR inhibition drastically changes the cell cycle duration in primate cells, however, scRNAseq showed that NPC differentiation was not delayed in mTORi. Analysis of the early neural marker PAX6 at higher temporal resolution also suggests that reporter onset was not affected on a smaller time scale. Collectively, these results suggest that NPC differentiation can be uncoupled from cell cycling and growth.

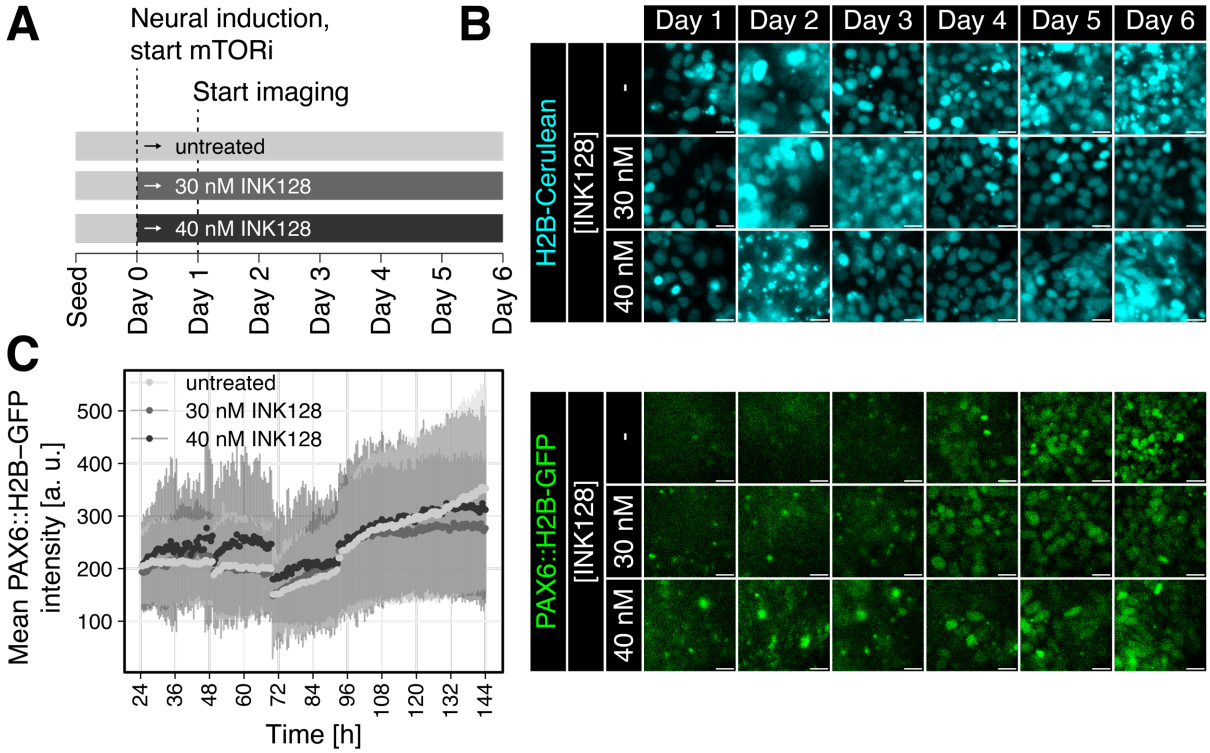

Figure 28: PAX6 onset is unaffected by mTOR inhibition.
A Schematic representation of experimental procedure. Cells were seeded and differentiation +/- mTORi inhibition (30 nM and 40 nM INK128 respectively) started at day 0. **B** Stills of a time-lapse imaging experiment, showing the nuclear H2B-Cerulean signal (top) and the PAX6::H2B-GFP reporter (bottom). **C** Average PAX6::H2B-GFP ± SD signal over a five-day differentiation time course. Representative data of N = 2 experiments are shown.

2.6.12 FOXG1 is upregulated upon mTOR inhibition

Despite its drastic effect on the cell cycle, mTOR inhibition did not delay early neural differentiation. To confirm that mTOR inhibition and, as a consequence, also cell cycling do not delay differentiation, I focused on a later time point of NPC differentiation. Later during differentiation, cells have been subjected to mTOR inhibition for longer and the discrepancy in cell cycle numbers between control and treated cells is larger. I differentiated cells with and without mTOR inhibitor for eight days and stained for the forebrain marker FOXG1 (Figure 29). FOXG1 is a transcription factor that localizes to the nucleus in NPCs and is cytoplasmic in differentiating cells (Regad et al., 2007). It inhibits early cortical differentiation and is associated with NPC proliferation (Hanashima et al., 2004; Hettige et al., 2022). If mTOR inhibition affects later differentiation, I expect a delay in FOXG1 expression. In mouse cells, I observed FOXG1 in the day 0 control along the whole cell body, suggesting unspecific antibody binding. The FOXG1 signal still outlined the cell body in mouse at days 7 and 8 of differentiation in the control condition, whereas in the mTORi cells, there was uniform background (Figure 29A, B). In cynomolgus, nuclear FOXG1 was faintly visible in very few cells at day 7 in the untreated control and in more cells upon mTORi treatment. The number of FOXG1 positive cells increased in both conditions at day 8 but surprisingly, there was more FOXG1 signal in the mTORi-treated cells.

(Figure 29A, B). No FOXG1 was detected in untreated human cells at days 7 and 8. Strikingly, nuclear FOXG1 was ubiquitously expressed in the mTORi-treated cells at days 7 and 8 (Figure 29A, B). Hence, mTOR inhibition did not delay FOXG1 expression but led to premature FOXG1 expression. This could suggest that neural differentiation is counterintuitively accelerated under mTOR inhibition. If this effect can be attributed to the cell cycle extension under mTOR inhibition or if it is a metabolic effect, has to be tested. Furthermore, it remains open whether other later NPC markers follow the same trend as FOXG1.

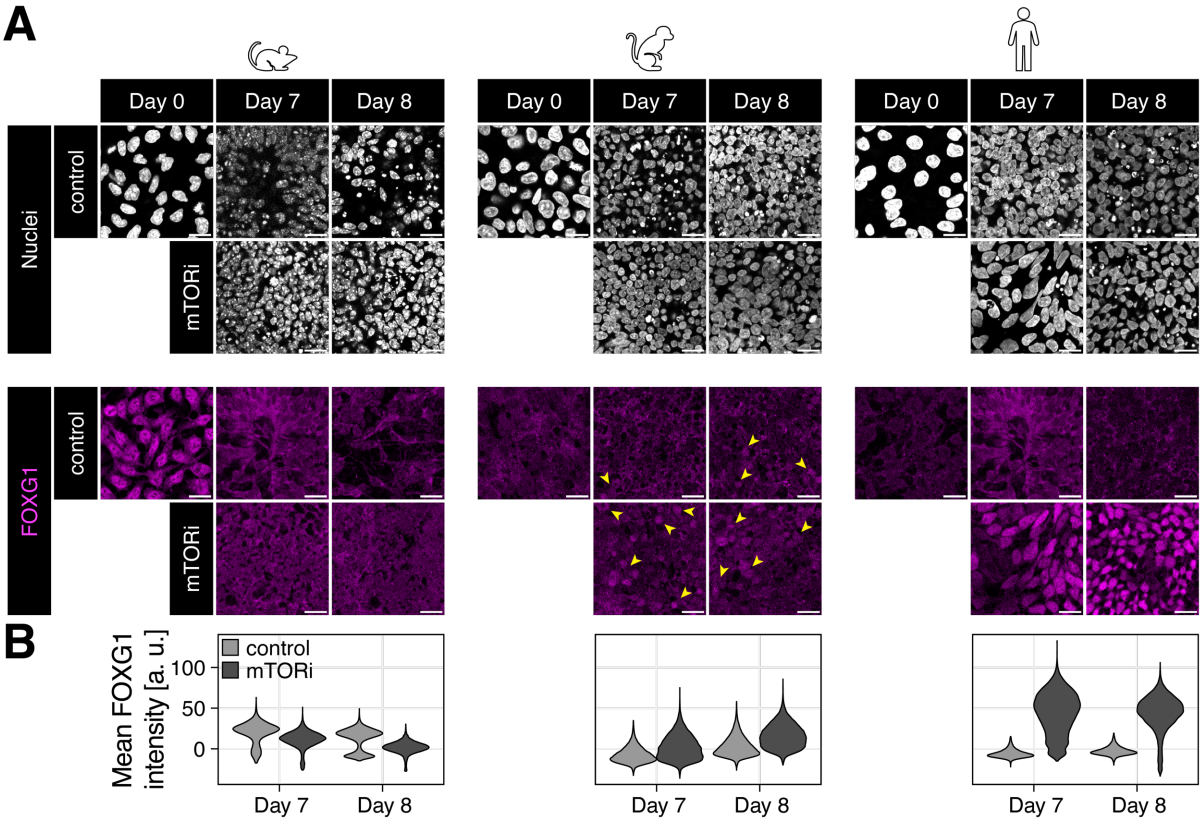

Figure 29: FOXG1 is upregulated in mTORi-treated cells.
A Immunostaining of a differentiation time course at days 0, 7 and 8. Nuclear staining (Hoechst33258) is shown in the top row (adjusted for each image), FOXG1 staining is shown in the bottom row (adjusted to the same minimum and maximum for all images). Arrow heads indicate FOXG1+ cells in cynomolgus. **B** Quantification of FOXG1 staining based on StarDist 2D segmentation as described in chapter 5.5.3. Violins were set to the same maximum width.

2.7 Glycogen metabolism influences NPC differentiation

Since I found that growth and differentiation speed can be uncoupled from each other, I explored alternative routes to find the underlying cause for species-specific differentiation timing. In an orthogonal approach to the hypothesis-driven cell cycle experiments, the time-resolved scRNAseq dataset of differentiating mouse, cynomolgus and human cells obtained by Alexandra de la Porte and Moritz Thomas (Helmholtz Munich) was used to identify candidate mechanisms to be involved in differentiation timing (Figure 8A). To reduce all differentially expressed genes between species and time points to a comprehensive list of candidate genes, we hypothesized

that timing regulation is most likely linked to metabolism. We used gene lists for several metabolic pathways and first compared the mean expression of all genes within a pathway between species and time points (Figure 30A). When a pathway showed different expression dynamics, i. e. genes were expressed more strongly at early time points in one species and more strongly at later time points in another, they were candidates for further analyses. In a second step, we focused on individual genes within a gene list (Figure 30A). Genes that exhibited different dynamics between species and time points were considered 'genes of interest'. These were then filtered further by comparing gene expression between cells which were assigned to the same differentiation state but stemmed from different sampling times (Figure 30A). For that, cells were grouped into differentiation states like 'pluripotency high' and 'pluripotency low'. If a cell from 'pluripotency low' was sampled at 8 h post induction, it was assigned to 'early cells'. A cell belonging to the same cluster but sampled at day 1 post induction was called 'late cell'. Of all genes, only the *UDP-glucose pyrophosphorylase 2* gene (*UGP2*) showed different expression dynamics between fast and slow species as well as between early and late cells (Figure 30B). *UGP2* catalyzes the generation of the glycogen precursor UDP-glucose + PP_i from glucose-1-phosphate + UTP (Adeva-Andany et al., 2016) and is thus crucial for glycogen sythesis. Therefore, we hypothesized that glycogen metabolism is a species-specific property.

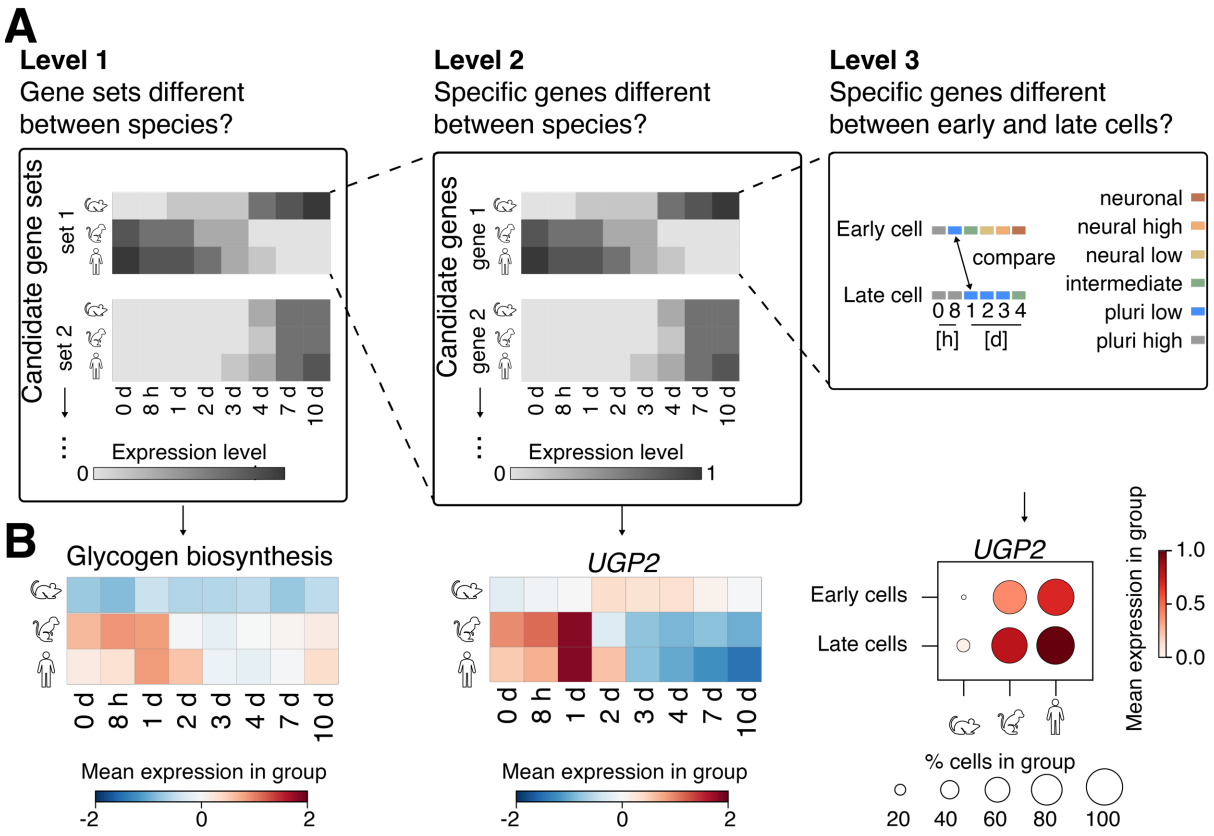

Figure 30: ScRNAseq identifies *UGP2* as a candidate gene for the regulation of differentiation timing.
A Schematic overview of filtering strategy to identify candidate mechanisms and genes that could be involved in differentiation timing. In level 1, a selection of candidate gene sets, typically revolving around a specific metabolic

pathway, is used to select potentially interesting gene sets. Gene sets were considered interesting, if the mean expression of all genes within the set exhibited different dynamics between species and time points. In level 2, gene sets of interest were screened for individual genes that exhibited different dynamics between species and time points. In level 3, genes of interest were compared between fast-differentiating (early) and slow-differentiating (late) cells within each species. For that, cells were assigned to different differentiation states (e. g. pluripotency high, pluripotency low). When a cell was sampled at 8 hours post induction but fell into pluripotency low, it was considered 'early', while a cell sampled at 1 day post induction and assigned to the same state was considered 'late'. **B** The strategy described in A was used to identify candidate genes. The gene set 'Glycogen biosynthesis' exhibited different dynamics in mouse and the primates. Within the gene set, *UGP2* showed the most striking difference between species. In the comparison of early and late cells, *UGP2* was also preferentially expressed in late cells.

2.7.1 Glycogen metabolism is species-specific

Using the single-cell sequencing data obtained for the mTOR inhibition experiment, I was able to reproduce previous results from my collaborators and saw that *UGP2* is highly expressed in the slower species and barely detectable in the mouse (Figure 31A). Next, I sought to examine the phenotypic relevance of differential *UGP2* expression between the species. Lower *UGP2* levels should result in low glycogen storage, thus, I determined glycogen concentrations in mouse, cynomolgus and human PSCs using a fluorometric assay where glycogen is hydrolyzed to glucose which is then oxidized and able to react with an OxiRed probe. Glycogen levels were significantly different between the three species (Figure 31B). At 0.058 ± 0.003 µg/10^3 cells, human PSCs showed the highest glycogen concentration, followed by cynomolgus PCS at 0.032 ± 0.002 µg/10^3 cells. Glycogen levels in mouse PSCs were lower than in primate PSCs by an order of magnitude at 0.004 ± 0.001 µg/10^3 cells (Figure 31B). Strikingly, glycogen content followed the same trend as differentiation speed and high glycogen levels were associated with slow differentiation. This makes UGP2 a promising candidate for the regulation of differentiation timing.

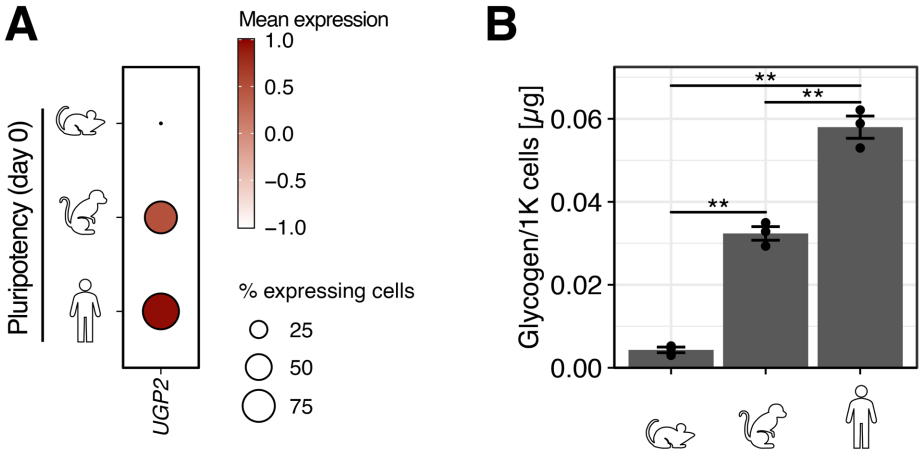

Figure 31: *UGP2* expression and glycogen content follow a species-dependent trend.
A Single-cell sequencing data showing the mean *UGP2* expression in PSCs of mouse, cynomolgus and human (color hue) and the percentage of *UGP2*-expressing cells (dot size). **B** Glycogen content in µg per 1000 cells in mouse, cynomolgus and human PSCs. Points indicate glycogen measurements of N = 3 experiments, the bar height shows the mean of the three measurements. Error bars correspond to the SE between experiments. **: adjusted p-value < 0.01, unpaired Student's t-test with Bonferroni correction.

2.7.2 Cellular glycogen content is drastically reduced upon UGP2 loss of function

Next, I wanted to test whether *UGP2* expression is linked to differentiation speed. In a 2020 publication, loss of *UGP2* in human ESCs led to premature neuronal differentiation (Perenthaler et al., 2020). If NPC differentiation is affected by *UGP2* loss, is unknown. We obtained two clones of the *UGP2* knock-out lines by Perenthaler et al. (2020) harboring an insertion in exon 2 of the *UGP2* gene, causing a frameshift and a premature stop codon. I measured glycogen levels in the *UGP2* knock-out lines and compared them to human wild type *UGP2* levels. The knock-out lines had significantly less glycogen than the wild type. *UGP2*-KO clone #1 and *UGP2*-KO clone #2 had barely detectable glycogen levels of 0.007 ± 0.001 µg glycogen/10^3 cells and 0.004 ± 0.001 µg glycogen/10^3 cells respectively (Figure 32). Thereby, *UGP2* knock-out glycogen levels were comparable to mouse levels (0.004 ± 0.001 µg/10^3 cells, Figure 31B) rather than human levels, showing that the species-specific trend in glycogen content depends on *UGP2* expression.

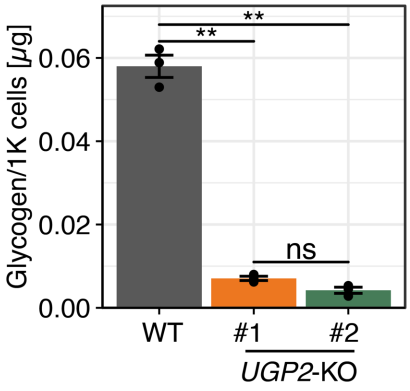

Figure 32: Knock-out of *UGP2* reduces glycogen levels.
Glycogen content in µg per 1000 cells in H9 wild type cells (data from Figure 31B) and two human *UGP2* knock-out lines (Perenthaler et al., 2020). Points indicate glycogen measurements of N = 3 experiments, the bar height shows the mean of the three measurements. Error bars correspond to the SE between experiments. ns: adjusted p-value > 0.05, **: adjusted p-value < 0.01, unpaired Student's t-test with Bonferroni correction.

2.7.3 Loss of UGP2 does not accelerate early NPC differentiation

If the low *UGP2* level and glycogen content observed in the mouse influences differentiation speed, the *UGP2* knock-out lines are expected to differentiate more quickly than the wild type. To test this, I performed a six-day differentiation time course in human wild type PSCs and the two *UGP2* knock-out lines and checked the timing of early neural marker emergence via immunofluorescence. PAX6 was detected in few cells at day 3 in all cell lines and was more prominently expressed from day 4 onwards (Figure 33A). Segmentation and intensity measurements revealed that PAX6 expression was even slightly higher in wild type than in the *UGP2* knock-outs (Figure 33B). SOX1 expression started at day 2 after neural induction and was indistinguishable between the wild type and both *UGP2* knock-out lines (Figure 33A, B). OCT4 was drastically decreased in all lines at day 3 of differentiation. At days 0 to 2, the *UGP2* knock-

out lines had higher OCT4 signal than the wild type, however, OCT4 was observed uniformly in all cells (Figure 33A, B).

In sum, loss of *UGP2* did not influence early NPC differentiation as assessed by PAX6 and SOX1 staining within the analyzed time intervals.

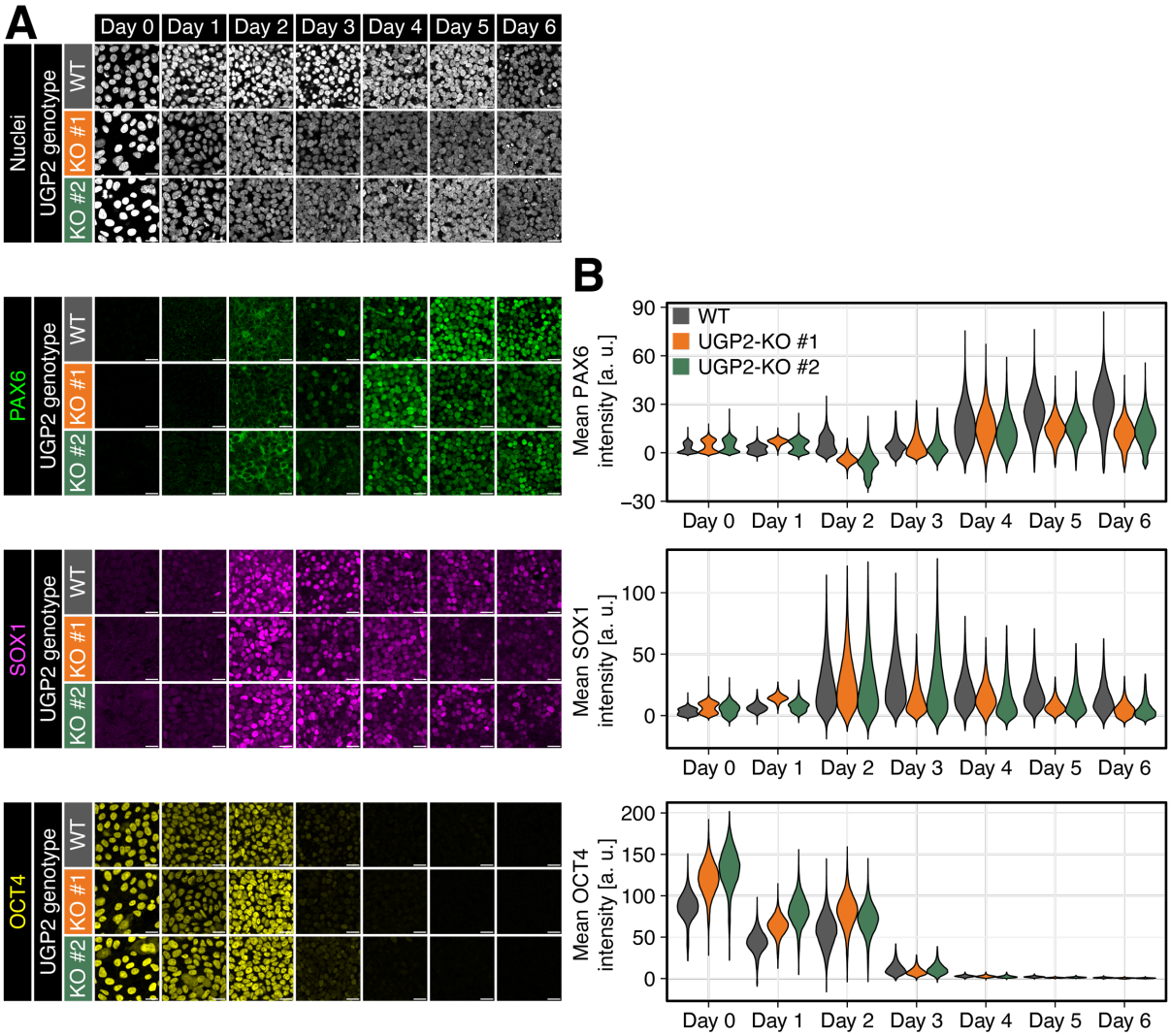

Figure 33: Loss of UGP2 does not alter early NPC differentiation.
A Immunostaining of a six-day time course differentiation. Representative images of N = 2 experiments are shown. The nuclear channel (Hoechst33342), PAX6, SOX1 and OCT4 are displayed for H9 wild type and the two *UGP2* kock-out lines. Images were adjusted to the same minimum/maximum for all genotypes, nuclei signal was adjusted individually. Scale bars = 20 µm. **B** Intensity measurements in single nuclei performed with StarDist 2D. Outlier removal and background subtraction were done as described in chapter 5.5.3. Violins were scaled to the same maximum width.

2.7.4 Glycogen metabolism influences late NPC differentiation

Since loss of UGP2 did not accelerate NPC differentiation at the earliest time points, I extended the differentiation time course to sixteen days. By that time, mRNA of the forebrain marker *FOXG1* can be detected in human wild type cells (Barry et al., 2017). Immunostaining on the differentiation time course revealed FOXG1 protein expression starting in single cells at day 14 in wild type and in clusters by day 16 (Figure 34A). Strikingly, *UGP2* knock-out line #1 had weak

FOXG1 expression already at day 9 and knock-out line #2 at day 10. In both knock-out lines, FOXG1 signal was uniform in all cells from day 12 on and kept rising until day 16 (Figure 34A). Quantification of FOXG1 signal confirmed that both *UGP2* knock-out lines expressed FOXG1 prematurely starting at day 9 (Figure 34B). These results suggest that glycogen metabolism affects NPC differentiation at later time points.

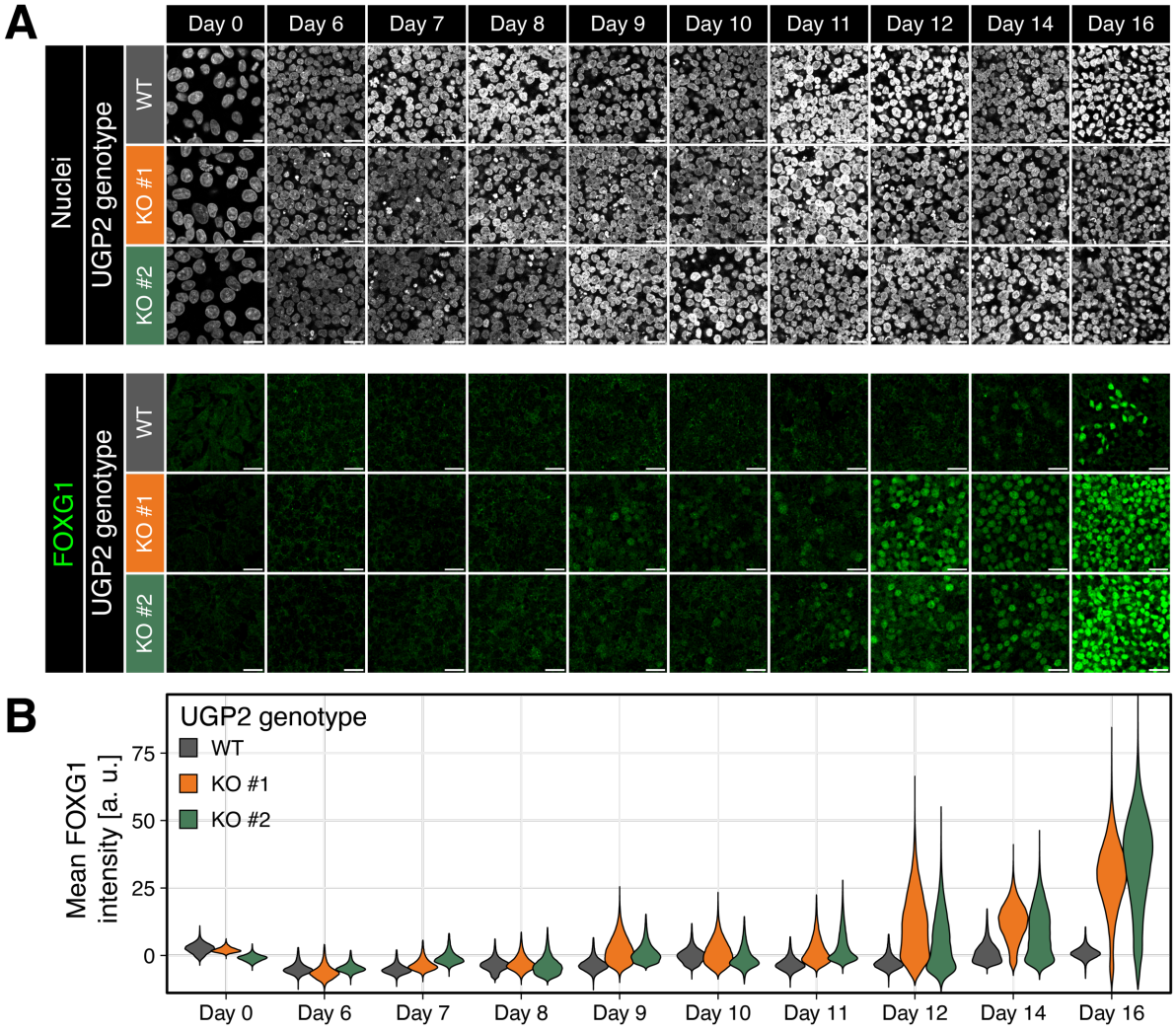

Figure 34: Loss of UGP2 leads to premature FOXG1 expression.
A Immunostaining on a differentiation time course. Day 0 and days 6 to 16 are shown for *UGP2* wild type H9s and the two *UGP2* knock-out lines. Nuclei staining (top) using Hoechst33258 (minimum and maximum intensity were adjusted individually for each image) and FOXG1 staining (adjusted to the same minimum and maximum) (bottom) are shown. Scale bars = 20 µm. **B** Distributions of FOXG1 signal intensities based on StarDist 2D segmentation. Outlier removal and background subtraction performed as described in chapter 5.5.3. Violins were scaled to the same maximum width.

Since NPC differentiation is marked by the onset of several neural genes, I sought to test the expression of another marker, neuronal Doublecortin (DCX). DCX is associated with microtubules and marks migrating, postmitotic neurons (Gleeson et al., 1999). Based on the FOXG1 staining, I expected premature DCX expression in the *UGP2* knock-out lines. In an immunostaining of a differentiation time course, DCX was detected in wild type cells from day 8 post neural induction

onwards and was very prominently expressed from day 10 on (Figure 35). Surprisingly, both *UGP2* knock-out lines showed a delayed onset of DCX starting faintly from day 10 on. By day 12, DCX had increased but never reached wild type levels within the time frame of the experiment (Figure 35). This stands in contrast to the expectation that UGP2 loss should lead to premature neural marker expression. However, it clearly shows that UGP2 and associated glycogen metabolism affects NPC differentiation timing. It remains to be tested whether the *UGP2* knock-out additionally changes differentiation outcome or if FOXG1 and DCX expression are mutually exclusive.

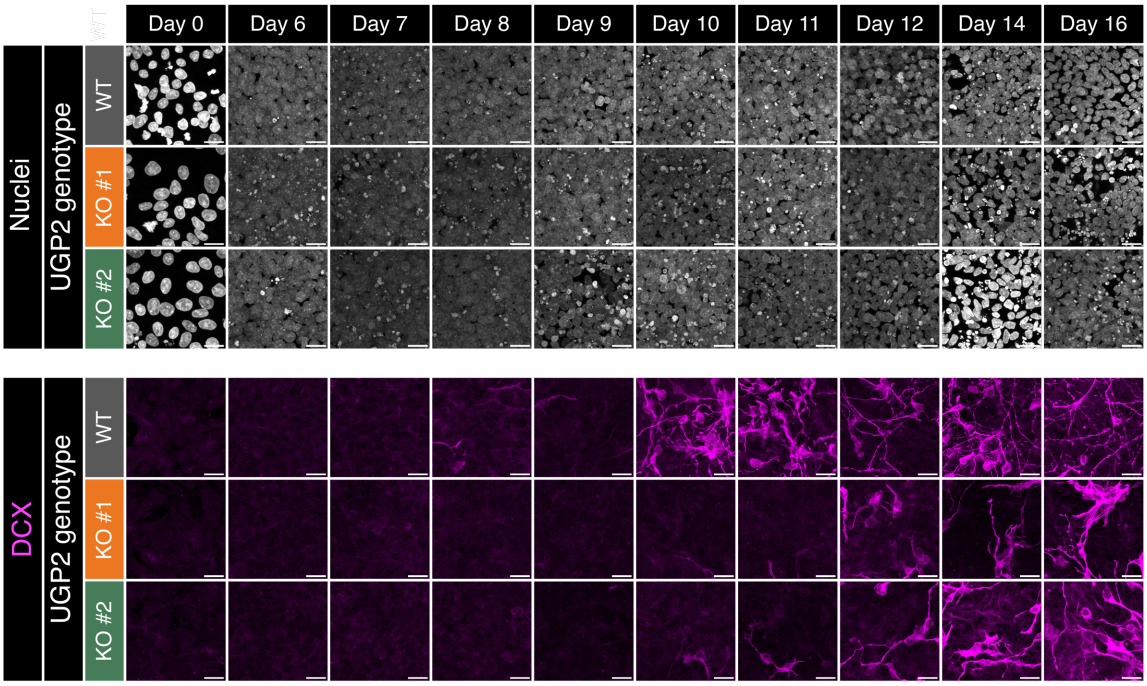

Figure 35: Doublecortin is expressed earlier in wild type than in *UGP2* knock-out cells.
Differentiation time course on human wild type and the two *UGP2* knock-out lines. Nuclear staining (Hoechst33258, top, minimum and maximum intensity were adjusted individually for each image) and a Doublecortin (DCX) staining (bottom, adjusted to the same minimum and maximum) are shown. All images shown are Z-maximum projections. Scale bars = 20 µm.

3 Discussion

Why species develop at different time scales has fascinated researchers for decades but especially since the introduction of pluripotent stem cells to the field of developmental biology, it has become a rising topic of interest. The fact that species-specific developmental timing is maintained during in vitro differentiation demonstrates that, unlike classically assumed, timing is not merely a consequence of varying body sizes in the animal kingdom, but rather regulated at the cellular level. Thus, we have to start thinking differentially about timing in biology. Not least due to the broad nature of the question, there are many theories on how species-specific time scales of development could be determined. Differentiation timing has been linked to several species-specific properties like metabolic rate, protein half-life, epigenetics and cell cycling (Ciceri et al., 2024; Diaz-Cuadros et al., 2023; Hergenreder et al., 2024; Rayon et al., 2020). However, most studies are correlative and, depending on the differentiation model, sometimes lead to contradictory conclusions.

In this project, I aimed to identify cell-intrinsic mechanisms that contribute to setting the developmental speed across species and alter developmental timing by manipulating these mechanisms. I used PSCs of mouse, cynomolgus and human in the context of neural progenitor differentiation and found that mouse cells expressed neural markers earliest, followed by cynomolgus and human. Through a single-cell transcriptomics experiment conducted by my collaborators Alexandra de la Porte and Moritz Thomas (Helmholtz Munich), a scaling factor of 2.2 between mouse and cynomolgus and 2.4 between mouse and human during neural differentiation was calculated, corresponding well with scaling factors from other differentiation systems described in the literature (Diaz-Cuadros et al., 2023; Rayon et al., 2020). To find out how this scaling factor arises, I performed two kinds of manipulations, either targeting the cell cycle directly or metabolism and growth and analyzed neural differentiation. Surprisingly, early neural differentiation was largely unaffected by the manipulations, suggesting that cell cycle, growth and metabolism can be uncoupled. Finally, single-cell transcriptomics (Helmholtz Munich) identified UGP2, responsible for glycogen synthesis, as a candidate gene to be involved in timing. In line with this, glycogen levels were negatively correlated with differentiation speed and late neural differentiation was affected by a *UGP2* knock-out in human.

Collectively, these results show that cell cycling is dispensable for differentiation and that differentiation could be tuned by glycogen metabolism.

3.1 Species-specific timing in mouse, cynomolgus and human

For this project, PSCs of three species were grown under identical conditions. So far, a harmonization of pluripotency media conditions between mouse and primates has not been reported and current studies compare species grown under highly different conditions (Diaz-Cuadros et al., 2023; Lázaro et al., 2023; Matsuda et al., 2020; Rayon et al., 2020). Here, I cultured cells in harmonized conditions using UPPS and thereby reduced cell culture artifacts for subsequent analyses. UPPS contains both a WNT inhibitor and a WNT agonist (Stauske et al., 2020). It has been reported that the pluripotency-maintaining effect of a combination of WNT inhibitor and agonist is mediated through Axin2-dependent retention of β-catenin in the cytoplasm (Kim et al., 2013). In UPPS, mouse cells already expressed SOX1, making them more biased towards differentiation than the primate cells. However, mouse cells in their original medium (FAX) differentiated along a similar timeline (Figure 12), indicating that UPPS did not drastically alter differentiation dynamics. Thus, in all species, UPPS supported self-renewal and preserved the cells' differentiation capacity.

The observed differentiation time shift between mouse and human (2.4-fold) corresponds well with time shifts observed in other systems like the segmentation clock (2- to 3-fold) and motor neuron differentiation (2.5-fold) (Matsuda et al., 2020; Rayon et al., 2020). With an observed differentiation time shift of 2.2-fold between mouse and cynomolgus, cynomolgus cells differentiated only slightly faster than human cells. Assuming a connection between differentiation speed and body mass, this could be expected since the body masses of cynomolgus and human are more similar than the body masses of any of the primates compared to mouse (Tacutu et al., 2018; Walpole et al., 2012). The same is true for gestational times and lifespans (Jewett & Dukelow, 1972; Tacutu et al., 2018). Another reason for similar differentiation speeds of cynomolgus and human could be phylogenetic similarity. However, given the differences between both primate species, it is still striking that their differentiation speeds are so alike.

3.2 Uncoupling of growth and differentiation

During motor neuron and presomitic mesoderm differentiation, differentiation speed of mouse and human correlated with the cell cycle duration (Diaz-Cuadros et al., 2023; Rayon et al., 2020). Here, I tested if cell cycle durations follow the same trend as differentiation speed in the species panel of mouse, cynomolgus and human during pluripotency and neural differentiation. I observed that mouse cycled fasted, followed by the two primate species which cycled at similar speeds. Thus qualitatively, the cell cycle followed the same trend as neural differentiation with mouse being fastest and cynomolgus and human close together. However, under the assumption that cells sense the number of cell divisions or the cumulative time spent in a specific cell cycle phase, the cell cycle difference between the species cannot explain the observed differentiation

time shift quantitatively (e. g. the cell cycle fold change between human and mouse is 1.47, while the differentiation fold-change is 2.4). It would however be possible that cell cycling is not linearly translated to differentiation timing or that differentiation timing is a result of a combined mechanisms including the cell cycle or, more generally, growth.

3.2.1 Neural differentiation in a retinoblastoma knock-out background

Functional coupling of the cell cycle to differentiation has been proposed in past studies. G1 phase has been described as a window of opportunity during the cell cycle. Cells only effectively responded to differentiation signals in G1 (Pauklin & Vallier, 2013; Sela et al., 2012). This could be explained by chromatin rearrangements and establishment of topology associating domains (TADs) during G1 phase (reviewed by Dekker, 2014; Thomson et al., 2004). Cell differentiation is concomitant with an extension of G1 phase (Calder et al., 2013) until cells finally exit the cell cycle when they are terminally differentiated. Consequently, artificial shortening of G1 phase would force cells to keep a pluripotency-like cell cycle structure while minimizing their window of opportunity to respond to differentiation signals.

One way to artificially decrease G1 duration is a knock-out of the pocket protein family, including the retinoblastoma protein (Dannenberg et al., 2000; Sage et al., 2000). Without RB, E2F is free to activate expression of S phase inducing genes (reviewed by Donjerkovic & Scott, 2000). During pluripotency, RbTKO mouse EpiSCs had a cell cycle that was indistinguishable from wild type EpiSCs. This strongly indicates that the cell cycle regulation in EpiSCs is very similar to ESCs which are characterized by inactive RB and unrestricted G1/S transit (Stead et al., 2002). Since cells establish G1/S control during differentiation, I hypothesized that while wild type cells extend their G1 phase, RbTKO cells would keep a short, pluripotency-like G1 phase. Time-lapse imaging of differentiating PIP-FUCCI wild type and RbTKO cells however showed that both lines exhibited an increase of G1 duration upon differentiation. Whilst the G1 extension indicates a gain of G1/S control, the G1/S checkpoint and associated RB activation might not have been fully established at this time of differentiation, explaining the lack of a cell cycle phenotype in RbTKO cells.

In contrast, scRNAseq indicated a reduction of RbTKO cells in G1 phase in comparison to the wild type. Although cell cycle phase inference from transcriptomics data is only an indirect measure of the cell cycle status, it suggests that wild type cells already activated gene expression programs indicative of cell cycle maturation while RbTKO cells remained immature. Single-cell transcriptomics during neural differentiation further showed that neurogenesis-related GO terms were among both the up- and downregulated genes in RbTKO compared to wild type. Integration of these data with a time-resolved reference data set (Helmholtz Munich) finally showed that neural differentiation was not delayed in RbTKO cells compared to the wild type; RbTKO actually had the tendency to differentiate slightly faster.

Together, these results suggest that the RbTKO does not delay early NPC differentiation. This could indicate that shortening of G1 phase does not disturb differentiation. This interpretation is supported by the fact that embryos can undergo diapause where they exit the cell cycle and still do not differentiate but remain pluripotent (reviewed by Fenelon et al., 2014). However, as different methods of cell cycle analysis yielded opposing results, it is also likely that the cell cycle phenotype was not strong enough at this time point of differentiation because the cells were still too immature. It would therefore be interesting to analyze later time points of NPC differentiation and check later neural markers like FOXG1 or DCX. A certain degree of G1/S transition control seems to be required for (terminal) differentiation, as subcutaneous injection of RbTKO cells into mice caused homogeneous teratomas composed of proliferating cells and lacking fully differentiated neurons and muscle cells (Dannenberg et al., 2000). An inducible RbTKO in differentiating cells could reveal, if cells with a maturing cell cycle regain stem-like properties or differentiate slower in response to induced G1 shortening.

3.2.2 Effect of mTOR inhibition on cell cycle and neural differentiation

In previous studies, differentiation timing has been linked to metabolism and protein turnover (Diaz-Cuadros et al., 2023; Rayon et al., 2020). While the connection between protein turnover and differentiation speed discovered during motor neuron differentiation was mainly correlative and could not be functionally confirmed in the segmentation clock model, metabolic interventions lowering the NAD+/NADH ratio were able to alter segmentation clock periods (Diaz-Cuadros et al., 2023; Rayon et al., 2020). A central hub of metabolism is mTOR which promotes cell growth through the upregulation of protein translation and ribosome biogenesis (reviewed by Liu & Sabatini, 2020). mTOR has been implicated in pluripotency and cell fate acquisition of human ESCs in different ways. Zhou et al. (2009) reported that mTOR supports self-renewal and prevents differentiation while Easley et al. (2010) found that ESCs generally have lower mTOR levels than terminally differentiated cells and that constitutively active mTOR effector S6K induces differentiation. Furthermore, inhibition of mTORC1/2 in mouse blastocysts and ESCs induced a diapause-like state in which growth was arrested and translation and transcription drastically reduced while cells maintained their developmental potential (Bulut-Karslioglu et al., 2016). To investigate whether cell growth and differentiation are coupled processes, I reduced mTOR signaling using an inhibitor of mTORC1/2 and assessed differentiation outcome. mTOR inhibition had a clear effect on cell growth. The cell cycle in all species was significantly slowed down upon mTOR inhibition. In agreement with mTOR's reported role in regulating the G1/S transition, I observed that G1 phases tended to be disproportionately extended upon mTOR inhibition (Fingar et al., 2004). Strikingly, the effect size of mTOR inhibition followed a species-specific trend with mouse being affected least and the primates strongest. Species-dependent differences in

sensitivity to mTOR inhibition could be the result of different mTOR protein levels and the degree of mTOR activity versus inhibition. It has been shown that longevity correlates with decreased mTOR protein levels, decreased mTOR activator levels and increased mTOR inhibition across different species (Mota-Martorell et al., 2020). It would therefore be interesting to examine the levels of active mTOR or its effectors in mouse, cynomolgus and human cells. In combination with previous studies where mTOR inhibition in adult organisms increased their lifespan (Kaeberlein et al., 2005; Kapahi et al., 2004; Vellai et al., 2003; Wu et al., 2013), this puts mTOR at the center of regulating timing in the context of aging.

Based on the observation that the fast-differentiating mouse tended to cycle faster and also had an increased metabolic rate compared to the slow-differentiating human (Diaz-Cuadros et al., 2023), I hypothesized that an mTORi-mediated metabolic and growth reduction could slow down differentiation. Under the assumption that differentiation is slowed down to the same degree as the cell cycle, I expected human and cynomolgus cells to acquire neural marker expression approximately 50% later under mTOR inhibition than in the control. Such a scenario would be true if cells sensed the number of cell divisions (Temple & Raff, 1986) or if there was a general requirement of cycling or growth for differentiation. Surprisingly, early neural markers emerged at the same time in mTOR-inhibited and control cells (within the time resolution of the experiment). Single-cell RNA sequencing revealed that several terms linked to purine metabolism were downregulated upon mTOR inhibition in human. This is in line with the well-established role of mTOR inducing purine synthesis to increase nucleotide availability for cell growth (Ben-Sahra et al., 2016). In cynomolgus, genes linked to neurodevelopmental processes were downregulated, indicating that mTOR inhibition could slow down differentiation. However, human cells upregulated GO terms linked to neurodevelopment upon mTORi, next to GO terms connected to alternative differentiation paths. The co-upregulation of genes indicative of alternative differentiation paths suggests that mTOR-inhibited cells could differentiate with decreased precision.

Mapping of the mTOR inhibition sequencing data onto a time-resolved reference data set allowed for the estimation of the differentiation status of mTORi-treated versus control cells. Mouse mTORi-treated and control cells preferentially mapped to the same time points which is to be expected because mouse cells were affected least by the treatment. In cynomolgus and human, mTORi-treated cells were delayed at day 2 but assigned to more advanced time points than the control at day 4. The latter observation stands in contrast to the working hypothesis that growth reduction slows down differentiation. It has been shown that mTOR inhibition in human ESCs can trigger differentiation, probably owing to reduced expression of pluripotency factors. However, only endo- and mesodermal differentiation were upregulated under mTOR inhibition, not

(neuro)ectodermal differentiation (Zhou et al., 2009) which could potentially explain the upregulation of genes linked to alternative cell fates observed in human.

The lack of a consistent differentiation delay in mTORi argues against a model where mTOR inhibition and therefore growth inhibition systematically slows down neural differentiation. Although mTOR inhibition is a metabolic intervention and only impacts the cell cycle indirectly, normal differentiation despite of the drastic cell cycle lengthening upon mTOR inhibition indicates that differentiation is independent of cell cycling. This is in agreement with the observation that a cell cycle arrest in apical progenitors does not change temporal gene expression. If the cell cycle was necessary for correct differentiation, a transient cell cycle arrest in apical progenitors would result in differentiation into early-born neurons, however, transiently arrested cells were able to differentiate into late-born upper layer neurons upon release (Okamoto et al., 2016). Since in this case the cell cycle arrest was only transient, this does not abrogate the possibility that cell cycling is necessary for differentiation progression but it clearly points against a cell-cycle-counting mechanism as proposed earlier (Takahashi et al., 1999; Temple & Raff, 1986). In zebrafish, it was shown that cell fate acquisition was not disturbed by a cell cycle arrest but the rate of differentiation was altered. The observed time shift was within the order of hours rather than days (Kukreja et al., 2023). Such a subtle change in differentiation timing would not be detectable with a 24-hour time resolution. Therefore, I employed a live-cell imaging approach that is more sensitive to small temporal shifts in marker expression using a human PAX6::H2B-GFP reporter line (Tchieu et al., 2017). While the data was too noisy to narrow PAX6 onset down to the hour, it showed that the timing of PAX6 increase was similar between untreated control and mTORi-treated cells.

While mTOR inhibition is a metabolic intervention rather than a targeted cell cycle perturbation, the absence of a differentiation delay upon mTOR inhibition-dependent cell cycle elongation clearly indicates that differentiation can be uncoupled from cell growth and cycling.

3.3 mTOR's role during neural differentiation

To test, if mTOR inhibition affected neural differentiation at a later stage, I differentiated cells for a longer period and checked FOXG1 expression. Surprisingly, I found that FOXG1 was strongly upregulated under mTOR inhibition in human cells. This was particularly unexpected as mTOR has been shown to promote insulin-induced neuron differentiation (Han et al., 2008), indicating that mTOR inhibition should perturb differentiation. FOXG1 is a forebrain marker that inhibits early cortical differentiation and is linked to NPC proliferation (Hanashima et al., 2004; Hettige et al., 2022). Premature FOXG1 expression upon mTOR inhibition either suggests an alternative role for mTOR during neural differentiation or the presence of a specific link between mTOR and FOXG1.

A regulatory relationship between mTOR and FOXG1 has been proposed in the context of different pathologies (lung cancer and Alzheimer's disease). In the former case, mTOR activation in a lung carcinoma cell line was upregulated upon FOXG1 overexpression (Chen et al., 2023). In contrast, FOXG1 overexpression led to reduced active mTOR and increased active AMPK in glioblastoma cells (Yun et al., 2024). Thus, there is an apparent connection between FOXG1 and mTOR, although the effect of FOXG1 overexpression on mTOR seems to be cell type-dependent and it is unclear whether there is a reciprocal relationship between FOXG1 and mTOR.

If increased FOXG1 expression observed under mTORi is indicative of enhanced neural differentiation, it is possible that this effect is caused by the mTORi-dependent cell cycle alteration. Terminal differentiation is always accompanied by cell cycle exit (reviewed by Boward et al., 2016). Since mTOR inhibition prolonged the cell cycle and especially G1 phase, it is possible that treatment counterintuitively accelerated differentiation by forcing the cell cycle to be more mature. It remains to be tested, if neuronal markers like DCX, βIII-tubulin or MAP2 are also upregulated in response to mTOR inhibition and thus, if mTOR inhibition actually promotes neural differentiation or if FOXG1 upregulation represents an outlier case due to a direct relationship between mTOR and FOXG1.

3.4 Linking UGP2 to differentiation dynamics

Single-cell transcriptome analysis of a time-resolved differentiation time course (Alexandra de la Porte and Moritz Thomas, Helmholtz Munich) uncovered UGP2 as a candidate gene to be involved in differentiation speed. UGP2 (for UDP-glucose pyrophosphorylase 2) is required for glycogen synthesis by catalyzing the reaction from glucose-1-phosphate and UTP to the glycogen precursor UDP-glucose (reviewed by Adeva-Andany et al., 2016). Glycogen is the storage form of glucose, consisting of multiple, branched glucose molecules (reviewed by Calder, 1991). Glucose can be released via glycogenolysis (reviewed by Roach, 2005). UGP2 is also involved in the synthesis of extracellular matrix components such as hyaluronan and its product UDP-glucose is a substrate for protein glycosylation (reviewed by Bieberich, 2014; Magee et al., 2001).

Higher expression of UGP2 in the slow-differentiating primate cells and in 'late' differentiating cells suggested that UGP2 is linked to differentiation speed. A mutation in the UGP2 gene was reported to be responsible for developmental and/or epileptic encephalopathies in humans. While the mutation was tolerable in the long isoform of the gene, it resulted in loss of the short isoform which is predominantly found in the brain. Human ESCs carrying a UGP2 loss of function mutation exhibited premature neuronal differentiation (Perenthaler et al., 2020). Based on these observations, I speculated that glycogen synthesis is involved in determining a cell's differentiation speed. Measurement of glycogen content in mouse, cynomolgus and human PSCs

showed that species differed significantly in their glycogen content with mouse exhibiting the lowest glycogen levels and human the highest. Thus, glycogen levels reflected the species-specific trend observed for differentiation speed, lifespan and body size.

In line with this, a study in the planarian S*chmidtea mediterranea* links body size-dependent energy storage to metabolic rate scaling following Kleiber's law (Thommen et al., 2019). The planarian's body size fluctuates drastically depending on food availability; when fed, it grows and when starved it shrinks, owing to changes in cell number. The metabolic rate scales with a ~ ¾ exponent to the body mass, thereby following Kleiber's law. Intriguingly, the mass per cell disproportionately increased with body mass (~ ¾ exponent) due to larger energy reserves in the form of triglycerides and glycogen (Thommen et al., 2019). Based on these observations, larger organisms are expected to have a higher mass per cell associated with higher energy storages. Indeed, the dry mass of human presomitic mesoderm cells is more than double that of mouse cells (Diaz-Cuadros et al., 2023). It will be interesting to test, if mass/cell scaling also applies to a multi-species comparison and how glycogen levels relate to cell mass.

But how can glycogen metabolism contribute to the pace of life? The recapitulation of the species-dependent trend in differentiation speeds at the level glycogen content and the finding of Thommen et al. (2019) that energy storage is at the root of metabolic rate scaling laws reinforced the hypothesis that glycogen metabolism is connected to differentiation speed. Therefore, low glycogen levels would favor fast differentiation and growth and high glycogen levels slow differentiation and growth.

The role of glycogen metabolism for growth is manifold. A variety of cancer cells hallmarked by high proliferative capacity, show an accumulation of glycogen (Rousset et al., 1981) which stands in apparent contrast to the idea that high glycogen levels are associated with slow growth. Both cancer and non-cancerous cells upregulate enzymes required for glycogen synthesis including UGP2 in hypoxic conditions, leading to an increase in glycogen levels. This has been shown to improve cell survival under hypoxic and glucose-deprived conditions (Pelletier et al., 2012; Pescador et al., 2010). In glioblastoma cells, expression of glycogen synthase 1 (GYS1) and glycogen phosphorylase (PYGL) increased upon hypoxia. As PYGL is required for the breakdown of glycogen, knock-down of PYGL led to glycogen accumulation and reduced growth of glioblastoma cells in hypoxia (Favaro et al., 2012). Hence, a balance between glucose storage as glycogen and glycogen breakdown appears important for growth under unfavorable conditions. However, I grew PSCs under normoxia and conclusions derived from cancer models under stress conditions might not be applicable to stem cell development.

One possible model to explain higher UGP2 and glycogen levels in the slow-differentiating species would be that glucose is shunted away from glycolysis by conversion to glycogen, reducing the amount of energy available for cell proliferation and differentiation. To test if differentiation

speed was sensitive to reduced glycogen levels, I used two human ESC lines carrying a *UGP2* knock-out and performed NPC differentiation. Both knock-out lines had barely detectable glycogen levels and were thereby more reminiscent of mouse cells than human cells in that respect. Comparison of the two human *UGP2* knock-out lines with the wild type showed that early neural marker emergence was unaffected by UGP2 loss, indicating that glycogen or UGP2 is dispensable for early neural differentiation. During later NPC differentiation however, both *UGP2* knock-out lines exhibited premature FOXG1 expression. This is in line with the observation that UGP2 loss leads to premature neuronal differentiation (Perenthaler et al., 2020). Surprisingly, the neuronal marker DCX showed delayed expression in both *UGP2* knock-out clones, indicating that *UGP2* knock-out cells differentiated slower. DCX is a microtubule-associated protein marking postmitotic neurons (Gleeson et al., 1999). A possible explanation for this observation is that premature FOXG1 expression in *UGP2* knock-out cells inhibits early cortical differentiation and thereby delays the emergence of DCX positive cortical neurons. FOXG1 has been shown to inhibit the differentiation of the early Cajal-Retzius neurons which have been suggested to express DCX (Hanashima et al., 2004; Meyer et al., 2002). In agreement with this, the onset of premature FOXG1 expression in the *UGP2* knock-out lines roughly coincided with the onset of DCX expression in the wild type.

In depth-analyses of several neural and neuronal markers will be required to understand the effect of a *UGP2* knock-out on neural differentiation. Since it is also possible that loss of UGP2 affects the cell type composition during differentiation, the precise differentiation status and cell fate of *UGP2* knock-out cells is currently being determined via single-cell transcriptomics (ongoing at Helmholtz Munich and Leiden Academic Centre for Drug Research LACDR). Rescue experiments and UGP2 overexpression in the fast-differentiating mouse cells could further confirm the role of UGP2 in neural differentiation. It would also be important to measure metabolic rates in the *UGP2* knock-out lines. Furthermore, the influence of UGP2 in other differentiation systems like mesodermal or endodermal differentiation needs to be tested to assess whether the level of glycogen metabolism is a general mechanism for regulating differentiation speed.

As UGP2 is not only required for glycogen synthesis but also for protein glycosylation, numerous mechanisms could influence the differentiation process. For example, it has been shown that UGP2 was responsible for the glycosylation of EGFR in pancreatic cancer cells and therefore critical for cancer maintenance (Wolfe et al., 2021). Thus, UGP2 could modulate the function of several proteins through posttranslational modification and be a central player in the regulation of cancer, growth and differentiation. Proteomics could reveal which proteins are modified through UGP2 and thus, if there are other players involved that could affect differentiation. Besides, it would be interesting to compare cycling times of wild type and *UGP2* knock-out cells

and measure glycogen content upon mTOR inhibition, as mTOR has been reported to be required for glycogen synthesis in the mouse liver, making it possible that glycogen contents were reduced in the mTOR inhibition experiments (Uehara et al., 2024).

3.5 Conclusions and outlook

This project deals with one of the most fundamental questions of biology, the question of how developmental time and the pace of life arises. I specifically aimed to identify cell-intrinsic mechanisms that regulate species-specific differentiation timing. The use of (induced) pluripotent stem cells enabled me to compare developmental speeds across three mammalian species. Cells recapitulated the species-specific time scales of development during in vitro neural progenitor differentiation, highlighting the relevance of stem cell models in developmental biology. As of now, many studies on developmental timing remain correlative. For this reason, I sought to alter differentiation timing through perturbation of candidate mechanism. As cell differentiation and growth have to be coordinated with each other during embryonic development, I hypothesized that growth could regulate differentiation timing. Surprisingly however, manipulation of growth and metabolism via mTOR inhibition did not systematically delay early neural differentiation. Two conclusions can be derived from this finding. First, reducing anabolic processes like translation and ribosome biogenesis does not inhibit differentiation and second, differentiation is independent of growth. As mTOR inhibition also slowed down the cell cycle, it appears unlikely that cell cycle progression regulates differentiation speed. It remains to be tested to what extent mTOR-mediated processes are reduced in the three species and if neural differentiation is affected by a complete cell cycle arrest. In sum, this line of experimentation raised the question how differentiation timing is regulated independent of growth and cell cycling and if all of these cellular properties are determined by an overlying process.

A promising candidate is the metabolic enzyme UGP2. As evident by clinical studies, loss of the short isoform of UGP2 has detrimental effects on brain development (Perenthaler et al., 2020), emphasizing the critical role of UGP2 in the developmental context. UGP2 is required for glycogen synthesis and its expression level followed a species-dependent trend. Consequently, glycogen levels were drastically different between species. Premature FOXG1 expression upon loss of UGP2 implicates UGP2 in the regulation of neural differentiation, however, the exact role of UGP2 in this context needs to be further explored through transcriptome analysis, as this will aid in determining the differentiation status and cell type composition in UGP2 loss-of-function mutants. Defining the role of UGP2 during development could uncover fundamental principles in biology. Since glycogen and triglyceride storage has been proposed as the reason for ¾ power law scaling of metabolic rates in planarians (Thommen et al., 2019), it would be interesting to

explore cellular energy storages and cell sizes in the inter-species comparison. This would potentially reveal unknown scaling relationships across species and possibly link UGP2 and glycogen storage to Kleiber's law.

The discovery of UGP2 as a candidate mechanism for timing implicates metabolism as the overlying processes that regulates growth and differentiation. However, unlike previous studies which focus on cellular metabolic rates, this project stresses the importance of energy storage for developmental timing. How metabolic rates correlate with UGP2 levels can be subject of future studies. Due to UGP2's role in posttranslational protein glycosylation, proteomics could reveal which proteins are modified by UGP2-mediated glycosylation and could therefore be part of a more complex network. Exploring the role of UGP2 in development will show if UGP2 or related metabolic processes can be used as a tool to modulate differentiation speed. Identifying factors that regulate differentiation time scales is relevant for clinical applications of pluripotent stem cells. The protracted differentiation time of human cells poses challenges for research and personalized medicine (Lu et al., 2017). Shortening the differentiation and maturation time line of human cells would therefore greatly aid in medical sciences.

4 Materials

4.1 Cell lines

Table 1: Parental cell lines used.

Name	Species	Source
H9	*Homo sapiens*	WiCell Institute, provided by Prof. Dr. James Thomson, Wisconsin
H9	*Homo sapiens*	Dr. Stefan Barakat, Rotterdam
cy iPSCs (56A1)	*Macaca fascicularis*	Prof. Dr. Wolfgang Enard, Munich
mEpiSCs (129S2C1a)	*Mus musculus*	Prof. Dr. Ludovic Vallier, Cambridge
RbTKO (129/Ola)	*Mus musculus*	Prof. Dr. Hein Te Riele, Amsterdam
H9 PAX6::H2B-GFP	*Homo sapiens*	Prof. Dr. Lorenz Studer, New York City
H9 UGP2-KO #3-2	*Homo sapiens*	Dr. Stefan Barakat, Rotterdam
H9 UGP2-KO #3-35	*Homo sapiens*	Dr. Stefan Barakat, Rotterdam

4.2 Basal media and supplements

Table 2: List of basal media and supplements.

Media	Source
Neuropan Basal Medium with L-Glutamine, 2.2 g/L NaHCO3	PAN Biotech
Neurobasal (minus phenol red)	Gibco
DMEM/F12 (1:1), with L-Glutamine, 15 mM HEPES, 1.2 g/L NaHCO3	PAN Biotech
DMEM/F12, HEPES, no phenol red-500 mL	Gibco
StemMACS iPS Brew XF	Miltenyi Biotech
Opti-MEM	Gibco
Bambanker	Nippon Genetics
100x N2 supplement	Gibco

50x B27 supplement	Gibco
50 mM β-mercaptoethanol	Gibco
100X MEM-NEAA	Gibco
100X Glutamax	Gibco
7.5 % BSA	Gibco
Recombinant Mouse Activin A	Cell Guidance Systems
FGF2	Peprotech
LIF	Protein facility, MPI Dortmund
Human recombinant insulin (4 mg/ml)	Gibco

4.3 Media and buffers

Table 3: List of media with compositions.

Medium/buffer	Composition
UPPS	StemMACS iPS Brew; 1 μM IWR-1; 0.5 μM CHIR99021
FAX	1:1 Neuropan:DMEM/F12; 0.5X N2 supplement; 0.5X B27 supplement; 0.1 mM β-mercaptoethanol; 0.5X Glutamax; 0.0025% BSA; 12 ng/ml FGF2; 25 ng/ml Activin A; 20 μM XAV939. Medium was sterile-filtered.
NPCSL	1:1 Neuropan:DMEM/F12; 0.5X N2 supplement; 0.5X B27 supplement; 0.1 mM β-mercaptoethanol; 1X Glutamax; 1X MEM-NEAA; 5 μg/ml human recombinant insulin; 10 μM SB431542; 100 nM LDN193189. Medium was sterile-filtered before inhibitor addition.
Imaging NPCSL	1:1 Neurobasal (minus phenol red):DMEM/F12 (HEPES, no phenol red); 0.5X N2 supplement; 0.5X B27 supplement; 0.1 mM β-mercaptoethanol; 1X Glutamax; 1X MEM-NEAA; 5 μg/ml human recombinant insulin; 10 μM SB431542; 100 nM LDN193189. Medium was sterile-filtered before inhibitor addition.
ES + LIF	GMEM; 10% FBS; 1X MEM-NEAA; 2 mM Glutamax; 0.1 mM β-mercaptoethanol; 10 mg/ml LIF. Medium was sterile-filtered.
Mounting medium	80% glycerol (99.5%); 20 % PBS; 4% w/v n-propyl-gallate
PBT-BSA	DPBS w/ Ca^{2+}/Mg^{2+}; 1% BSA; 0.1% Triton X-100

4.4 Chemicals and reagents

Table 4: List of chemical reagents.

Chemical/reagent	Source
DPBS w/o Ca^{2+}/Mg^{2+}	PAN Biotech
DPBS w/ Ca^{2+}/Mg^{2+}	PAN Biotech
0.5 M EDTA	Invitrogen
Accutase	Sigma-Aldrich
Trypsin	PAN Biotech
Matrigel Basement Membrane Matrix, LDEV-free	Corning
Dimethyl sulfoxide (DMSO)	Signa-Aldrich
Histofix	Carl Roth
Triton X-100	Thermo Scientific
Bovine serum albumin (BSA)	Carl Roth
Lipofectamine2000	Thermo Fisher Scientific

4.5 Inhibitors

Table 5: List of inhibitors.

Inhibitor	Source
CHIR99021	Tocris
IWR-1	Sigma Aldrich
XAV939	Cell Guidance Systems
Y-27632	R&D Systems
SB431542	Peprotech
LDN-193189 HCl	Peprotech
INK128	Cell Signaling

4.6 Antibodies

Table 6: List of primary and secondary antibodies.

Antibody	Host	Concentration	Source
anti-PAX6 (901301)	rabbit	10 µg/ml	BioLegend
anti-SOX1 (AF3369)	goat	1 µg/ml	biotechne/R&D Systems
anti-OCT3/4 (sc-5279)	mouse	2 µg/ml	Santa Cruz
anti-FOXG1 (ab18259)	rabbit	7-9 µg/ml	Abcam
anti-DCX (13925-1-AP)	rabbit	6 µg/ml	Proteintech
anti-rabbit AlexaFluor-488	donkey	4 µg/ml	Invitrogen/Life Technologies
anti-goat AlexaFluor-555	donkey	4 µg/ml	Invitrogen/Life Technologies
anti-goat AlexaFluor-568	donkey	4 µg/ml	Invitrogen/Life Technologies
anti-rabbit AlexaFluor-568	donkey	4 µg/ml	Invitrogen/Life Technologies
anti-mouse AlexaFluor-647	donkey	4 µg/ml	Invitrogen/Life Technologies

4.7 Commerical kits

Table 7: List of commercial kits.

Kit	Source
Glycogen Assay Kit ab65620	Abcam
NEBuilder HiFi DNA Assembly Cloning Kit	New England Biolabs
QIAGEN Plasmid Midi Kit (12143)	Qiagen
Chromium Next GEM Single Cell 3' Kit v3.1 (PN-1000269)	10x Genomics
3' CellPlex Kit Set A (PN-1000261)	10x Genomics
3' Feature Barcode Kit (PN-1000262)	10x Genomics
Chromium Next GEM Chip G Single Cell Kit (PN-1000127)	10x Genomics
Dual Index Kit TT Set A (PN-1000215)	10x Genomics
Dual Index Kit NN Set A (PN-1000243)	10x Genomics
Neon Transfection System 100 µL Kit	Invitrogen

Agilent High Sensitivity DNA Kit 5067-4626	Agilent

4.8 Constructs

Table 8: List of plasmid constructs.

Plasmid name	Function
pENTR-PIP-FUCCI, Addgene #118621	Original PIP-FUCCI plasmid
pCAG pBase HN 2545	Transposase plasmid for piggyBAC transgenesis
pPB-CAG-cHA-IRES-Puro	PiggyBAC vector with a CAG promoter and IRES-Puro for selection
pPBCAG-PIP-FUCCI-IRES-Puro	PiggyBAC vector carrying the PIP-FUCCI sensor with an IRES-*pac* for selection
pPBCAG-H2BmCER-I_Blsd	PiggyBAC vector carrying an H2B-Cerulean reporter with an IRES-*bsd* for selection
pPBCAG-H2BmCER-IP	PiggyBAC vector carrying an H2B-Cerulean reporter with an IRES-*pac* for selection

4.9 Laboratorial equipment

Table 9: List of laboratorial equipment.

Material	Source
Cell culture plates (different sizes)	Sarstedt
Cell culture flasks (different sizes)	Sarstedt
μ-Slide 8 Well high ibiTreat	Ibidi
Serological pipettes (different sizes)	Sarstedt
Filtropur sterile filters, mesh size 0.2 μm	Sarstedt
Bottletop sterile filters, mesh size 0.2 μm	Thermo Fisher Scientific, Nalgene
Cell strainer, mesh size 35 μm	Falcon

4.10 Software

Table 10: List of software.

Software	Source
R 4.3.2	R Core Team, 2022
Seurat v5	Hao et al., 2023
CellRanger 7.2.0	10x Genomics
Fiji v2.9.0/1.53t	Schindelin et al., 2012
StarDist 2D	Schmidt et al., 2018
TrackMate v7.9.2	Ershov et al., 2022; Tinevez et al., 2017
Micro Manager 2.0	Edelstein et al., 2010
LASX	Leica Microsystems
FlowJo v9	BD Biosciences
ShinyGO 8.0	Ge et al., 2020
Scanpy 1.9.8	Wolf et al., 2018

5 Methods

5.1 Cell culture

Cells were grown at 37 °C and 5% CO_2 in a sterile environment. For cell culture harmonization across cell lines and species, primed PSCs were cultured in UPPS medium on 1:100 Matrigel in DMEM/F12 and routine-passaged with 0.5 mM EDTA. For RbTKO experiments, mouse wild type and RbTKO EpiSCs were cultivated in FAX medium on Matrigel. UPPS-adapted cells were frozen in Bambanker and FAX-adapted cells in 70% FAX/20% KSR/10% DMSO. All primed cells were thawed in the presence of 10 µM ROCK inhibitor (Y-27632). Mouse cells were passaged every 2-3 days and primate cells every 3-5 days. RbTKO mESCs were grown on 0.1% gelatine-coated dishes in ES + LIF medium. They were routine-passaged using trypsin. Cell brightfield images were taken using a Zeiss Axiovert 40 CFL microscope with a Leica MC170HD camera.

5.2 Neural progenitor differentiation

All cell lines were differentiated using dual SMAD inhibition (Chambers et al., 2009). Prior to differentiation, cells were detached with Accutase and resuspended in pluripotency medium containing 10 µM ROCK inhibitor. Cells were counted using a Countess Automated Cell Counter in a 1:1 dilution with trypan blue. Mouse cells were seeded at a density of 62,500 cells/cm^2 and primate cells at 125,000 cells/cm^2 and kept in pluripotency medium with ROCK inhibitor overnight. Differentiation was induced by changing the cells to NPC medium supplemented with 10 µM SB431542 and 100 nM LDN193189 (SMAD2/3 and SMAD1/5/8 inhibition). During differentiation, cells were washed daily with DPBS (w/o Ca^{2+}/Mg^{2+}) and the medium was changed.

5.3 Differentiation of RbTKO mESCs to Epi-like cells

RbTKO mESCs (Dannenberg et al., 2000) were grown in ES + LIF on gelatine. For Epi differentiation, they were passaged onto fibronectin-coated plates and changed to FAX medium. They were kept in FAX for 10 passages and transferred to Matrigel-coating before further experiments were performed. Routine-splitting was performed using EDTA.

5.4 mTOR inhibition

mTORC1/2 was inhibited using 50 nM INK128 (unless stated otherwise). INK128 is an mTOR ATP site inhibitor (Hsieh et al., 2012) and affects both mTORC1 and mTORC2. mTOR inhibition

was typically started simultaneously with neural induction. For PIP-FUCCI measurements during pluripotency, INK128 was added to pluripotency medium shortly before acquisition start.

5.5 Immunostainings

5.5.1 Fixation and staining procedure

For immunostainings, cells were grown on chambered µ-Slides (Ibidi). Prior to fixation, they were rinsed with DPBS containing Ca^{2+}/Mg^{2+}. Fixation was performed for 15 min at room temperature in Histofix (4% PFA). Fixed cells were rinsed in PBT-BSA, followed by blocking and permeabilization in PBT-BSA three times for 15 min at room temperature. Primary antibodies were diluted in PBT-BSA and added overnight at 4 °C. The next day, antibodies were removed and cells were rinsed and washed again three times for 15 min in PBT-BSA. Secondary antibodies were added for 1-2 hours at room temperature in PBT-BSA, protected from light. After incubation, cells were washed twice with PBT-BSA for 15 min and twice with DPBS + Ca^{2+}/Mg^{2+} for 10 min. Finally, cells were mounted by adding home-made mounting medium.

5.5.2 Confocal microscopy

Immunostainings were imaged on a Leica SP8 confocal microscope (Leica Microsystems) with a 63X 1.4 NA oil immersion objective. Typically, tile scans with 75-225 single tiles of 512x512 px were acquired and merged for analysis.

5.5.3 Image segmentation for immunostainings

Merged tile scans of immunostainings were segmented using StarDist 2D (Schmidt et al., 2018) with the Versatile (fluorescent nuclei) model (nTiles = 10, otherwise default parameters) in the nuclei channel. Spots with an area < 10 µm² were filtered out. For background subtraction, the background was measured in a central region of each tile scan (200x200 µm). To obtain a background value inside this region for each channel, it was segmented with StarDist 2D (same parameters) in the nuclei channel and all spots were combined to a single region of interest (ROI) after which the ROI was inverted and background outside the segmented nuclei was measured in all channels. The channel-specific mean background value was subtracted from each measurement in the corresponding channel. Outliers were defined as all values outside the range of 3 times the interquartile range below or above the first and third quartile respectively in any channel.

5.6 Flow cytometry

For cell sorting, cells were detached using Accutase. The cell suspension was centrifuged at 200 g for 5 min and pellets were resuspended in DPBS (w/ Ca^{2+}/Mg^{2+}) + 0.5% BSA. To obtain a single-cell solution, cells were passed through a cell strainer. Sorting was performed using a FACS Aria Fusion (BD Biosciences). Data analysis was performed with FlowJo v9 (BD Biosciences).

5.7 Nucleofection

Nucleofection was performed with a Neon Transfection System (Life Technologies), following the manufacturer's instructions. Cells were detached using Accutase and centrifuged for 5 min at 200 g. Cell pellets were resuspended in pluripotency medium supplemented with 10 µM ROCK inhibitor and $1.5 \cdot 10^6$ cells were taken off and centrifuged for 5 min at 200 g again. Afterwards, the cells were washed in 5 ml DPBS (w/o Ca^{2+}/Mg^{2+}) and pellets resuspended in 105 µl Buffer R. The cell suspension was transferred to a reaction tube containing 5 µg plasmid DNA. The Neon tube was filled with 3 ml Buffer E2 and inserted into the pipette station. Electroporation was performed with two pulses at 1000 V for 20 ms. Cells were seeded in pluripotency medium with 10 µM ROCK inhibitor and antibiotic selection was started after one or two days.

5.8 Lipofection

For lipofection, 4 µl Lipofectamine2000 and 2 µg plasmid DNA were mixed with 50 µl Opti-MEM respectively. Both mixes were combined, vortexted and incubated for 10 min at room temperature. Cells were detached using Accutase and centrifuged for 5 min at 200 g. Pellets were resuspended in DPBS (w/o Ca^{2+}/Mg^{2+}) and $5 \cdot 10^5$ – $1 \cdot 10^6$ cells were transferred to a new tube and centrifuged again. The cells were resuspended in the Lipofectamine2000/DNA/Opti-MEM mixture and incubated for 10 min at room temperature. Finally, the cells were seeded in pluripotency medium supplemented with 10 µM ROCK inhibitor. Depending on the cell survival, selection was started after one or two days.

5.9 PIP-FUCCI measurements

5.9.1 Generation of a PIP-FUCCI expression vector

All FUCCI experiments were performed with the PIP-FUCCI construct from Grant et al., (2018, Addgene plasmid #118621). I used the piggyBAC system to randomly integrate the PIP-FUCCI construct into cells. The PIP-FUCCI construct was amplified with 25 nt overhangs for the target vector pPB-CAG-cHA-IRES-Puro using the following primers:

Fw_gibson_pip_fucci:
5′-GTCTCATCATTTTGGCAAAGAATTCATGGAGCAGCGCCGCGTCAC-3′
Rev_gibson_pip_fucci:
5′-CGGAATTCGATATCAAGCTTATCGAGTTACAGCGCCTTTCTCCGTTTTTCTGC-3′

The target vector was opened by *Not*I-HF and *Xho*I digest and both fragments were ligated using NEB HiFi Assembly following the manufacturer's instructions. Plasmids were isolated with the QIAGEN Plasmid Midi Kit (Qiagen) and tested for successful sensor integration by Sanger sequencing.

5.9.2 Generation of PIP-FUCCI cell lines

The PIP-FUCCI-carrying pPB-CAG-cHA-IRES-Puro vector was randomly integrated into human and mouse cells in UPPS, mouse cells in FAX and mouse RbTKO cells in FAX using Lipofectamine2000. Cynomolgus cells were nucleofected using the NEON system. pPB-CAG-PIP-FUCCI-IRES-Puro was used in a 1:1 ratio with a pCAG pBase HN 2545 plasmid carrying a transposase for genomic integration of the PIP-FUCCI construct (Wang et al., 2008). Successful transfection was selected for under 1.5 mg/ml puromycin. Polyclonal cell lines were kept under selection to prevent transgene silencing. Prior to flow cytometry analysis, PIP-FUCCI cells were sorted for the 20-30% cells with highest mCherry expression.

5.9.3 Time-lapse imaging of PIP-FUCCI lines

PIP-FUCCI imaging was performed in chimeric cultures comprised of PIP-FUCCI sensor cells and unlabeled, parental cells in ratios ranging from 1:10 to 1:100. This enabled me to track cells even in dense colonies and during NPC differentiation when cells are seeded at particularly high densities. Cells were seeded a day prior to acquisition start as single cells in pluripotency medium supplemented with 10 µM ROCK inhibitor. Primate cells were typically seeded at 80,000 cells/cm^2 and mouse cells at 40,000 cells/cm^2. Immediately before imaging, cells were washed and transferred to the desired media condition. For measurements in pluripotency, either pluripotency medium or pluripotency medium supplemented with 50 nM INK128 was added. Cells for differentiation measurements were seeded three days before imaging start at 62,500 cells/cm^2 (mouse), 80,000 cells/cm^2 (human) and 125,000 cells/cm^2 (cynomolgus) and differentiated +/- 50 nM INK128 from day 0 onwards. Imaging was started at day 2 of differentiation. Images were acquired every 10 min for 48 to 72 h on an Olympus IX81 widefield microscope with a 20X 0.75 NA objective. Cells were kept in a humidified stage top incubator (Ibidi) at 37 °C and 5% CO_2.

5.9.4 Cell tracking and PIP-FUCCI analysis

Tracking was performed in Fiji (ImageJ v2.9.0) with TrackMate v7.9.2 using the "Manual Tracking" option. Here, a circular region of interest (ROI) with a radius of 2.24 px was manually placed in the center of a nucleus in each frame of a track. mVenus and mCherry fluorescence were measured inside the ROI. Each track started at the first frame after cell division and ended with the last frame before the next division, so the total cell cycle duration was calculated as *end frame – start frame*. Cell cycle phase durations were calculated based on mVenus fluorescence. The G1/S transition was defined as the frame in which mVenus signal in the first half of the track (scaled between 1 and 2) was closest to its half maximum ($PIP_{half\text{-}max}$). The S/G2M transition was the frame in which mVenus signal had an increase of > 0 and kept rising at an average of ≥ 1.5% over the following five frames (PIP_{rise}) in the second half of the track (scaled between 1 and 2). Thus, phase durations were calculated as follows:

$$G1_{duration} = PIP_{half-max} - start$$

$$S_{duration} = PIP_{rise} - PIP_{half-max}$$

$$G2M_{duration} = end - PIP_{rise}$$

5.10 Human PAX6::H2B-GFP reporter

5.10.1 Generation of H9 PAX6::H2B-GFP cells with a nuclear reporter

The H9 PAX6::H2B-GFP reporter line (Tchieu et al., 2017) was nucleofected with a piggyBAC vector containing an H2B-Cerulean reporter under the control of a CAG promoter. Two constructs with either a *puromycin N-acetyltransferase* gene (*pac*) or a *blasticidin S-deaminase* (*bsd*) gene for selection located downstream of the reporter after an IRES sequence were used. Cells were nucleofected with the piggyBAC vector and a pCAG pBase HN 2545 transposase plasmid for random integration of the transgene (Wang et al., 2008). Successfully transfected cells were selected under 1.5 µg/ml puromycin or 15 µg/ml blasticidin. Polyclonal populations were used for all experiments and kept under constant selection.

5.10.2 Time-lapse imaging of H9 PAX6::H2B-GFP; H2B-Cerulean reporter cells

H9 PAX6::H2B-GFP; H2B-Cerulean reporter cells were seeded onto µ-slides (Ibidi) at a density of 250,000 cells/cm^2 and grown in UPPS + 10 µM ROCK inhibitor overnight. NPC differentiation was induced with imaging NPCSL at day 0, either without or with 30 nM/40 nM mTOR inhibitor INK128 and cells were allowed to differentiate for one day before imaging start. At day 1 of NPC

differentiation, image acquisition was started on an Olympus IX81 widefield microscope with an iXon 888 EM-CCD camera (Andor) and LED illumination (pE4000, CoolLED) on a 40X 1.30 NA oil immersion objective. All hardware components were controlled by MicroManager 2.0 (Edelstein et al., 2010). Images were taken in 30 min intervals for up to five days. Cells were washed daily and medium was changed.

5.10.3 Analysis of H9 PAX6::H2B-GFP; H2B-Cerulean time-lapse series

Time series of H9 PAX6::H2B-GFP; H2B-Cerulean reporter cells were segmented based on the nuclear H2B-Cerulean signal using StarDist 2D and the *Versatile (fluorescent nuclei) model* (Schmidt et al., 2018) with the probability threshold set to 0.70 and otherwise default parameters. During differentiation, cells accumulated debris which was largely removed by washing and media changes. This introduced shifts in PAX6::H2B-GFP signal intensity. To reduce these artificial shifts, I generated a Gaussian blur image (radius = 50 µm) of the PAX6::H2B-GFP channel in each frame and subtracted it from the original image. PAX6::H2B-GFP intensity was measured on the resulting corrected image. Nuclei with an area ≤ 50 µm² were filtered out and the frame average of PAX6::H2B-GFP intensity was calculated across all remaining nuclei per condition.

5.11 Glycogen measurements

Glycogen contents were measured using the Glycogen Assay Kit ab65620. Glycogen is first hydrolyzed to glucose which is then oxidized and thereby generates a product that reacts with an OxiRed probe. Cells were harvested after DPBS (w/o Ca^{2+}/Mg^{2+})-washing by Accutase and centrifugation at 200 g for 5 min. The cells were again washed with DPBS (w/o Ca^{2+}/Mg^{2+}) and finally resuspended in cold H_2O. For glycogen content normalization, cells were counted using a Countess Automated Cell Counter in a 1:1 trypan blue dilution. Cell lysis and enzymatic inactivation were performed by boiling the cell suspension for 10 min. The homogenate was centrifuged for 10 min at 18,000 g and 4 °C and the supernatant containing all soluble cellular contents was subsequently assayed for glycogen contents. Different amounts of supernatant were transferred to a 96-well plate and adjusted to 50 µl reaction volume with Hydrolysis Buffer. Each sample concentration was measured in duplicate. The hydrolysis reaction was performed by addition of 1 µl Hydrolysis Enzyme Mix at room temperature for 30 min. Glucose was detected by adding 50 µl of Reaction Mix (48.7 µl Development Buffer; 1 µl Development Enzyme Mix; 0.3 µl OxiRed Probe) to each sample for 30 min at room temperature, protected from light. To reduce background signal caused by intracellular glucose, sample background controls without Hydrolysis Enzyme Mix to convert glycogen to glucose were performed in parallel. A standard curve with glycogen concentrations ranging from 0 (blank) to 0.2 µg glycogen/well was used to calculate glycogen contents. All sample, sample background and standard wells were measured

at 535/587 nm (Ex/Em) on a Tecan Plate Reader. Duplicate measurements were averaged and sample background readings subtracted from sample readings. Next, the blank measurement was subtracted from all measurements. The standard readings were plotted against the glycogen concentration/well and a linear fit was performed to calculate glycogen contents in each sample well. Since different amounts of supernatant were measured, glycogen contents per µl supernatant were averaged for each sample. The resulting glycogen content [µg/µl supernatant] was then normalized to the number of cells in solution before homogenization.

5.12 Single-cell RNA-sequencing

For Single-cell RNA sequencing, I used the Chromium Next GEM Single Cells 3' Reagent Kits v3.1 (Dual Index) with Feature Barcode technology for Cell Multiplexing (10x Genomics) according to the manufacturer's instructions with minor modifications. This protocol allows for multiplexing of several samples and pooled sequencing. In 10x single-cell applications, lipid droplets containing single cells and a gel bead are formed (Gel Beads-in-emulsion, GEMs). The gel beads contain oligos required for reverse transcription of mRNAs including sequencing primers, a 10x Barcode specific to individual gel beads, unique molecular identifiers (UMIs), poly(dT) oligos and Capture Sequences. Thereby, cDNA libraries of single cells can be generated to obtain transcriptome data with single-cell resolution.

5.12.1 Experimental set-up for RbTKO scRNAseq

For the RbTKO experiment, mouse wild type and RbTKO cells were seeded into six-well plates according to the NPC differentiation protocol (Chapter 5.2). To obtain a time-resolved data set, multiple wells per cell line were seeded. NPC induction was performed one day after seeding. Uninduced cells (day 0) and day 2 and 4 NPCs were harvested for library generation as described in chapter 5.12.3.

5.12.2 Experimental set-up for mTORi scRNAseq

For the mTORi-related line of experiments, five six-wells of mouse, cynomolgus and human cells each were seeded one day before neural induction as described before (Chapter 5.2). At day 0, NPC differentiation was induced in four wells, two of which were also subsequently treated with 50 nM INK128. The uninduced well served as the day 0 pluripotency control. Day 0 PSCs and day 2 and 4 NPCs were used for cDNA library generation.

Therefore, the procedure described in the following was performed at days 0, 2 and 4 of differentiation for both experiments.

5.12.3 Cell preparation and multiplexing

Cells were harvested after thorough washing by detaching with Accutase. Cells in suspension were centrifuged for 5 min at 200 g and pellets resuspended in DPBS (w/o Ca^{2+}/Mg^{2+}) + 0.04% BSA. The washing step was repeated once. To obtain a single-cell suspension, cells were passed through a cell strainer and counted using a Countess Automated Cell Counter (Invitrogen) in a 1:1 dilution with trypan blue. Where possible, $1 \cdot 10^6$ cells were transferred to DNA LoBind tubes and centrifuged again at 4 °C.

In a next step, the individual samples were labeled for sample demultiplexing in the analysis process. Each pellet was resuspended in 100 µl specific Cell Multiplexing Oligo (CMO) and incubated for 5 min at room temperature to allow for CMO binding to the plasma membrane. The labeling reaction was stopped by addition of 1.9 ml DPBS (w/o Ca^{2+}/Mg^{2+}) + 1% BSA and cells were centrifuged again at 4 °C. Pelleted cells were resuspended in DPBS (w/o Ca^{2+}/Mg^{2+}) + 1% BSA and samples were pooled at equal ratios to obtain a suspension of $1.5 \cdot 10^6$ cells. Since neural differentiation sometimes led to increased cell death and cell debris, the pooled samples were sorted with an FACS Aria Fusion (BD Biosciences) to remove small particles and cell clumps based on forward and side scatter (FSC and SSC) gating.

5.12.4 GEM generation and library preparation

Sorted cells were counted again and the appropriate volume of cells for a target cell recovery of 12,000 cells for day 0 and 22,000 cells for days 2 and 4 was added to a GEM-RT master mix for reverse transcription and loaded onto a Chromium Next GEM Chip according to the manufacturer's instructions. Immediately after GEM generation, the gel beads are dissolved. Cells are lysed and exposed to the oligos within the gel bead. During the GEM-RT, two kinds of DNA molecules are synthesized, (1) a cDNA molecule containing a 10x barcode specific to an individual cell and a UMI specific to the individual cDNA molecule captured by the poly(dT) oligo and (2) a multiplexing DNA containing the 10x barcode and UMI as well as the Feature Barcode (Cell Multiplexing Oligo) that identifies each sample within a pool, captured by a specific Capture Sequence.

Following GEM-RT, cDNA libraries were generated. For each GEM-RT, two separate libraries were made; a 3' Gene Expression library and a Cell Multiplexing library, allowing for sample demultiplexing based on CMO labeling. cDNA was amplified and cDNA fragments were separated by size through SPRIselect cleanup. Larger fragments were used for gene expression library generation while smaller fragments were used for multiplexing library generation. For the 3' Gene Expression library, cDNA fragment size was optimized by enzymatic fragmentation followed by A-tailing and adapter ligation. For cDNA amplification and library demultiplexing, a sample index PCR was performed. Similarly, a sample index PCR was performed on the shorter

DNA fragments obtained through the SPRIselect cleanup. Library quality and fragment size was evaluated with a BioAnalyzer using the BioAnalyzer High Sensitivity DNA Assay (Agilent).

5.12.5 Sequencing, mapping and demultiplexing

The 3' Gene Expression libraries were sequenced with a target sequencing depth of 25,000 read pairs/cell. The Cell Multiplexing libraries were sequenced at a depth of 5,000 read pairs/cell. Sequencing reads were obtained through NovaSeq X Plus PE150.

Each 3' Gene Expression library contained reads of mouse, cynomolgus and human cells. Therefore, 3' Gene Expression libraries of each time point (days 0, 2 and 4) were mapped against each genome separately. The mouse genome mm10 (GENCODE vM23/Ensembl98) and the human genome GRCh38 (GENCODE v32/Ensembl98) were obtained from 10x Genomics, the cynomolgus genome GCA_011100615.1 (Genome assembly 6.0) was obtained from Ensembl. Mapping was performed using CellRanger 7.2.0 (10x Genomics). Using the *cellranger multi* function, sample demultiplexing occurred in parallel to read alignment. Downstream analyses were performed in Seurat v5 (Hao et al., 2023). Only cells with a minimum feature count of > 3000 and a maximum mitochondrial gene percentage of < 15% were considered. Depending on the sample, between 281 and 2034 cells per sample were retained with a mean read count between 12,781 and 39,916 reads/cell. Each cell's feature counts were divided by the total count number for that cell, multiplied by a scaling factor of 10,000 and log1p-transformed. Data were then scaled to obtain a mean expression of 0 and a variance of 1 across cells.

5.12.6 Clustering and cell cycle phase annotations

Clustering analysis was performed using unsupervised Louvain clustering at the indicated resolution. Cell cycle phase annotation was based on the cell cycle phase-specific gene sets from Tirosh et al. (2016) and performed with the Seurat function *CellCycleScoring*. Quantification and heatmap visualization of clustering and cell cycle scoring were done using a custom-made pheatmap-based heatmap (Schumacher et al., 2023).

5.12.7 Gene ontology analysis

GO terms were obtained using ShinyGO 8.0 (Ge et al., 2020) selecting either human genes GRCh38.p13, mouse genes GRCm39 or Crab-eating macaque genes Macaca_fascicularis_6.0. Only *Biological Processes* were considered. Figures show the top 10 most significantly enriched GO terms.

5.12.8 Data integration

For single-cell data set integration, I used the Python-based Scanpy function *ingest* (Wolf et al., 2018). A pre-processed, time-resolved scRNAseq data set of a differentiation time course in mouse, cynomolgus and human obtained by Alexandra de la Porte and Moritz Thomas (Helmholtz Munich) served as a reference. Query sequencing data was processed as described before and all time points were concatenated. Reference time point assignments were quantified using the custom-made pheatmap-based heatmap (Schumacher et al., 2023).

6 References

Adeva-Andany, M. M., González-Lucán, M., Donapetry-García, C., Fernández-Fernández, C., & Ameneiros-Rodríguez, E. (2016). Glycogen metabolism in humans. *BBA Clinical*, *5*, 85–100. https://doi.org/10.1016/J.BBACLI.2016.02.001

Aladjem, M. I., Spike, B. T., Rodewald, L. W., Hope, T. J., Klemm, M., Jaenisch, R., & Wahl, G. M. (1998). ES cells do not activate p53-dependent stress responses and undergo p53-independent apoptosis in response to DNA damage. *Current Biology : CB*, *8*(3), 145–155. https://doi.org/10.1016/S0960-9822(98)70061-2

Allis, C. D., & Jenuwein, T. (2016). The molecular hallmarks of epigenetic control. *Nature Reviews Genetics*, *17*(8), 487–500. https://doi.org/10.1038/nrg.2016.59

Arias, E. E., & Walter, J. C. (2005). PCNA functions as a molecular platform to trigger Cdt1 destruction and prevent re-replication. *Nature Cell Biology 2005 8:1*, *8*(1), 84–90. https://doi.org/10.1038/ncb1346

Barry, C., Schmitz, M. T., Jiang, P., Schwartz, M. P., Duffin, B. M., Swanson, S., Bacher, R., Bolin, J. M., Elwell, A. L., McIntosh, B. E., Stewart, R., & Thomson, J. A. (2017). Species-specific developmental timing is maintained by pluripotent stem cells ex utero. *Developmental Biology*, *423*(2), 101–110. https://doi.org/10.1016/j.ydbio.2017.02.002

Becker, K. A., Ghule, P. N., Therrien, J. A., Lian, J. B., Stein, J. L., Van Wijnen, A. J., & Stein, G. S. (2006). Self-renewal of human embryonic stem cells is supported by a shortened G1 cell cycle phase. *Journal of Cellular Physiology*, *209*(3), 883–893. https://doi.org/10.1002/jcp.20776

Ben-Sahra, I., Howell, J. J., Asara, J. M., & Manning, B. D. (2013). Stimulation of de novo pyrimidine synthesis by growth signaling through mTOR and S6K1. *Science (New York, N.Y.)*, *339*(6125), 1323–1328. https://doi.org/10.1126/SCIENCE.1228792

Ben-Sahra, I., Hoxhaj, G., Ricoult, S. J. H., Asara, J. M., & Manning, B. D. (2016). mTORC1 induces purine synthesis through control of the mitochondrial tetrahydrofolate cycle. *Science (New York, N.Y.)*, *351*(6274), 728–733. https://doi.org/10.1126/SCIENCE.AAD0489

Bieberich, E. (2014). Synthesis, processing, and function of N-glycans in N-glycoproteins. *Advances in Neurobiology*, *9*, 47. https://doi.org/10.1007/978-1-4939-1154-7_3

Birket, M. J., Orr, A. L., Gerencser, A. A., Madden, D. T., Vitelli, C., Swistowski, A., Brand, M. D., & Zeng, X. (2011). A reduction in ATP demand and mitochondrial activity with neural differentiation of human embryonic stem cells. *Journal of Cell Science*, *124*(3), 348–358. https://doi.org/10.1242/jcs.072272

Boward, B., Wu, T., & Dalton, S. (2016). Concise Review: Control of Cell Fate Through Cell Cycle and Pluripotency Networks. *Stem Cells*, *34*(6), 1427–1436. https://doi.org/10.1002/stem.2345

Brons, I. G. M., Smithers, L. E., Trotter, M. W. B., Rugg-Gunn, P., Sun, B., Chuva De Sousa Lopes, S. M., Howlett, S. K., Clarkson, A., Ahrlund-Richter, L., Pedersen, R. A., & Vallier, L. (2007). Derivation of pluripotent epiblast stem cells from mammalian embryos. *Nature*, *448*(7150), 191–195. https://doi.org/10.1038/nature05950

Brown, E. J., Albers, M. W., Bum Shin, T., Ichikawa, K., Keith, C. T., Lane, W. S., & Schreiber, S. L. (1994). A mammalian protein targeted by G1-arresting rapamycin–receptor complex. *Nature*, *369*(6483), 756–758. https://doi.org/10.1038/369756a0

Brunn, G. J., Hudson, C. C., Sekulić, A., Williams, J. M., Hosoi, H., Houghton, P. J., Lawrence, J. C., & Abraham, R. T. (1997). Phosphorylation of the translational repressor PHAS-I by the

mammalian target of rapamycin. *Science*, *277*(5322), 99–101. https://doi.org/10.1126/science.277.5322.99

Buchkovich, K., Duffy, L. A., & Harlow, E. (1989). The retinoblastoma protein is phosphorylated during specific phases of the cell cycle. *Cell*, *58*(6), 1097–1105. https://doi.org/10.1016/0092-8674(89)90508-4

Buffenstein, R., & Jarvis, J. U. M. (2002). The Naked Mole Rat--A New Record for the Oldest Living Rodent. *Science of Aging Knowledge Environment*, *2002*(21). https://doi.org/10.1126/SAGEKE.2002.21.PE7

Bulut-Karslioglu, A., Biechele, S., Jin, H., MacRae, T. A., Hejna, M., Gertsenstein, M., Song, J. S., & Ramalho-Santos, M. (2016). Inhibition of mTOR induces a paused pluripotent state. *Nature*, *540*(7631), 119–123. https://doi.org/10.1038/nature20578

Burnett, P. E., Barrow, R. K., Cohen, N. A., Snyder, S. H., & Sabatini, D. M. (1998). RAFT1 phosphorylation of the translational regulators p70 S6 kinase and 4E-BP1. *Proceedings of the National Academy of Sciences of the United States of America*, *95*(4), 1432–1437. https://doi.org/10.1073/pnas.95.4.1432

Bylund, M., Andersson, E., Novitch, B. G., & Muhr, J. (2003). Vertebrate neurogenesis is counteracted by Sox1-3 activity. *Nature Neuroscience*, *6*(11), 1162–1168. https://doi.org/10.1038/NN1131

Calder, A., Roth-Albin, I., Bhatia, S., Pilquil, C., Lee, J. H., Bhatia, M., Levadoux-Martin, M., McNicol, J., Russell, J., Collins, T., & Draper, J. S. (2013). Lengthened G1 phase indicates differentiation status in human embryonic stem cells. *Stem Cells and Development*, *22*(2), 279–295. https://doi.org/10.1089/scd.2012.0168

Calder, P. C. (1991). Glycogen structure and biogenesis. *J. Biochem*, *23*(12), 1335–1352. https://doi.org/10.1016/0020-711X(91)90274-Q

Carrieri, F. A., Murray, P. J., Ditsova, D., Ferris, M. A., Davies, P., & Dale, J. K. (2019). CDK 1 and CDK 2 regulate NICD 1 turnover and the periodicity of the segmentation clock. *EMBO Reports*, *20*(7). https://doi.org/10.15252/embr.201846436

Carroll, B., Nelson, G., Rabanal-Ruiz, Y., Kucheryavenko, O., Dunhill-Turner, N. A., Chesterman, C. C., Zahari, Q., Zhang, T., Conduit, S. E., Mitchell, C. A., Maddocks, O. D. K., Lovat, P., von Zglinicki, T., & Korolchuk, V. I. (2017). Persistent mTORC1 signaling in cell senescence results from defects in amino acid and growth factor sensing. *The Journal of Cell Biology*, *216*(7), 1949–1957. https://doi.org/10.1083/JCB.201610113

Cavanaugh, A. H., Hempel, W. M., Taylor, L. J., Rogalsky, V., Todorov, G., & Rothblum, L. I. (1995). Activity of RNA polymerase I transcription factor UBF blocked by Rb gene product. *Nature 1995 374:6518*, *374*(6518), 177–180. https://doi.org/10.1038/374177a0

Chambers, S. M., Fasano, C. A., Papapetrou, E. P., Tomishima, M., Sadelain, M., & Studer, L. (2009). Highly efficient neural conversion of human ES and iPS cells by dual inhibition of SMAD signaling. *Nature Biotechnology*, *27*(3), 275–280. https://doi.org/10.1038/nbt.1529

Chen, P.-L., Scully, P., Shew, J.-H., Wang, J. Y. J., & Lee, W.-H. (1989). Phosphorylation of the Retinoblastoma Gene Product Is Modulated during the Cell Cycle and Cellular Differentiation. *Cell*, *58*(6), 1193–1198. https://doi.org/10.1016/0092-8674(89)90517-5

Chen, Y., Wang, Y., Yang, C., Zhang, X., Liu, Y., Pu, G., Jiang, H., Pan, Y., Li, Z., & Lai, M. (2023). FOXG1 regulates the proliferation and apoptosis of human lung cancer cells. *Heliyon*, *9*(9), e19540. https://doi.org/10.1016/J.HELIYON.2023.E19540

Chotiner, J. Y., Wolgemuth, D. J., & Jeremy Wang, P. (2019). Functions of cyclins and CDKs in mammalian gametogenesis. *Biology of Reproduction*, *101*(3), 591. https://doi.org/10.1093/BIOLRE/IOZ070

Chung, J., Kuo, C. J., Crabtree, G. R., & Blenis, J. (1992). Rapamycin-FKBP specifically blocks growth-dependent activation of and signaling by the 70 kd S6 protein kinases. *Cell*, *69*(7), 1227–1236. https://doi.org/10.1016/0092-8674(92)90643-Q

Chung, S., Dzeja, P. P., Faustino, R. S., Perez-Terzic, C., Behfar, A., & Terzic, A. (2007). Mitochondrial oxidative metabolism is required for the cardiac differentiation of stem cells. *Nature Clinical Practice. Cardiovascular Medicine*, *4*(Suppl 1), S60. https://doi.org/10.1038/NCPCARDIO0766

Ciceri, G., Baggiolini, A., Cho, H. S., Kshirsagar, M., Benito-Kwiecinski, S., Walsh, R. M., Aromolaran, K. A., Gonzalez-Hernandez, A. J., Munguba, H., Koo, S. Y., Xu, N., Sevilla, K. J., Goldstein, P. A., Levitz, J., Leslie, C. S., Koche, R. P., & Studer, L. (2024). An epigenetic barrier sets the timing of human neuronal maturation. *Nature 2024 626:8000*, *626*(8000), 881–890. https://doi.org/10.1038/s41586-023-06984-8

Cockburn, K., & Rossant, J. (2010). Making the blastocyst: Lessons from the mouse. *Journal of Clinical Investigation*, *120*(4), 995–1003. https://doi.org/10.1172/JCI41229

Cooper, G. M. (2000). *The Eukaryotic Cell Cycle*. https://www.ncbi.nlm.nih.gov/books/NBK9876/

Copp, A. J. (2005). Neurulation in the cranial region - Normal and abnormal. *Journal of Anatomy*, *207*(5), 623–635. https://doi.org/10.1111/j.1469-7580.2005.00476.x

Coronado, D., Godet, M., Bourillot, P. Y., Tapponnier, Y., Bernat, A., Petit, M., Afanassieff, M., Markossian, S., Malashicheva, A., Iacone, R., Anastassiadis, K., & Savatier, P. (2013). A short G1 phase is an intrinsic determinant of naïve embryonic stem cell pluripotency. *Stem Cell Research*, *10*(1), 118–131. https://doi.org/10.1016/j.scr.2012.10.004

Dannenberg, J. H., Van Rossum, A., Schuijff, L., & Te Riele, H. (2000). Ablation of the retinoblastoma gene family deregulates G1 control causing immortalization and increased cell turnover under growth-restricting conditions. *Genes and Development*, *14*(23), 3051–3064. https://doi.org/10.1101/gad.847700

de Magalhães, J. P., Costa, J., & Church, G. M. (2007). An Analysis of the Relationship Between Metabolism, Developmental Schedules, and Longevity Using Phylogenetic Independent Contrasts. *The Journals of Gerontology. Series A, Biological Sciences and Medical Sciences*, *62*(2), 149. https://doi.org/10.1093/GERONA/62.2.149

DeCaprio, J. A., Ludlow, J. W., Lynch, D., Furukawa, Y., Griffin, J., Piwnica-Worms, H., Huang, C.-M., & Livingston', D. M. (1989). The Product of the Retinoblastoma Susceptibility Gene Has Properties of a Cell Cycle Regulatory Element. *Cell*, *58*(6), 1085–1095. https://doi.org/10.1016/0092-8674(89)90507-2

Dekker, J. (2014). Two ways to fold the genome during the cell cycle: insights obtained with chromosome conformation capture. *Epigenetics & Chromatin*, *7*(1), 25. https://doi.org/10.1186/1756-8935-7-25

Diaz-Cuadros, M., Miettinen, T. P., Skinner, O. S., Sheedy, D., Díaz-García, C. M., Gapon, S., Hubaud, A., Yellen, G., Manalis, S. R., Oldham, W. M., & Pourquié, O. (2023). Metabolic regulation of species-specific developmental rates. *Nature*, *613*(7944), 550–557. https://doi.org/10.1038/s41586-022-05574-4

Donjerkovic, D., & Scott, D. W. (2000). Regulation of the G1 phase of the mammalian cell cycle. *Cell Research 2000 10:1*, *10*(1), 1–16. https://doi.org/10.1038/sj.cr.7290031

Dunphy, W. G., Brizuela, L., Beach, D., & Newport, J. (1988). The Xenopus cdc2 protein is a component of MPF, a cytoplasmic regulator of mitosis. *Cell*, *54*(3), 423–431. https://doi.org/10.1016/0092-8674(88)90205-X

Easley, C. A., Ben-Yehudah, A., Redinger, C. J., Oliver, S. L., Varum, S. T., Eisinger, V. M., Carlisle, D. L., Donovan, P. J., & Schatten, G. P. (2010). mTOR-mediated activation of p70 S6K induces

differentiation of pluripotent human embryonic stem cells. *Cellular Reprogramming*, *12*(3), 263–273. https://doi.org/10.1089/CELL.2010.0011

Edelstein, A., Amodaj, N., Hoover, K., Vale, R., & Stuurman, N. (2010). Computer control of microscopes using μManager. *Current Protocols in Molecular Biology*, *Chapter 14*(SUPPL. 92). https://doi.org/10.1002/0471142727.MB1420S92

Edwards, R. G., Purdy, J. M., Steptoe, P. C., & Walters, D. E. (1981). The growth of human preimplantation embryos in vitro. *American Journal of Obstetrics and Gynecology*, *141*(4), 408–416. https://doi.org/10.1016/0002-9378(81)90603-7

Ershov, D., Phan, M. S., Pylvänäinen, J. W., Rigaud, S. U., Le Blanc, L., Charles-Orszag, A., Conway, J. R. W., Laine, R. F., Roy, N. H., Bonazzi, D., Duménil, G., Jacquemet, G., & Tinevez, J. Y. (2022). TrackMate 7: integrating state-of-the-art segmentation algorithms into tracking pipelines. *Nature Methods 2022 19:7*, *19*(7), 829–832. https://doi.org/10.1038/s41592-022-01507-1

Evans, M. J., & Kaufman, M. H. (1981). Establishment in culture of pluripotential cells from mouse embryos. *Nature 1981 292:5819*, *292*(5819), 154–156. https://doi.org/10.1038/292154a0

Evans, T., Rosenthal, E. T., Youngblom, J., Distel, D., & Hunt, T. (1983). Cyclin: A Protein Specified by Maternal mRNA in Sea Urchin Eggs That Is Destroyed at Each Cleavage Division. *Cell*, *33*(2), 389–396. https://doi.org/10.1016/0092-8674(83)90420-8

Ezhevsky, S. A., Ho, A., Becker-Hapak, M., Davis, P. K., & Dowdy, S. F. (2001). Differential regulation of retinoblastoma tumor suppressor protein by G(1) cyclin-dependent kinase complexes in vivo. *Molecular and Cellular Biology*, *21*(14), 4773–4784. https://doi.org/10.1128/MCB.21.14.4773-4784.2001

Ezhevsky, S. A., Nagahara, H., Vocero-Akbani, A. M., Gius, D. R., Wei, M. C., & Dowdy, S. F. (1997). Hypo-phosphorylation of the retinoblastoma protein (pRb) by cyclin D:Cdk4/6 complexes results in active pRb. *Proceedings of the National Academy of Sciences of the United States of America*, *94*(20), 10699. https://doi.org/10.1073/PNAS.94.20.10699

Favaro, E., Bensaad, K., Chong, M. G., Tennant, D. A., Ferguson, D. J. P., Snell, C., Steers, G., Turley, H., Li, J. L., Günther, U. L., Buffa, F. M., McIntyre, A., & Harris, A. L. (2012). Glucose Utilization via Glycogen Phosphorylase Sustains Proliferation and Prevents Premature Senescence in Cancer Cells. *Cell Metabolism*, *16*(6), 751–764. https://doi.org/10.1016/J.CMET.2012.10.017

Fenelon, J. C., Banerjee, A., & Murphy, B. D. (2014). Embryonic diapause: development on hold. *The International Journal of Developmental Biology*, *58*(2-3–4), 163–174. https://doi.org/10.1387/ijdb.140074bm

Fingar, D. C., Richardson, C. J., Tee, A. R., Cheatham, L., Tsou, C., & Blenis, J. (2004). mTOR Controls Cell Cycle Progression through Its Cell Growth Effectors S6K1 and 4E-BP1/Eukaryotic Translation Initiation Factor 4E. *Molecular and Cellular Biology*, *24*(1), 200. https://doi.org/10.1128/MCB.24.1.200-216.2004

Flemington, E. K., Speck, S. H., & Kaelin, W. G. (1993). E2F-1-mediated transactivation is inhibited by complex formation with the retinoblastoma susceptibility gene product. *Proceedings of the National Academy of Sciences of the United States of America*, *90*(15), 6914–6918. https://doi.org/10.1073/PNAS.90.15.6914

Fluckiger, A.-C., Marcy, G., Marchand, M., Négre, D., Cosset, F.-L., Mitalipov, S., Wolf, D., Savatier, P., & Dehay, C. (2006). Cell cycle features of primate embryonic stem cells. *Stem Cells (Dayton, Ohio)*, *24*(3), 547. https://doi.org/10.1634/STEMCELLS.2005-0194

Folmes, C. D. L., Dzeja, P. P., Nelson, T. J., & Terzic, A. (2012). Metabolic Plasticity in Stem Cell Homeostasis and Differentiation. *Cell Stem Cell*, *11*(5), 596–606. https://doi.org/10.1016/J.STEM.2012.10.002

Folmes, C. D. L., Nelson, T. J., Martinez-Fernandez, A., Arrell, D. K., Lindor, J. Z., Dzeja, P. P., Ikeda, Y., Perez-Terzic, C., & Terzic, A. (2011). Somatic Oxidative Bioenergetics Transitions into Pluripotency-Dependent Glycolysis to Facilitate Nuclear Reprogramming. *Cell Metabolism*, *14*(2), 264–271. https://doi.org/10.1016/J.CMET.2011.06.011

Gao, F.-B., Durand, B., & Raff, M. (1997). Oligodendrocyte precursor cells count time but not cell divisions before differentiation. *Current Biology*, *7*, 152–155.

Gautier, J., Minshull, J., Lohka, M., Glotzer, M., Hunt, T., & Maller, J. L. (1990). Cyclin is a component of maturation-promoting factor from Xenopus. *Cell*, *60*(3), 487–494. https://doi.org/10.1016/0092-8674(90)90599-A

Gautier, J., Norbury, C., Lohka, M., Nurse, P., & Maller, J. (1988). Purified maturation-promoting factor contains the product of a Xenopus homolog of the fission yeast cell cycle control gene cdc2+. *Cell*, *54*(3), 433–439. https://doi.org/10.1016/0092-8674(88)90206-1

Ge, S. X., Jung, D., Jung, D., & Yao, R. (2020). ShinyGO: a graphical gene-set enrichment tool for animals and plants. *Bioinformatics*, *36*(8), 2628–2629. https://doi.org/10.1093/BIOINFORMATICS/BTZ931

Gingras, A. C., Gygi, S. P., Raught, B., Polakiewicz, R. D., Abraham, R. T., Hoekstra, M. F., Aebersold, R., & Sonenberg, N. (1999). Regulation of 4E-BP1 phosphorylation: a novel two-step mechanism. *Genes & Development*, *13*(11), 1422. https://doi.org/10.1101/GAD.13.11.1422

Gleeson, J. G., Peter T, L., Flanagan, L. A., & Walsh, C. A. (1999). Doublecortin Is a Microtubule-Associated Protein and Is Expressed Widely by Migrating Neurons. *Neuron*, *23*(2), 257–271. https://doi.org/10.1016/S0896-6273(00)80778-3

Gökbuget, D., & Blelloch, R. (2019). Epigenetic control of transcriptional regulation in pluripotency and early differentiation. *Development (Cambridge, England)*, *146*(19), dev164772. https://doi.org/10.1242/DEV.164772

Goodrich, D. W., Wang, N. P., Qian, Y. W., Lee, E. Y. H. P., & Lee, W. H. (1991). The retinoblastoma gene product regulates progression through the G1 phase of the cell cycle. *Cell*, *67*(2), 293–302. https://doi.org/10.1016/0092-8674(91)90181-W

Gowans, G. J., & Hardie, D. G. (2014). AMPK: a cellular energy sensor primarily regulated by AMP. *Biochemical Society Transactions*, *42*(1), 71–75. https://doi.org/10.1042/BST20130244

Grandison, R. C., Piper, M. D. W., & Partridge, L. (2009). Amino-acid imbalance explains extension of lifespan by dietary restriction in Drosophila. *Nature*, *462*(7276), 1061–1064. https://doi.org/10.1038/NATURE08619

Grant, G. D., Kedziora, K. M., Limas, J. C., Cook, J. G., & Purvis, J. E. (2018). Accurate delineation of cell cycle phase transitions in living cells with PIP-FUCCI. *Cell Cycle*, *17*(21–22), 2496–2516. https://doi.org/10.1080/15384101.2018.1547001

Grunz, H., & Tacke, L. (1989). Neural differentiation of Xenopus laevis ectoderm takes place after disaggregation and delayed reaggregation without inducer. *Cell Differentiation and Development : The Official Journal of the International Society of Developmental Biologists*, *28*(3), 211–217. https://doi.org/10.1016/0922-3371(89)90006-3

Günther, B., & Morgado, E. (2004). Time in physics and biology. *Biological Research*, *37*(4), 759–765. https://doi.org/10.4067/S0716-97602004000500005

Gwinn, D. M., Shackelford, D. B., Egan, D. F., Mihaylova, M. M., Mery, A., Vasquez, D. S., Turk, B. E., & Shaw, R. J. (2008). AMPK phosphorylation of raptor mediates a metabolic checkpoint. *Molecular Cell*, *30*(2), 214. https://doi.org/10.1016/J.MOLCEL.2008.03.003

Han, J., Wang, B., Xiao, Z., Gao, Y., Zhao, Y., Zhang, J., Chen, B., Wang, X., & Dai, J. (2008). Mammalian target of rapamycin (mTOR) is involved in the neuronal differentiation of neural progenitors induced by insulin. *Molecular and Cellular Neuroscience*, *39*(1), 118–124.

https://doi.org/10.1016/J.MCN.2008.06.003

Hanahan, D., & Weinberg, R. A. (2000). The Hallmarks of Cancer. *Cell*, *100*(1), 57–70. https://doi.org/10.1016/S0092-8674(00)81683-9

Hanashima, C., Li, S. C., Shen, L., Lai, E., & Fishell, G. (2004). Foxg1 Suppresses Early Cortical Cell Fate. *Science*, *303*(5654), 56–59. https://doi.org/10.1126/SCIENCE.1090674/SUPPL_FILE/HANASHIMA.SOM.PDF

Hannan, K. M., Brandenburger, Y., Jenkins, A., Sharkey, K., Cavanaugh, A., Rothblum, L., Moss, T., Poortinga, G., McArthur, G. A., Pearson, R. B., & Hannan, R. D. (2003). mTOR-Dependent Regulation of Ribosomal Gene Transcription Requires S6K1 and Is Mediated by Phosphorylation of the Carboxy-Terminal Activation Domain of the Nucleolar Transcription Factor UBF. *Molecular and Cellular Biology*, *23*(23), 8862–8877. https://doi.org/10.1128/MCB.23.23.8862-8877.2003

Hao, Y., Stuart, T., Kowalski, M. H., Choudhary, S., Hoffman, P., Hartman, A., Srivastava, A., Molla, G., Madad, S., Fernandez-Granda, C., & Satija, R. (2023). Dictionary learning for integrative, multimodal and scalable single-cell analysis. *Nature Biotechnology 2023 42:2*, *42*(2), 293–304. https://doi.org/10.1038/s41587-023-01767-y

Hara, K., Yonezawa, K., Kozlowski, M. T., Sugimoto, T., Andrabi, K., Weng, Q. P., Kasuga, M., Nishimoto, I., & Avruch, J. (1997). Regulation of eIF-4E BP1 Phosphorylation by mTOR. *Journal of Biological Chemistry*, *272*(42), 26457–26463. https://doi.org/10.1074/JBC.272.42.26457

Harima, Y., Takashima, Y., Ueda, Y., Ohtsuka, T., & Kageyama, R. (2013). Accelerating the Tempo of the Segmentation Clock by Reducing the Number of Introns in the Hes7 Gene. *Cell Reports*, *3*(1), 1–7. https://doi.org/10.1016/j.celrep.2012.11.012

Harman, D. (1968). Free Radical Theory of Aging: Effect of Free Radical Reaction Inhibitors on the Mortality Rate of Male LAF1 Mice. *Journal of Gerontology*, *23*(4), 476–482. https://doi.org/10.1093/GERONJ/23.4.476

Harman, Denham. (1972). The Biologic Clock: The Mitochondria? *Journal of the American Geriatrics Society*, *20*(4), 145–147. https://doi.org/10.1111/j.1532-5415.1972.tb00787.x

Harman, Denham. (1992). Free radical theory of aging. *Mutation Research*, *275*(3–6), 257–266. https://doi.org/10.1016/0921-8734(92)90030-s

Hartwell, L. H. (1967). Macromolecule synthesis in temperature-sensitive mutants of yeast. *Journal of Bacteriology*, *93*(5), 1662–1670. https://doi.org/10.1128/JB.93.5.1662-1670.1967

Hartwell, L. H. (1973). Three Additional Genes Required for Deoxyribonucleic Acid Synthesis in Saccharomyces cerevisiae. *Journal of Bacteriology*, *115*(3), 966. https://doi.org/10.1128/JB.115.3.966-974.1973

Hartwell, L. H., Mortimer, R. K., Culotti, J., & Culotti, M. (1973). Genetic Control of the Cell Division Cycle in Yeast: V. Genetic Analysis of cdc Mutants. *Genetics*, *74*(2), 267–286. https://doi.org/10.1093/GENETICS/74.2.267

Helin, K., Harlow, E. D., & Fattaey, A. (1993). Inhibition of E2F-1 Transactivation by Direct Binding of the Retinoblastoma Protein. *MOLECULAR AND CELLULAR BIOLOGY*, *13*(10), 6501–6508.

Helin, K., Lees, J. A., Vidal, M., Dyson, N., Harlow, E., & Fattaey, A. (1992). A cDNA encoding a pRB-binding protein with properties of the transcription factor E2F. *Cell*, *70*(2), 337–350. https://doi.org/10.1016/0092-8674(92)90107-N

Hemmati-Brivanlou, A., & Melton, D. A. (1994). Inhibition of activin receptor signaling promotes neuralization in Xenopus. *Cell*, *77*(2), 273–281. https://doi.org/10.1016/0092-8674(94)90319-0

Henley, S. A., & Dick, F. A. (2012). The retinoblastoma family of proteins and their regulatory functions in the mammalian cell division cycle. *Cell Division*, *7*(1). https://doi.org/10.1186/1747-1028-7-10

Hergenreder, E., Minotti, A. P., Zorina, Y., Oberst, P., Zhao, Z., Munguba, H., Calder, E. L., Baggiolini, A., Walsh, R. M., Liston, C., Levitz, J., Garippa, R., Chen, S., Ciceri, G., & Studer, L. (2024). Combined small-molecule treatment accelerates maturation of human pluripotent stem cell-derived neurons. *Nature Biotechnology 2024*, 1–11. https://doi.org/10.1038/s41587-023-02031-z

Hettige, N. C., Peng, H., Wu, H., Zhang, X., Yerko, V., Zhang, Y., Jefri, M., Soubannier, V., Maussion, G., Alsuwaidi, S., Ni, A., Rocha, C., Krishnan, J., McCarty, V., Antonyan, L., Schuppert, A., Turecki, G., Fon, E. A., Durcan, T. M., & Ernst, C. (2022). FOXG1 dose tunes cell proliferation dynamics in human forebrain progenitor cells. *Stem Cell Reports*, *17*(3), 475. https://doi.org/10.1016/J.STEMCR.2022.01.010

Hiebert, S. W., Blake, M., Azizkhan, J., & Nevins, J. R. (1991). Role of E2F transcription factor in E1A-mediated trans activation of cellular genes. *Journal of Virology*, *65*(7), 3547–3552. https://doi.org/10.1128/JVI.65.7.3547-3552.1991

Hofmann, J. F. X., & Beach, D. (1994). cdt 1 is an essential target of the Cdc 1 O/Sct 1 transcription factor: requirement for DNA replication and inhibition of mitosis. *The EMBO Journal*, *13*(2), 425–434.

Hong, Y., & Stambrook, P. J. (2004). *Restoration of an absent G 1 arrest and protection from apoptosis in embryonic stem cells after ionizing radiation*. www.pnas.orgcgidoi10.1073pnas.0401346101

Howard, A., & Pelc, S. R. (1951). Nuclear incorporation of P32 as demonstrated by autoradiographs. *Experimental Cell Research*, *2*(2), 178–187. https://doi.org/10.1016/0014-4827(51)90083-3

Hsieh, A. C., Liu, Y., Edlind, M. P., Ingolia, N. T., Janes, M. R., Sher, A., Shi, E. Y., Stumpf, C. R., Christensen, C., Bonham, M. J., Wang, S., Ren, P., Martin, M., Jessen, K., Feldman, M. E., Weissman, J. S., Shokat, K. M., Rommel, C., & Ruggero, D. (2012). The translational landscape of mTOR signalling steers cancer initiation and metastasis. *Nature*, *485*(7396), 55. https://doi.org/10.1038/NATURE10912

Hu, D., Linders, A., Yamak, A., Correia, C., Kijlstra, J. D., Garakani, A., Xiao, L., Milan, D. J., Van Der Meer, P., Serra, M., Alves, P. M., & Domian, I. J. (2018). Metabolic Maturation of Human Pluripotent Stem Cell-Derived Cardiomyocytes by Inhibition of HIF1α and LDHA. *Circulation Research*, *123*(9), 1066–1079. https://doi.org/10.1161/CIRCRESAHA.118.313249

Hubaud, A., & Pourquié, O. (2014). Signalling dynamics in vertebrate segmentation. *Nature Reviews Molecular Cell Biology*, *15*(11), 709–721. https://doi.org/10.1038/nrm3891

Inoki, K., Li, Y., Xu, T., & Guan, K. L. (2003). Rheb GTPase is a direct target of TSC2 GAP activity and regulates mTOR signaling. *Genes & Development*, *17*(15), 1829–1834. https://doi.org/10.1101/GAD.1110003

Inoki, K., Li, Y., Zhu, T., Wu, J., & Guan, K. L. (2002). TSC2 is phosphorylated and inhibited by Akt and suppresses mTOR signalling. *Nature Cell Biology 2002 4:9*, *4*(9), 648–657. https://doi.org/10.1038/ncb839

Inoki, K., Zhu, T., & Guan, K. L. (2003). TSC2 Mediates Cellular Energy Response to Control Cell Growth and Survival. *Cell*, *115*(5), 577–590. https://doi.org/10.1016/S0092-8674(03)00929-2

Iwata, R., Casimir, P., Erkol, E., Boubakar, L., Planque, M., Gallego López, I. M., Ditkowska, M., Gaspariunaite, V., Beckers, S., Remans, D., Vints, K., Vandekeere, A., Poovathingal, S., Bird, M., Corthout, N., Vermeersch, P., Carpentier, S., Davie, K., Mazzone, M., … Vanderhaeghen, P.

(2023). *Mitochondria metabolism sets the species-specific tempo of neuronal development*. *4705*(January), 1–17.

Jackson, M., Krassowska, A., Gilbert, N., Chevassut, T., Forrester, L., Ansell, J., & Ramsahoye, B. (2004). Severe Global DNA Hypomethylation Blocks Differentiation and Induces Histone Hyperacetylation in Embryonic Stem Cells. *Molecular and Cellular Biology*, *24*(20), 8862–8871. https://doi.org/10.1128/MCB.24.20.8862-8871.2004

James, D., Levine, A. J., Besser, D., & Hemmati-Brivanlou, A. (2005). TGFbeta/activin/nodal signaling is necessary for the maintenance of pluripotency in human embryonic stem cells. *Development (Cambridge, England)*, *132*(6), 1273–1282. https://doi.org/10.1242/DEV.01706

Jenuwein, T., & Allis, C. D. (2001). Translating the histone code. *Science*, *293*(5532), 1074–1080. https://doi.org/10.1126/SCIENCE.1063127/ASSET/FCD15CEA-ECDC-41AF-AE32-FEDCEA8620CC/ASSETS/GRAPHIC/SE3119652003.JPEG

Jewett, D. A., & Dukelow, W. R. (1972). Cyclicity and gestation length of Macaca fascicularis. *Primates*, *13*(3), 327–332. https://doi.org/10.1007/BF01730578/METRICS

Kaeberlein, M., Powers, R. W., Steffen, K. K., Westman, E. A., Hu, D., Dang, N., Kerr, E. O., Kirkland, K. T., Fields, S., & Kennedy, B. K. (2005). Regulation of yeast replicative life span by TOR and Sch9 in response to nutrients. *Science (New York, N.Y.)*, *310*(5751), 1193–1196. https://doi.org/10.1126/SCIENCE.1115535

Kapahi, P., Zid, B. M., Harper, T., Koslover, D., Sapin, V., & Benzer, S. (2004). Regulation of lifespan in Drosophila by modulation of genes in the TOR signaling pathway. *Current Biology : CB*, *14*(10), 885–890. https://doi.org/10.1016/J.CUB.2004.03.059

Kawasaki, H., Mizuseki, K., Nishikawa, S., Kaneko, S., Kuwana, Y., Nakanishi, S., Nishikawa, S. I., & Sasai, Y. (2000). Induction of midbrain dopaminergic neurons from ES cells by stromal cell-derived inducing activity. *Neuron*, *28*(1), 31–40. https://doi.org/10.1016/S0896-6273(00)00083-0

Keller, G. M. (1995). In vitro differentiation of embryonic stem cells. *Current Opinion in Cell Biology*, *7*(6), 862–869. https://doi.org/10.1016/0955-0674(95)80071-9

Kim, D.-H., Sarbassov, D. D., Ali, S. M., King, J. E., Latek, R. R., Erdjument-Bromage, H., Tempst, P., & Sabatini, D. M. (2002). mTOR Interacts with Raptor to Form a Nutrient-Sensitive Complex that Signals to the Cell Growth Machinery pathway. *Cell*, *110*(2), 163–175. http://www.cell.com/cgi/content/full/110/

Kim, H., Wu, J., Ye, S., Tai, C. I., Zhou, X., Yan, H., Li, P., Pera, M., & Ying, Q. L. (2013). Modulation of β-catenin function maintains mouse epiblast stem cell and human embryonic stem cell self-renewal. *Nature Communications*, *4*, 2403. https://doi.org/10.1038/NCOMMS3403

Kleiber, M. (1932). Body Size and Metabolism. *Hilgardia Journal of Agricultural Science*, *6*(11), 315–353.

Kojima, Y., Tam, O. H., & Tam, P. P. L. (2014). Timing of developmental events in the early mouse embryo. *Seminars in Cell & Developmental Biology*, *34*, 65–75. https://doi.org/10.1016/J.SEMCDB.2014.06.010

Kukreja, K., Patel, N., Megason, S. G., & Klein, A. M. (2023). Global decoupling of cell differentiation from cell division in early embryo development. *BioRxiv*.

Labuschagne, C. F., van den Broek, N. J. F., Mackay, G. M., Vousden, K. H., & Maddocks, O. D. K. (2014). Serine, but not glycine, supports one-carbon metabolism and proliferation of cancer cells. *Cell Reports*, *7*(4), 1248–1258. https://doi.org/10.1016/j.celrep.2014.04.045

Lázaro, J., Costanzo, M., Sanaki-Matsumiya, M., Girardot, C., Hayashi, M., Hayashi, K., Diecke, S., Hildebrandt, T. B., Lazzari, G., Wu, J., Petkov, S., Behr, R., Trivedi, V., Matsuda, M., & Ebisuya,

M. (2023). A stem cell zoo uncovers intracellular scaling of developmental tempo across mammals. *Cell Stem Cell*, 938–949. https://doi.org/10.1016/j.stem.2023.05.014

Lee, M. H., Reynisdóttir, I., & Massagué, J. (1995). Cloning of p57KIP2, a cyclin-dependent kinase inhibitor with unique domain structure and tissue distribution. *Genes & Development*, *9*(6), 639–649. https://doi.org/10.1101/GAD.9.6.639

Lee, S. H., Lumelsky, N., Studer, L., Auerbach, J. M., & McKay, R. D. (2000). Efficient generation of midbrain and hindbrain neurons from mouse embryonic stem cells. *Nature Biotechnology*, *18*(6), 675–679. https://doi.org/10.1038/76536

Lees, E., Faha, B., Dulic, V., Reed, S. I., & Harlow, E. (1992). Cyclin E/cdk2 and cyclin A/cdk2 kinases associate with p107 and E2F in a temporally distinct manner. *Genes & Development*, *6*(10), 1874–1885. https://doi.org/10.1101/GAD.6.10.1874

Lestienne, R. (1988). From physical to biological time. *Mechanisms of Ageing and Development*, *43*(3), 189–228. https://doi.org/10.1016/0047-6374(88)90032-2

Lian, X., Zhang, J., Azarin, S. M., Zhu, K., Hazeltine, L. B., Bao, X., Hsiao, C., Kamp, T. J., & Palecek, S. P. (2012). Directed cardiomyocyte differentiation from human pluripotent stem cells by modulating Wnt/β-catenin signaling under fully defined conditions. *Nature Protocols 2013 8:1*, *8*(1), 162–175. https://doi.org/10.1038/nprot.2012.150

Libé-Philippot, B., & Vanderhaeghen, P. (2021). *Annual Review of Genetics Cellular and Molecular Mechanisms Linking Human Cortical Development and Evolution*. https://doi.org/10.1146/annurev-genet-071719

Linaro, D., Vermaercke, B., Iwata, R., Ramaswamy, A., Libé-Philippot, B., Boubakar, L., Davis, B. A., Wierda, K., Davie, K., Poovathingal, S., Penttila, P. A., Bilheu, A., De Bruyne, L., Gall, D., Conzelmann, K. K., Bonin, V., & Vanderhaeghen, P. (2019). Xenotransplanted Human Cortical Neurons Reveal Species-Specific Development and Functional Integration into Mouse Visual Circuits. *Neuron*, *104*(5), 972-986.e6. https://doi.org/10.1016/j.neuron.2019.10.002

Lindstedt, S. L., & Calder, W. A. (1981). Body Size, Physiological Time, and Longevity of Homeothermic Animals. *Quarterly Review of Biology*, *56*(1), 1–16. https://doi.org/10.1086/412080

Liu, G. Y., & Sabatini, D. M. (2020). mTOR at the nexus of nutrition, growth, ageing and disease. *Nature Reviews Molecular Cell Biology 2020 21:4*, *21*(4), 183–203. https://doi.org/10.1038/s41580-019-0199-y

Lohka, M. J., Hayes, M. K., & Maller, J. L. (1988). Purification of maturation-promoting factor, an intracellular regulator of early mitotic events. *Proceedings of the National Academy of Sciences of the United States of America*, *85*(9), 3009–3013. https://doi.org/10.1073/PNAS.85.9.3009

Lu, P., Ceto, S., Wang, Y., Graham, L., Wu, D., Kumamaru, H., Staufenberg, E., & Tuszynski, M. H. (2017). Prolonged human neural stem cell maturation supports recovery in injured rodent CNS. *The Journal of Clinical Investigation*, *127*(9), 3287. https://doi.org/10.1172/JCI92955

Mac Auley, A., Werb, Z., & Mirkes, P. E. (1993). Characterization of the unusually rapid cell cycles during rat gastrulation. *Development*, *117*(3), 873–883. https://doi.org/10.1242/dev.117.3.873

Madhavan, J., Mallikarjuna, K., Vikas, K., George, R., Bremner, R., & Kumaramanickavel, G. (2010). CDKN1C (p57KIP2) mRNA expression in human retinoblastomas. *Ophthalmic Genetics*, *31*(3), 141–146. https://doi.org/10.3109/13816810.2010.490544

Magee, C., Nurminskaya, M., & Linsenmayer, T. F. (2001). UDP-glucose pyrophosphorylase: up-regulation in hypertrophic cartilage and role in hyaluronan synthesis. *Biochemical Journal*, *360*(Pt 3), 667. https://doi.org/10.1042/0264-6021:3600667

Mahmoud, A. I. (2023). Metabolic switches during development and regeneration. *Development (Cambridge)*, *150*(20). https://doi.org/10.1242/DEV.202008/334166

Malumbres, M., & Barbacid, M. (2005). Mammalian cyclin-dependent kinases. *Trends in Biochemical Sciences*, *30*(11), 630–641. https://doi.org/10.1016/J.TIBS.2005.09.005

Martínez-Alonso, D., & Malumbres, M. (2020). Mammalian cell cycle cyclins. *Seminars in Cell & Developmental Biology*, *107*, 28–35. https://doi.org/10.1016/J.SEMCDB.2020.03.009

Martínez-Reyes, I., & Chandel, N. S. (2020). Mitochondrial TCA cycle metabolites control physiology and disease. *Nature Communications*, *11*(1). https://doi.org/10.1038/s41467-019-13668-3

Matsuda, M., Hayashi, H., Garcia-Ojalvo, J., Yoshioka-Kobayashi, K., Kageyama, R., Yamanaka, Y., Ikeya, M., Toguchida, J., Alev, C., & Ebisuya, M. (2020). Species-specific segmentation clock periods are due to differential biochemical reaction speeds. *Science*, *369*(6509), 1450–1455. https://doi.org/10.1126/SCIENCE.ABA7668

Matsuoka, S., Edwards, M. C., Bai, C., Parker, S., Zhang, P., Baldini, A., Harper, J. W., & Elledge, S. J. (1995). p57KIP2, a structurally distinct member of the p21CIP1 Cdk inhibitor family, is a candidate tumor suppressor gene. *Genes & Development*, *9*(6), 650–662. https://doi.org/10.1101/GAD.9.6.650

Mayer, C., Zhao, J., Yuan, X., & Grummt, I. (2004). mTOR-dependent activation of the transcription factor TIF-IA links rRNA synthesis to nutrient availability. *Genes & Development*, *18*(4), 423–434. https://doi.org/10.1101/GAD.285504

McGhee, J. D., & Felsenfeld, G. (1980). Nucleosome structure. *Annual Review of Biochemistry*, *49*, 1115–1156. https://doi.org/10.1146/annurev.bi.49.070180.005343

McInnes, L., Healy, J., & Melville, J. (2020). *UMAP: Uniform Manifold Approximation and Projection for Dimension Reduction*.

Meyer, G., Perez-Garcia, C. G., & Gleeson, J. G. (2002). Selective Expression of Doublecortin and LIS1 in Developing Human Cortex Suggests Unique Modes of Neuronal Movement. *Cerebral Cortex*, *12*(12), 1225–1236. https://doi.org/10.1093/CERCOR/12.12.1225

Michels, A. A., Robitaille, A. M., Buczynski-Ruchonnet, D., Hodroj, W., Reina, J. H., Hall, M. N., & Hernandez, N. (2010). mTORC1 Directly Phosphorylates and Regulates Human MAF1. *Molecular and Cellular Biology*, *30*(15), 3749. https://doi.org/10.1128/MCB.00319-10

Mota-Martorell, N., Jove, M., Pradas, I., Berdún, R., Sanchez, I., Naudi, A., Gari, E., Barja, G., & Pamplona, R. (2020). Gene expression and regulatory factors of the mechanistic target of rapamycin (mTOR) complex 1 predict mammalian longevity. *GeroScience*, *42*(4), 1157–1173. https://doi.org/10.1007/S11357-020-00210-3

Mudryj, M., Hiebert, S. W., & Nevins, J. R. (1990). A role for the adenovirus inducible E2F transcription factor in a proliferation dependent signal transduction pathway. *The EMBO Journal*, *9*(7), 2179–2184. https://doi.org/10.1002/J.1460-2075.1990.TB07387.X

Muñoz-Sanjuán, I., & Brivanlou, A. H. (2002). Neural induction, the default model and embryonic stem cells. *Nature Reviews. Neuroscience*, *3*(4), 271–280. https://doi.org/10.1038/NRN786

Narasimha, A. M., Kaulich, M., Shapiro, G. S., Choi, Y. J., Sicinski, P., & Dowdy, S. F. (2014). Cyclin D activates the Rb tumor suppressor by mono-phosphorylation. *ELife*, *3*. https://doi.org/10.7554/ELIFE.02872

Neganova, I., Zhang, X., Atkinson, S., & Lako, M. (2009). Expression and functional analysis of G1 to S regulatory components reveals an important role for CDK2 in cell cycle regulation in human embryonic stem cells. *Oncogene*, *28*(1), 20–30. https://doi.org/10.1038/onc.2008.358

Nichols, J., & Smith, A. (2009). Naive and Primed Pluripotent States. *Cell Stem Cell*, *4*(6), 487–492. https://doi.org/10.1016/j.stem.2009.05.015

Nishitani, H., Lygerou, Z., Nishimoto, T., & Nurse, P. (2000). The Cdt1 protein is required to license DNA for replication in fission yeast. *Nature 2000 404:6778*, *404*(6778), 625–628. https://doi.org/10.1038/35007110

Niwa, H., Burdon, T., Chambers, I., & Smith, A. (1998). Self-renewal of pluripotent embryonic stem cells is mediated via activation of STAT3. *Genes & Development*, *12*(13), 2048–2060. https://doi.org/10.1101/GAD.12.13.2048

O'Neill, C. (2015). The epigenetics of embryo development. *Animal Frontiers*, *5*(1), 42–49. https://doi.org/10.2527/AF.2015-0007

Ohtani, K., Degregori, J., & Nevins, J. R. (1995). Regulation of the cyclin E gene by transcription factor E2F1. *Proceedings of the National Academy of Sciences*, *92*(26), 12146–12150. https://doi.org/10.1073/PNAS.92.26.12146

Okamoto, M., Miyata, T., Konno, D., Ueda, H. R., Kasukawa, T., Hashimoto, M., Matsuzaki, F., & Kawaguchi, A. (2016). Cell-cycle-independent transitions in temporal identity of mammalian neural progenitor cells. *Nature Communications*, *7*. https://doi.org/10.1038/ncomms11349

Otani, T., Marchetto, M. C., Gage, F. H., Simons, B. D., & Livesey, F. J. (2016). 2D and 3D Stem Cell Models of Primate Cortical Development Identify Species-Specific Differences in Progenitor Behavior Contributing to Brain Size. *Cell Stem Cell*, *18*(4), 467–480. https://doi.org/10.1016/J.STEM.2016.03.003

Otis, E. M., & Brent, R. (1954). Equivalent ages in mouse and human embryos. *The Anatomical Record*, *120*(1), 33–63. https://doi.org/10.1002/ar.1091200104

Padgett, J., & Santos, S. D. M. (2020). From clocks to dominoes: lessons on cell cycle remodelling from embryonic stem cells. *FEBS Letters*, *594*(13), 2031–2045. https://doi.org/10.1002/1873-3468.13862

Pagano, M., Pepperkok, R., Lukas, J., Baldin, V., Ansorge, W., Bartek, J., & Draetta, G. (1993). Regulation of the Cell Cycle by the cdk2 Protein Kinase in Cultured Human Fibroblasts. *The Journal of Cell Biology*, *121*(1), 101–111. https://doi.org/10.1083/jcb.121.1.101

Panopoulos, A. D., Yanes, O., Ruiz, S., Kida, Y. S., Diep, D., Tautenhahn, R., Herrerías, A., Batchelder, E. M., Plongthongkum, N., Lutz, M., Berggren, W. T., Zhang, K., Evans, R. M., Siuzdak, G., & Belmonte, J. C. I. (2011). The metabolome of induced pluripotent stem cells reveals metabolic changes occurring in somatic cell reprogramming. *Cell Research 2011 22:1*, *22*(1), 168–177. https://doi.org/10.1038/cr.2011.177

Pardee, A. B. (1974). A restriction point for control of normal animal cell proliferation. *Proceedings of the National Academy of Sciences of the United States of America*, *71*(4), 1286–1290. https://doi.org/10.1073/PNAS.71.4.1286

Pauklin, S., & Vallier, L. (2013). The cell-cycle state of stem cells determines cell fate propensity. *Cell*, *155*(1), 135–147. https://doi.org/10.1016/j.cell.2013.08.031

Pearl, R. (1928). *The rate of living*. University of London press ltd.

Pelletier, J., Bellot, G., Gounon, P., Lacas-Gervais, S., Pouysségur, J., & Mazure, N. M. (2012). Glycogen Synthesis is Induced in Hypoxia by the Hypoxia-Inducible Factor and Promotes Cancer Cell Survival. *Frontiers in Oncology*, *2*(FEB). https://doi.org/10.3389/FONC.2012.00018

Perenthaler, E., Nikoncuk, A., Yousefi, S., Berdowski, W. M., Alsagob, M., Capo, I., van der Linde, H. C., van den Berg, P., Jacobs, E. H., Putar, D., Ghazvini, M., Aronica, E., van IJcken, W. F. J., de Valk, W. G., Medici-van den Herik, E., van Slegtenhorst, M., Brick, L., Kozenko, M., Kohler, J.

N., … Barakat, T. S. (2020). Loss of UGP2 in brain leads to a severe epileptic encephalopathy, emphasizing that bi-allelic isoform-specific start-loss mutations of essential genes can cause genetic diseases. *Acta Neuropathologica*, *139*(3), 415–442. https://doi.org/10.1007/s00401-019-02109-6

Pescador, N., Villar, D., Cifuentes, D., Garcia-Rocha, M., Ortiz-Barahona, A., Vazquez, S., Ordoñez, A., Cuevas, Y., Saez-Morales, D., Garcia-Bermejo, M. L., Landazuri, M. O., Guinovart, J., & Del Peso, L. (2010). Hypoxia promotes glycogen accumulation through hypoxia inducible factor (HIF)-mediated induction of glycogen synthase 1. *PloS One*, *5*(3). https://doi.org/10.1371/JOURNAL.PONE.0009644

Pevny, L. H., Sockanathan, S., Placzek, M., & Lovell-Badge, R. (1998). A role for SOX1 in neural determination. *Development*, *125*(10), 1967–1978. https://doi.org/10.1242/DEV.125.10.1967

Phifer-Rixey, M., & Nachman, M. W. (2015). Insights into mammalian biology from the wild house mouse Mus musculus. *ELife*, *4*(4), 1–13. https://doi.org/10.7554/ELIFE.05959

R-Core-Team. (2022). R: A Language and Environment for Statistical Computing | BibSonomy. *Foundation for Statistical Computing*. https://www.bibsonomy.org/bibtex/7469ffee3b07f9167cf47e7555041ee7

Rayon, T., Stamataki, D., Perez-Carrasco, R., Garcia-Perez, L., Barrington, C., Melchionda, M., Exelby, K., Lazaro, J., Tybulewicz, V. L. J., Fisher, E. M. C., & Briscoe, J. (2020). Species-specific pace of development is associated with differences in protein stability. *Science*, *369*(6509). https://doi.org/10.1126/SCIENCE.ABA7667

Regad, T., Roth, M., Bredenkamp, N., Illing, N., & Papalopulu, N. (2007). The neural progenitor-specifying activity of FoxG1 is antagonistically regulated by CKI and FGF. *Nature Cell Biology 2007 9:5*, *9*(5), 531–540. https://doi.org/10.1038/ncb1573

Richardson, M. K. (1995). Heterochrony and the Phylotypic Period. *Developmental Biology*, *172*(2), 412–421. https://doi.org/10.1006/dbio.1995.8041

Rigoulet, M., Bouchez, C. L., Paumard, P., Ransac, S., Cuvellier, S., Duvezin-Caubet, S., Mazat, J. P., & Devin, A. (2020). Cell energy metabolism: An update. *Biochimica et Biophysica Acta (BBA) - Bioenergetics*, *1861*(11), 148276. https://doi.org/10.1016/J.BBABIO.2020.148276

Roach, P. (2005). Glycogen and its Metabolism. *Current Molecular Medicine*, *2*(2), 101–120. https://doi.org/10.2174/1566524024605761

Robitaille, A. M., Christen, S., Shimobayashi, M., Cornu, M., Fava, L. L., Moes, S., Prescianotto-Baschong, C., Sauer, U., Jenoe, P., & Hall, M. N. (2013). Quantitative phosphoproteomics reveal mTORC1 activates de novo pyrimidine synthesis. *Science (New York, N.Y.)*, *339*(6125), 1320–1323. https://doi.org/10.1126/SCIENCE.1228771

Rosenblatt, J., Gu, Y., & Morgan, D. O. (1992). Human cyclin-dependent kinase 2 is activated during the S and G2 phases of the cell cycle and associates with cyclin A. *Proceedings of the National Academy of Sciences of the United States of America*, *89*(7), 2824. https://doi.org/10.1073/PNAS.89.7.2824

Rossant, J., & Tam, P. P. L. (2022). Early human embryonic development: Blastocyst formation to gastrulation. *Developmental Cell*, *57*(2), 152–165. https://doi.org/10.1016/J.DEVCEL.2021.12.022

Rousset, M., Zweibaum, A., & Fogh, J. (1981). Presence of Glycogen and Growth-related Variations in 58 Cultured Human Tumor Cell Lines of Various Tissue Origins. *Cancer Research*, *41*(3), 1165–1170.

Rubner, M. (1908). *Das Problem der Lebensdauer und seine Beziehungen zu Wachstum und Ernährung*.

Ruiz, S., Panopoulos, A. D., Herrerías, A., Bissig, K. D., Lutz, M., Berggren, W. T., Verma, I. M., & Izpisua Belmonte, J. C. (2011). A High Proliferation Rate Is Required for Cell Reprogramming and Maintenance of Human Embryonic Stem Cell Identity. *Current Biology*, *21*(1), 45–52. https://doi.org/10.1016/J.CUB.2010.11.049

Sage, J., Mulligan, G. J., Attardi, L. D., Miller, A., Chen, S., Williams, B., Theodorou, E., & Jacks, T. (2000). Targeted disruption of the three Rb-related genes leads to loss of G1 control and immortalization. *Genes and Development*, *14*(23), 3037–3050. https://doi.org/10.1101/gad.843200

Sakai, Y. (1989). Neurulation in the mouse: Manner and timing of neural tube closure. *The Anatomical Record*, *223*(2), 194–203. https://doi.org/10.1002/ar.1092230212

Sakaue-Sawano, A., Kurokawa, H., Morimura, T., Hanyu, A., Hama, H., Osawa, H., Kashiwagi, S., Fukami, K., Miyata, T., Miyoshi, H., Imamura, T., Ogawa, M., Masai, H., & Miyawaki, A. (2008). Visualizing Spatiotemporal Dynamics of Multicellular Cell-Cycle Progression. *Cell*, *132*(3), 487–498. https://doi.org/10.1016/j.cell.2007.12.033

Samanta, M., & Kalantry, S. (2020). Generating primed pluripotent epiblast stem cells: A methodology chapter. *Current Topics in Developmental Biology*, *138*, 139–174. https://doi.org/10.1016/BS.CTDB.2020.01.005

Savatier, P., Huang, S., Szekely, L., Wiman, K. G., & Samarut, J. (1994). Contrasting patterns of retinoblastoma protein expression in mouse embryonic stem cells and embryonic fibroblasts. *Oncogene*, *9*(3), 809–818. https://europepmc.org/article/med/8108123

Savatier, P., Lapillonne, H., van Grunsven, L., Rudkin, B., & Samarut, J. (1995). Withdrawal of differentiation inhibitory activity/leukemia inhibitory factor upregulates D-type cyclins and cyclin-dependent kinase inhibitors in mouse embryonic stem cells. *Oncogene*, *12*(2), 309–322.

Schindelin, J., Arganda-Carreras, I., Frise, E., Kaynig, V., Longair, M., Pietzsch, T., Preibisch, S., Rueden, C., Saalfeld, S., Schmid, B., Tinevez, J. Y., White, D. J., Hartenstein, V., Eliceiri, K., Tomancak, P., & Cardona, A. (2012). Fiji: an open-source platform for biological-image analysis. *Nature Methods 2012 9:7*, *9*(7), 676–682. https://doi.org/10.1038/nmeth.2019

Schmidt, U., Weigert, M., Broaddus, C., & Myers, G. (2018). Cell detection with star-convex polygons. *Lecture Notes in Computer Science (Including Subseries Lecture Notes in Artificial Intelligence and Lecture Notes in Bioinformatics)*, *11071 LNCS*, 265–273. https://doi.org/10.1007/978-3-030-00934-2_30

Schulze, A., Zerfass, K., Spitkovsky, D., Middendorp, S., Bergès, J., Helin, K., Jansen-Dürr, P., & Henglein, B. (1995). Cell cycle regulation of the cyclin A gene promoter is mediated by a variant E2F site. *Proceedings of the National Academy of Sciences*, *92*(24), 11264–11268. https://doi.org/10.1073/PNAS.92.24.11264

Schumacher, S., Fernkorn, M., Marten, M., Kim, Y. S., Bedzhov, I., & Schröter, C. (2023). Tissue-intrinsic Wnt signals antagonize Nodal-driven AVE differentiation. *BioRxiv*, 2023.05.19.541432. https://doi.org/10.1101/2023.05.19.541432

Sela, Y., Molotski, N., Golan, S., Itskovitz-Eldor, J., & Soen, Y. (2012). Human embryonic stem cells exhibit increased propensity to differentiate during the G1 phase prior to phosphorylation of retinoblastoma protein. *Stem Cells*, *30*(6), 1097–1108. https://doi.org/10.1002/stem.1078

Smith, F. A., & Lyons, S. K. (2011). How big should a mammal be? A macroecological look at mammalian body size over space and time. *Philosophical Transactions of the Royal Society B: Biological Sciences*, *366*(1576), 2364. https://doi.org/10.1098/RSTB.2011.0067

Snow, M. H. L. (1977). Gastrulation in the mouse: growth and regionalization of the epiblast. *Journal of Embryology and Experimental Morphology*, *Vol. 42*(2), 293–303.

Spence, J. R., Mayhew, C. N., Rankin, S. A., Kuhar, M. F., Vallance, J. E., Tolle, K., Hoskins, E. E., Kalinichenko, V. V., Wells, S. I., Zorn, A. M., Shroyer, N. F., & Wells, J. M. (2010). Directed differentiation of human pluripotent stem cells into intestinal tissue in vitro. *Nature 2010 470:7332*, *470*(7332), 105–109. https://doi.org/10.1038/nature09691

Sperber, H., Mathieu, J., Wang, Y., Ferreccio, A., Hesson, J., Xu, Z., Fischer, K. A., Devi, A., Detraux, D., Gu, H., Battle, S. L., Showalter, M., Valensisi, C., Bielas, J. H., Ericson, N. G., Margaretha, L., Robitaille, A. M., Margineantu, D., Fiehn, O., … Ruohola-Baker, H. (2015). The metabolome regulates the epigenetic landscape during naive-to-primed human embryonic stem cell transition. *Nature Cell Biology 2015 17:12*, *17*(12), 1523–1535. https://doi.org/10.1038/ncb3264

Stauske, M., Polo, I. R., Haas, W., Knorr, D. Y., Borchert, T., Streckfuss-bömeke, K., Dressel, R., Bartels, I., Tiburcy, M., Zimmermann, W., & Behr, R. (2020). Non-Human Primate iPSC Generation, Cultivation, and Cardiac Differentiation under Chemically Defined Conditions. *Cells*, *9*(6), 1349. https://doi.org/10.3390/cells9061349

Stead, E., White, J., Faast, R., Conn, S., Goldstone, S., Rathjen, J., Dhingra, U., Rathjen, P., Walker, D., & Dalton, S. (2002). Pluripotent cell division cycles are driven by ectopic Cdk2, cyclin A/E and E2F activities. *Oncogene*, *21*(54), 8320–8333. https://doi.org/10.1038/sj.onc.1206015

Stiles, J., & Jernigan, T. L. (2010). The Basics of Brain Development. *Neuropsychology Review*, *20*(4), 327. https://doi.org/10.1007/S11065-010-9148-4

Swovick, K., Firsanov, D., Welle, K. A., Hryhorenko, J. R., Wise, J. P., George, C., Sformo, T. L., Seluanov, A., Gorbunova, V., & Ghaemmaghami, S. (2021). Interspecies Differences in Proteome Turnover Kinetics Are Correlated with Life Spans and Energetic Demands. *Molecular and Cellular Proteomics*, *20*, 100041. https://doi.org/10.1074/MCP.RA120.002301

Tacutu, R., Thornton, D., Johnson, E., Budovsky, A., Barardo, Di., Craig, T., DIana, E., Lehmann, G., Toren, D., Wang, J., Fraifeld, V. E., & De Magalhães, J. P. (2018). Human Ageing Genomic Resources: new and updated databases. *Nucleic Acids Research*, *46*(D1), D1083–D1090. https://doi.org/10.1093/NAR/GKX1042

Takahashi, K., & Yamanaka, S. (2006). Induction of Pluripotent Stem Cells from Mouse Embryonic and Adult Fibroblast Cultures by Defined Factors. *Cell*, *126*(4), 663–676. https://doi.org/10.1016/j.cell.2006.07.024

Takahashi, T., Goto, T., Miyama, S., Nowakowski, R. S., & Caviness, V. S. (1999). Sequence of Neuron Origin and Neocortical Laminar Fate: Relation to Cell Cycle of Origin in the Developing Murine Cerebral Wall. *The Journal of Neuroscience*, *19*(23), 10357–10371. https://doi.org/10.1523/JNEUROSCI.19-23-10357.1999

Tchieu, J., Zimmer, B., Fattahi, F., Amin, S., Zeltner, N., Chen, S., & Studer, L. (2017). A Modular Platform for Differentiation of Human PSCs into All Major Ectodermal Lineages. *Cell Stem Cell*, *21*(3), 399-410.e7. https://doi.org/10.1016/j.stem.2017.08.015

Temple, S., & Raff, M. C. (1986). Clonal Analysis of Oligodendrocyte Development in Culture: Evidence for a Developmental Clock That Counts Cell Divisions. *Cell*, *44*, 773–779.

ter Huurne, M., Chappell, J., Dalton, S., & Stunnenberg, H. G. (2017). Distinct Cell-Cycle Control in Two Different States of Mouse Pluripotency. *Cell Stem Cell*, *21*(4), 449-455.e4. https://doi.org/10.1016/j.stem.2017.09.004

Tesar, P. J., Chenoweth, J. G., Brook, F. A., Davies, T. J., Evans, E. P., Mack, D. L., Gardner, R. L., & McKay, R. D. G. (2007). New cell lines from mouse epiblast share defining features with human embryonic stem cells. *Nature*, *448*(7150), 196–199. https://doi.org/10.1038/NATURE05972

Thommen, A., Werner, S., Frank, O., Philipp, J., Knittelfelder, O., Quek, Y., Fahmy, K., Shevchenko,

A., Friedrich, B. M., Jülicher, F., & Rink, J. C. (2019). Body size-dependent energy storage causes Kleiber's law scaling of the metabolic rate in planarians. *ELife*, *8*. https://doi.org/10.7554/ELIFE.38187

Thomson, I., Gilchrist, S., Bickmore, W. A., & Chubb, J. R. (2004). The radial positioning of chromatin is not inherited through mitosis but is established de novo in early G1. *Current Biology*, *14*(2), 166–172. https://doi.org/10.1016/J.CUB.2003.12.024

Thomson, J. A. (1998). Embryonic stem cell lines derived from human blastocysts. *Science*, *282*(5391), 1145–1147. https://doi.org/10.1126/science.282.5391.1145

Tinevez, J. Y., Perry, N., Schindelin, J., Hoopes, G. M., Reynolds, G. D., Laplantine, E., Bednarek, S. Y., Shorte, S. L., & Eliceiri, K. W. (2017). TrackMate: An open and extensible platform for single-particle tracking. *Methods*, *115*, 80–90. https://doi.org/10.1016/J.YMETH.2016.09.016

Tippetts, T. S., Sieber, M. H., & Solmonson, A. (2023). Beyond energy and growth: the role of metabolism in developmental signaling, cell behavior and diapause. *Development (Cambridge)*, *150*(20). https://doi.org/10.1242/DEV.201610/334163

Tirosh, I., Izar, B., Prakadan, S. M., Wadsworth, M. H., Treacy, D., Trombetta, J. J., Rotem, A., Rodman, C., Lian, C., Murphy, G., Fallahi-Sichani, M., Dutton-Regester, K., Lin, J. R., Cohen, O., Shah, P., Lu, D., Genshaft, A. S., Hughes, T. K., Ziegler, C. G. K., … Garraway, L. A. (2016). Dissecting the multicellular ecosystem of metastatic melanoma by single-cell RNA-seq. *Science*, *352*(6282), 189–196. https://doi.org/10.1126/science.aad0501

Toma, K., Wang, T. C., & Hanashima, C. (2016). Encoding and decoding time in neural development. *Development Growth and Differentiation*, *58*(1), 59–72. https://doi.org/10.1111/dgd.12257

Tsai, L. H., Harlow, E., & Meyerson, M. (1991). Isolation of the human cdk2 gene that encodes the cyclin A- and adenovirus E1A-associated p33 kinase. *Nature*, *353*(6340), 174–177. https://doi.org/10.1038/353174A0

Uchikawa, M., Kamachi, Y., & Kondoh, H. (1999). Two distinct subgroups of Group B Sox genes for transcriptional activators and repressors: their expression during embryonic organogenesis of the chicken. *Mechanisms of Development*, *84*(1–2), 103–120. https://doi.org/10.1016/s0925-4773(99)00083-0

Uehara, K., Lee, W. D., Stefkovich, M., Biswas, D., Santoleri, D., Whitlock, A. G., Quinn, W., Coopersmith, T., Creasy, K. T., Rader, D. J., Sakamoto, K., Rabinowitz, J. D., & Titchenell, P. M. (2024). mTORC1 controls murine postprandial hepatic glycogen synthesis via Ppp1r3b. *The Journal of Clinical Investigation*, *134*(7). https://doi.org/10.1172/JCI173782

Vallier, L., Reynolds, D., & Pedersen, R. A. (2004). Nodal inhibits differentiation of human embryonic stem cells along the neuroectodermal default pathway. *Developmental Biology*, *275*(2), 403–421. https://doi.org/10.1016/J.YDBIO.2004.08.031

Vander Heiden, M. G., Cantley, L. C., & Thompson, C. B. (2009). Understanding the Warburg Effect: The Metabolic Requirements of Cell Proliferation. *Science (New York, N.Y.)*, *324*(5930), 1029. https://doi.org/10.1126/SCIENCE.1160809

Vellai, T., Takacs-Vellai, K., Zhang, Y., Kovacs, A. L., Orosz, L., & Müller, F. (2003). Influence of TOR kinase on lifespan in C. elegans. *Nature 2003 426:6967*, *426*(6967), 620–620. https://doi.org/10.1038/426620a

Vercellino, I., & Sazanov, L. A. (2021). The assembly, regulation and function of the mitochondrial respiratory chain. *Nature Reviews Molecular Cell Biology 2021 23:2*, *23*(2), 141–161. https://doi.org/10.1038/s41580-021-00415-0

Voit, R., Schäfer, K., & Grummt, I. (1997). Mechanism of repression of RNA polymerase I transcription by the retinoblastoma protein. *Molecular and Cellular Biology*, *17*(8), 4230.

https://doi.org/10.1128/MCB.17.8.4230

Walpole, S. C., Prieto-Merino, D., Edwards, P., Cleland, J., Stevens, G., & Roberts, I. (2012). The weight of nations: An estimation of adult human biomass. *BMC Public Health*, *12*(1), 1–6. https://doi.org/10.1186/1471-2458-12-439

Walther, C., & Gruss, P. (1991). Pax-6, a murine paired box gene, is expressed in the developing CNS. *Development*, *113*(4), 1435–1450.

Wang, W., Lin, C., Lu, D., Ning, Z., Cox, T., Melvin, D., Wang, X., Bradley, A., & Liu, P. (2008). Chromosomal transposition of PiggyBac in mouse embryonic stem cells. *Proceedings of the National Academy of Sciences of the United States of America*, *105*(27), 9290–9295. https://doi.org/10.1073/pnas.0801017105

Warburg, O. (1924). Über den Stoffwechsel der Carcinomzelle. *Die Naturwissenschaften*, *12*(50), 1131–1137. https://doi.org/10.1007/BF01504608

Warburg, O. (1956). On the origin of cancer cells. *Science*, *123*(3191), 309–314. https://doi.org/10.1126/science.123.3191.309

Weinberg, R. A. (1995). The retinoblastoma protein and cell cycle control. *Cell*, *81*(3), 323–330. https://doi.org/10.1016/0092-8674(95)90385-2

Weindruch, R. (1996). The Retardation of Aging by Caloric Restriction: Studies in Rodents and Primates. *Toxicologic Pathology*, *24*(6), 742–745. https://doi.org/10.1177/019262339602400618

West, G. B., Brown, J. H., & Enquist, B. J. (1997). A general model for the origin of allometric scaling laws in biology. *Science*, *276*(5309), 122–126. https://doi.org/10.1126/science.276.5309.122

Wiles, M. V., & Johansson, B. M. (1999). Embryonic stem cell development in a chemically defined medium. *Experimental Cell Research*, *247*(1), 241–248. https://doi.org/10.1006/EXCR.1998.4353

Wilson, P. A., & Hemmati-Brivanlou, A. (1995). Induction of epidermis and inhibition of neural fate by Bmp-4. *Nature*, *376*(6538), 331–333. https://doi.org/10.1038/376331A0

Wohlschlegel, J. A., Dwyer, B. T., Dhar, S. K., Cvetic, C., Walter, J. C., & Dutta, A. (2000). Inhibition of Eukaryotic DNA Replication by Geminin Binding to Cdt1. *Science*, *290*(5500), 2309–2312. https://doi.org/10.1126/science.290.5500.2309

Wolf, F. A., Angerer, P., & Theis, F. J. (2018). SCANPY: large-scale single-cell gene expression data analysis. *Genome Biology*, *19*(1), 15. https://doi.org/10.1186/S13059-017-1382-0

Wolfe, A. L., Zhou, Q., Toska, E., Galeas, J., Ku, A. A., & Koche, R. P. (2021). UDP-glucose pyrophosphorylase 2, a regulator of glycogen synthesis and glycosylation, is critical for pancreatic cancer growth. *Proceedings of the National Academy of Sciences*, *118*(31). https://doi.org/10.1073/pnas.2103592118

Wu, J. J., Liu, J., Chen, E. B., Wang, J. J., Cao, L., Narayan, N., Fergusson, M. M., Rovira, I. I., Allen, M., Springer, D. A., Lago, C. U., Zhang, S., DuBois, W., Ward, T., deCabo, R., Gavrilova, O., Mock, B., & Finkel, T. (2013). Increased mammalian lifespan and a segmental and tissue-specific slowing of aging after genetic reduction of mTOR expression. *Cell Reports*, *4*(5), 913–920. https://doi.org/10.1016/j.celrep.2013.07.030

Yang, X., Rodriguez, M. L., Leonard, A., Sun, L., Fischer, K. A., Wang, Y., Ritterhoff, J., Zhao, L., Kolwicz, S. C., Pabon, L., Reinecke, H., Sniadecki, N. J., Tian, R., Ruohola-Baker, H., Xu, H., & Murry, C. E. (2019). Fatty Acids Enhance the Maturation of Cardiomyocytes Derived from Human Pluripotent Stem Cells. *Stem Cell Reports*, *13*(4), 657–668. https://doi.org/10.1016/j.stemcr.2019.08.013

Ying, Q. L., Stavridis, M., Griffiths, D., Li, M., & Smith, A. (2003). Conversion of embryonic stem cells into neuroectodermal precursors in adherent monoculture. *Nature Biotechnology*, *21*(2), 183–186. https://doi.org/10.1038/nbt780

Yoshihara, E., Wei, Z., Lin, C. S., Fang, S., Ahmadian, M., Kida, Y., Tseng, T., Dai, Y., Yu, R. T., Liddle, C., Atkins, A. R., Downes, M., & Evans, R. M. (2016). ERRγ Is Required for the Metabolic Maturation of Therapeutically Functional Glucose-Responsive β Cells. *Cell Metabolism*, *23*(4), 622–634. https://doi.org/10.1016/j.cmet.2016.03.005

Yun, Q., Ma, S. F., Zhang, W. N., Gu, M., & Wang, J. (2024). FoxG1 as a Potential Therapeutic Target for Alzheimer's Disease: Modulating NLRP3 Inflammasome via AMPK/mTOR Autophagy Pathway. *Cellular and Molecular Neurobiology*, *44*(1), 35. https://doi.org/10.1007/S10571-024-01467-4

Zhang, X., Huang, C. T., Chen, J., Pankratz, M. T., Xi, J., Li, J., Yang, Y., LaVaute, T. M., Li, X. J., Ayala, M., Bondarenko, G. I., Du, Z. W., Jin, Y., Golos, T. G., & Zhang, S. C. (2010). Pax6 is a human neuroectoderm cell fate determinant. *Cell Stem Cell*, *7*(1), 90–100. https://doi.org/10.1016/j.stem.2010.04.017

Zhou, J., Su, P., Wang, L., Chen, J., Zimmermann, M., Genbacev, O., Afonja, O., Horne, M. C., Tanaka, T., Duan, E., Fisher, S. J., Liao, J., Chen, J., & Wang, F. (2009). mTOR supports long-term self-renewal and suppresses mesoderm and endoderm activities of human embryonic stem cells. *Proceedings of the National Academy of Sciences of the United States of America*, *106*(19), 7840–7845. https://doi.org/10.1073/pnas.0901854106

Zhou, W., Choi, M., Margineantu, D., Margaretha, L., Hesson, J., Cavanaugh, C., Blau, C. A., Horwitz, M. S., Hockenbery, D., Ware, C., & Ruohola-Baker, H. (2012). HIF1α induced switch from bivalent to exclusively glycolytic metabolism during ESC-to-EpiSC/hESC transition. *EMBO Journal*, *31*(9), 2103–2116. https://doi.org/10.1038/emboj.2012.71

7 Appendix

7.1 List of figures

7.2 List of tables

7.3 Commonly used abbreviations

Abbreviation	Meaning
AMP	Adenosine-monophosphate
AMPK	AMP-activated protein kinase
ATP	Adenosine-triphosphate
BSA	Bovine serum albumin
CDK	Cyclin-dependent kinase
cDNA	Complementary desoxyribonucleic acid
CMO	Cell multiplexing oligo
DNA	Desoxyribonucleic acid
EpiSC	Epiblast stem cell
ESC	Embryonic stem cell
FACS	Fluorescence-activated cell sorting
$FADH_2$	Flavin adenine dinucleotide (reduced form)
FAX	FGF2; Activin A, XAV939 medium
FBS	Fetal bovine serum
FDR	False discovery rate
FSC	Forward scatter
FUCCI	Fluorescent ubiquitination-based cell cycle indicator
GEM	Gel bead-in-emulsion
GFP	Green fluorescent protein
GO	Gene ontology
hESCs	Human embryonic stem cells
ICM	Inner cell mass
iPSC	induced pluripotent stem cell
KO	Knock-out
log2FC	Log2 fold change

mESCs	Mouse embryonic stem cells
mTOR	Mammalian target of rapamycin
mTORi	mTOR inhibition
NAD	Nicotinamide adenine dinucleotide (oxidized form)
NADH	Nicotinamide adenine dinucleotide (reduced form)
NADPH	Nicotinamide adenine dinucleotide phosphate (reduced form)
NPCs	Neural progenitor cells
NPCSL	NPC differentiation medium plus SB431542 and LDN193189
OXPHOS	Oxidative phosphorylation
PBS	Phosphate-buffered saline
PCNA	Proliferating cell nuclear antigen
PIP	PCNA-interacting protein
PSCs	Pluripotent stem cells
PYGL	Glycogen phosphorylase
RbTKO	Retinoblastoma triple knock-out
RNA	Ribonucleic acid
ROI	Region of interest
RT	Reverse transcription
scRNAseq	Single-cell RNA sequencing
SSC	Side scatter
TCA	Tricarboxylic acid cycle
TSC	Tuberous sclerosis complex
UDP	Uridine diphosphate glucose
UGP2	UDP-glucose pyrophosphorylase 2
UMI	Unique molecular identifier
UPPS	Universal primate pluripotent stem cell medium
WT	Wild type

Acknowledgments

It has been an exciting time at the institute and I am grateful for everyone who has been part of it. First and foremost, I would like to thank Dr. Christian Schröter, without whom this project would not have happened, for his constant support, inspiring discussions, and not least for always believing in the project. Thank you for always taking the time and offering advice. It has been a pleasure to be part of your group.

I would also like to express my gratitude towards Prof. Dr. Philippe Bastiaens for giving me the opportunity to be part of the Department of Systemic Cell Biology. I am thankful for all the support and discussions that shaped my project. Dr. Peter Bieling as well as my TAC members Prof. Dr. Stefan Westermann and Dr. Jonathan Rodenfels also contributed valuable advice and new ideas for which I am very grateful.

Thank you also to the whole department for your great input, your kindness, support and all the fun moments we shared. It would not have been the same without you.

Many thanks also to Christa and Lucia, for making our IMPRS such a great community and for always taking the time to help us students wherever you can. Your work is truly appreciated.

This project was a collaboration of the Schröter lab and the groups of Prof. Dr. Micha Drukker and Dr. Carsten Marr. Our meetings and discussions, online and in person, took the project to a place we did not imagine before. Thank you for creating such a collaborative, productive and friendly atmosphere in all our conversations and always pushing the project forward. Furthermore, I would like to extent my gratitude to the PhD students involved in the project, Alexandra de la Porte and Moritz Thomas. You did incredible work and I had a lot of fun with you (during and after work).

I would also like to thank all present and past members of the Schröter lab, namely Michelle, Sina, Max, Marina and Dhruv, as well as all temporary members (Fiorella, Caro, Sarah, Pauliine, Shamya and Pablo). Thanks to Michelle for all her support in the lab, be it FACS or the single-cell experiment, your help was indispensable. Thanks also to Max for sharing so much of your R expertise and helping me tremendously with my data analyses. To all of you, it was my honor to share a workplace with you guys, I could not have been luckier. I really appreciate you as colleagues and friends and I will truly miss working with you. Let's just never TGA.

My gratitude also extents to Ankit, Mike and Svenja for all the fun moments and all the absurd lunch discussions. You made every day just so much funnier.

Special thanks go to Yannic whose constant support and patience kept me going these past months. Thank you for always being there and finding the right words to turn a moment of stress into a moment of fun, I deeply appreciate it.

Finally, I thank my parents for always having my back, supporting me no matter what and being such an important constant in my life. Thank you.